7-30-2015 12:00 AM

Evaluation of gauge-radar merging methods for quantitative precipitation estimation in hydrology: a case study in the Upper Thames River basin

Jack L. McKee
The University of Western Ontario

Supervisor
Dr. Andrew Binns
The University of Western Ontario

Graduate Program in Civil and Environmental Engineering
A thesis submitted in partial fulfillment of the requirements for the degree in Master of Engineering Science

EVALUATION OF GAUGE-RADAR MERGING METHODS FOR QUANTITATIVE PRECIPITATION ESTIMATION IN HYDROLOGY: A CASE STUDY IN THE UPPER THAMES RIVER BASIN

(Thesis format: Monograph)

By

Jack L. McKee

Graduate Program in Civil and Environmental Engineering

A thesis submitted in partial fulfillment
of the requirements for the degree of
Master of Engineering Science

The School of Graduate and Postdoctoral Studies
The University of Western Ontario
London, Ontario, Canada

Abstract

Hydrological models rely on accurate precipitation data in order to produce results with a high degree of confidence and serve as valuable flood forecasting and warning tools. Gauge-radar merging methods combine rainfall estimates from rain gauges and weather radar in order to capitalize on the strengths of the individual instruments and produce precipitation data with greater accuracy for input to hydrological models. A comprehensive review of gauge-radar merging methods reveals that there is an opportunity for near-real time application in hydrological models. The performance of four well known gauge-radar merging methods, including mean field bias correction, Brandes spatial adjustment, local bias correction using kriging and conditional merging, are examined using Environment Canada radar and the Upper Thames River basin in southwestern Ontario, Canada, as a case study. The analysis assesses the effect of gauge-radar merging methods on: 1) the accuracy of predicted rainfall accumulations; and 2) the accuracy of predicted stream flows using a semi-distributed hydrological model. In addition, several influencing factors (i.e., gauge density, storm type, basin type, proximity to the radar tower and time-step of adjustment) are analysed to determine their effect on the performance of the rainfall estimation techniques. Results indicate that gauge-radar merging methods can increase the accuracy of both rainfall accumulation estimations and predicted stream flows over the use of raw radar and rain gauges alone. Results from this study provide guidance for hydrologists and engineers assessing whether the addition of corrected radar products will improve rainfall estimation and hydrological modelling accuracy.

Keywords

Water resources, quantitative precipitation estimation, weather radar, rain gauge, gauge-radar merging, hydrology, hydrological modelling.

Co-Authorship

The work presented here is a collaborative effort by the present author, Dr. Andrew Binns, Mark Helsten and Mark Shifflett. Chapter 2 has been accepted for publication in the *Canadian Water Resources Journal* (ID: TCWR-2014-0082) with the present author as primary author and Dr. Binns providing significant assistance in the set-up, organization and editing of the manuscript. The work completed in Chapter 4 and Chapter 5 will be submitted for publication in the near future, with the present author as the primary author, Dr. Binns providing assistance with the design of the study and interpretation of the results, and Mr. Helsten and Mr. Shifflett providing contributions and feedback on the original work in preparation for submission.

Acknowledgements

I would like to express my deepest gratitude to Dr. Andrew Binns for his guidance and support. His constant assistance and mentorship was invaluable in steering me towards my goals. I could not have hoped for a better supervisor and I look forward to working with him again in the future.

I am tremendously appreciative of the financial support provided by the Natural Sciences and Engineering Research Council of Canada (NSERC). While completing my thesis I had the privilege to work at the Watershed Conservation Centre (WCC) for the Upper Thames River Conservation Authority (UTRCA) as part of an NSERC Industrial Postgraduate Scholarship. Thank you to everyone at the WCC for welcoming me into the UTRCA family and making my time there truly great. A special thanks to Mark Helsten, Mark Shifflett, Imtiaz Shah and Phil Simm for their direction and help with this thesis. I would like to thank Environment Canada and Dr. Vincent Fortin for providing me with the data needed to complete this work.

Thank you to all the members of my research group for your support throughout my thesis. In particular I would like to thank Etta Gunsolus for always getting me to look at the bright side of things. As well I would like to thank Chris Howlett for his hard work during the summer of 2014.

This thesis would not have been possible without the love and support of my parents, Anne and John, throughout my academic studies. Their encouraging words and unwavering faith kept my confidence high.

I am forever grateful to my partner Lauren, for her constant love and belief in me. Her determination and hard work inspire me every day, and drove me to complete this thesis. I am excited to see what the future has to bring for us!

Table of Contents

List of Tables

List of Figures

List of Appendices

List of Abbreviations

BDC	Bayesian Data Combination
BSA	Brandes Spatial Adjustment
CaPA	Canadian Precipitation Analysis
CAPPI	Constant Altitude Plan Position Indicator
CM	Conditional Merging
CMC	Canadian Meteorological Centre
CV	Cross-Validation
CV (RMSE)	Coefficient of Variation of the Root Mean Square Error
EBK	Empirical Bayesian Kriging
EC	Environment Canada
GEM	Global Environmental Multiscale model
HEC-HMS	Hydrologic Engineering Centers – Hydrologic Modeling System
IN	Independent Network
KED	Kriging with External Drift
LB	Local Bias correction with ordinary kriging
MAE	Mean Absolute Error
MRE	Mean Relative Error
NSE	Nash Sutcliffe Efficiency
PEPF	Percent Error in Peak Flow
PEV	Percent Error in Volume
PTE	Peak Timing Error
PWRMSE	Peak Weighted Root Mean Square Error
QPE	Quantitative Precipitation Estimation
RGO (OK)	Rain Gauge Only using Ordinary Kriging

RMSE	Root Mean Square Error
SG	Stream Gauge
SOA	Statistical Objective Analysis
TB	Tipping Bucket
UH	Unit Hydrograph
URP	Unified Radar Processor
USACE	United States Army Corps of Engineers
UTRb	Upper Thames River basin
UTRCA	Upper Thames River Conservation Authority
WMO	World Meteorological Organization
WRST	Wilcoxon Rank Sum Test

Chapter 1

1 Introduction

1.1 Motivation

Throughout Canadian history flooding events have had a major impact on society, causing billions of dollars in damage and resulting in the loss of life. Flooding events are by far the most common natural disaster experienced in Canada (Sandink et al. 2010). The Institute for Catastrophic Loss Reduction estimates that currently preventable damages due to extreme rainfall exceed $2 billion a year in Canada (Kovacs et al. 2014). In recent years costs associated with flooding have been rapidly escalating (Insurance Bureau of Canada 2015). Flooding events in 2011 in Manitoba and Quebec resulted in damages of $1.1 billion and $78 million, respectively (Thistlethwaite and Feltmate 2013). Damages due to 2013 flooding in Alberta caused by a combination of snowmelt in the headwater regions and extreme rainfall resulted in damages exceeding $6 billion (Environment Canada 2014). Flash flooding in Toronto in July 2013 due to a high-intensity, short-duration rainfall event resulted in damages of approximately $1 billion (Environment Canada 2014). The federal, provincial and municipal governments of Canada have largely been responsible for covering the rising costs of these damages which has resulted in significant impacts to the Canadian economy (Environment Canada 2013a).

Riverine flooding events are a result of increased runoff from the surrounding contributing basin which causes the stream to exceed the level of the banks (Dingman 2008). While this increase in flow can be due to a number of hydrological, meteorological, and human-induced factors (Takeuchi 2001), precipitation is one of the most influential factors controlling the frequency and magnitude of flooding events (Environment Canada 2013b). One of the most important tools for flood mitigation is the use of hydrological models for flow prediction (Takeuchi 2001). A hydrological model, which conceptualizes the complex physical characteristics of a basin (Dingman 2008), is used to analyze stream flow rates and water levels in near real-time as they respond to rainfall events. Output from these models is used to provide early flood warning,

allowing for time to evacuate affected areas, shut down vulnerable transportation infrastructure, deploy emergency workers and establish emergency short-term flood protection for important structures (Looper and Vieux 2012).

Despite their many benefits, a lack of confidence in hydrological modelling outputs often leads to under-utilization of this tool for flood mitigation (McMillan et al. 2011). The validity of a model depends on the accuracy and reliability of input parameters and initial and boundary conditions (Zhu et al. 2013). Of these parameters and data, rainfall inputs play an integral role in the final accuracy of the model outputs (Golding 2009). In addition, accurate rainfall is often needed for hydrological model calibration to produce parameter sets which represent basin characteristics. Widespread use of hydrological models has demonstrated the need for accurate rainfall fields in order to produce runoff and stream flow predictions with a high degree of confidence (see, e.g., Beven and Hornberger 1982; Kalinga and Gan 2006; Cole and Moore 2008; Xu et al. 2013; Berne and Krajewski 2013; etc.). According to McMillan et al. (2011, p. 84): "No model, however well founded in physical theory or empirically justified by past performance, can produce accurate runoff predictions if forced with inaccurate rainfall data." Inaccurate rainfall data directly compromise the integrity of the model and the associated critical decisions made using model output (Golding 2009; McMillan et al. 2011). In particular, for small watersheds, the timing and location of rainfall is critical in reproducing hydrographs. There is thus an urgent need to acquire reliable precipitation estimates at high spatial (e.g., a few km or less) and temporal (e.g., hourly or less) resolutions (Berne and Krajewski 2013). As a result, in recent years substantial efforts have been made to develop accurate methods to estimate rainfall accumulations at higher spatial and temporal resolutions during precipitation events.

Currently, rain gauges and weather radar (radar) are the most widely accepted and used instruments for acquiring near-real time estimates of rainfall accumulations (Sene 2013). While these rainfall measurement techniques have their individual strengths, both techniques result in errors which can limit their ability to produce accurate input for hydrological models. Considering this, numerous techniques have been proposed to adjust and merge rain gauge and radar measurements (hereafter referred to as gauge-radar

merging methods) at high spatial and temporal resolutions in order to obtain greater accuracy in rainfall accumulations. The choice of a suitable rainfall estimation technique is a critical decision for hydrologists and engineers developing hydrological models for reliable operational use. The vast number of gauge-radar merging methods present in the literature makes this decision a challenging task.

In addition, several location-specific operational, hydrological and environmental factors can influence the accuracy and performance of individual gauge-radar merging methods. These factors include: the density of the rain gauge network, climate and storm characteristics, temporal resolution of adjustment, basin characteristics and proximity of the radar station. These factors have demonstrated to adversely affect the accuracy of gauge-radar merging methods by decreasing the reliability of the precipitation estimates (see, e.g., Kitchen and Blackall 1992; Michelson and Koistinen 2000; Kalinga and Gan 2006; Smith et al. 2007; Goudenhoofdt and Delobbe 2009; Berne and Krajewski 2013). The influence of each factor needs to be considered in the selection of an appropriate estimation technique. This highlights the need to both assess performance of gauge-radar merging methods on a case-by-case basis and to quantify the effect of these five factors on the performance of gauge-radar merging methods.

1.2 Goals and objectives of the thesis

The goal of this thesis is to evaluate the performance of gauge-radar merging methods for hydrological applications. This thesis will use radar data supplied by Environment Canada (EC) and will use the Upper Thames River basin (UTRb), located in southwestern Ontario, Canada, as a case study. This goal will be accomplished by satisfying the following three central objectives:

(1) conduct a comprehensive review of the literature to assess the performance of rain gauges, radar and gauge-radar merging methods for quantitative precipitation estimation;
(2) evaluate the effect of gauge-radar merging methods on the accuracy of estimated rainfall accumulations; and

(3) evaluate the effect of gauge-radar merging methods on the accuracy of predicted flows using a semi-distributed hydrological model.

Through the accomplishment of these objectives the effect of the aforementioned location-specific environmental, hydrological and operational influencing factors will be characterized and evaluated.

1.3 Structure of the thesis

This thesis is prepared in the classical monograph format. Following Chapter 1, five chapters are included. These are organized as follows.

Chapter 2 presents the literature review and provides a comprehensive review of the use of rain gauges and radar in hydrology as well as detailed descriptions of well-known gauge-radar merging methods for the near-real time estimation of rainfall accumulations.

Chapter 3 provides the description of the study area and the data used in the thesis.

Chapter 4 presents the results from an investigation of the effect of several well-known gauge-radar merging methods on rainfall accumulation accuracy, providing a particular focus on the effect of several hydrological, environmental and operational factors on the accuracy of the final rainfall estimates.

Chapter 5 presents the results from an investigation to evaluate the effect of several well-known gauge-radar merging methods on the accuracy of predicted hydrographs using a semi-distributed hydrological model.

Chapter 6 provides a discussion of the results from Chapters 2 through 5 and summarizes the main conclusions and contributions of the thesis. Opportunities for future research are also presented.

Chapter 2

2 Literature review

This Chapter provides a comprehensive review of the acquisition and merging of rain gauge and radar rainfall data for input into hydrological models. The aim of this literature review is to satisfy the following objectives:

(1) provide a review and description of the uncertainty associated with the use of rain gauges and radar for the acquisition of rainfall data;
(2) describe and compare pertinent gauge-radar merging methods to produce greater accuracy in rainfall accumulations; and
(3) identify and discuss factors which influence the accuracy of gauge-radar merging methods as input into hydrological models in order to aid in the selection of an appropriate rainfall estimation technique.

The use of radar in hydrological modelling is widely studied academically; however, it is not yet widely implemented operationally. This Chapter will assist in identifying circumstances in which the addition of radar rainfall data is beneficial in hydrological modelling.

2.2 Rainfall estimation: rain gauges

Historically, rain gauges have been the main source for quantitative precipitation estimation (QPE) for use in hydrological models, and remain one of the most popular and widely used rainfall accumulation collection methods today (Environment Canada 2013c). Rain gauges measure the depth of rainfall over a set time for a given location. Therefore, the primary goal of a rain gauge is to obtain representative measurements of rainfall over the area which the measurement represents (World Meteorological Organization [WMO] 2008). Rain gauges typically cover an area of 200 cm^2 (Vuerich et al. 2009). Several types of recording rain gauges are used in practice, including: tipping bucket rain gauges, weighing rain gauges, optical rain gauges and disdrometers. The majority of automatic recording rain gauge networks in Canada consist of a series of automatic weighing gauges and tipping bucket rain gauges (Environment Canada 2013c).

While rain gauges have the ability to provide accurate point measurements, they are subject to numerous sources of error and uncertainty that limit their use in operational flood forecasting models (Sinclair and Pegram 2005). These sources of uncertainty and the effect of this uncertainty on hydrological modelling capabilities are discussed in the following two sub-sections.

2.2.1 Uncertainty associated with rain gauge measurements

Wilson and Brandes (1979) identified two critical sources of error which have a considerable effect on the ability to use rain gauge measurements for hydrological modelling purposes. These include:

(1) the inability of point measurements to accurately characterize the spatial distribution of the rainfall field; and
(2) systematic and calibration errors.

The first error relates to the inability of a rain gauge to measure the spatial variability in a rainfall field. Hydrological models require a spatial distribution of rainfall over a basin in order to determine the rainfall-runoff response in the watershed. Rain gauges can provide only fractional coverage of the entire spatial domain and are thus often unable to provide an accurate representation of the variability in a rainfall field. Considering this, a network of gauges (consisting of a series of gauges distributed throughout the basin) is used to produce a spatial distribution and approximate rainfall accumulations at ungauged locations. Spatial distribution of rainfall from point rain gauge values can be determined using well-known distance averaging techniques such as inverse distance weighting, kriging, Thiessen polygons and splines (Dingman 2008). Rainfall fields, however, often exhibit a high degree of spatial variability (Tao et al. 2009), which is often uncaptured through the interpolation of point rain gauge values that generally produce a uniform rainfall field (Sinclair and Pegram 2005). According to previous research investigating the effect of gauge network design on interpolation accuracy, (see, e.g., Rodriguez-Iturbe and Mejia 1974; Xu et al. 2013) the interpolation accuracy of rainfall data sets is dependent on optimal network density and spacing. However, optimal gauge density and spacing is for the most part never achieved in a river basin (Smith et al. 2007). Economic

and practical considerations result in gauge networks that often provide poor representation of the rainfall field over a watershed (Volkmann et al. 2010). Huff (1970) demonstrated that a rain gauge network density of one gauge per 65 km^2 is required in order to achieve an average sampling error in recorded rainfall accumulations of less than 5% for six hour rainfall accumulations. The density required, however, will change depending on operational considerations. According to the US Army Corps of Engineers (1996), the optimal network design should consist of evenly distributed gauges at a spatial density determined by:

$$N = A^{0.33}, \quad (1)$$

where N = the number of gauges, and A = the area of the basin in mi^2. The WMO recommends rain gauge network densities dependent on catchment type (e.g., one gauge per 250 km^2 for a mountainous catchment or one gauge per 900 km^2 for a plains catchment) (WMO 2008). A number of different factors affect the optimal network density of rain gauges, including climatic patterns, topography (Lobligeois et al. 2014) and storm type (Huff 1970). For example, Barge et al. (1979) assessed that during a summer thunderstorm in southern Alberta, a recording rain gauge measured a rainfall depth representative of an extreme rainfall event. If the hydrological model had been based on rainfall recorded by this rain gauge alone a flood warning would have been issued. However, through subsequent qualitative observations of weather radar and a review of the subsequent stream flow data, it was evident that the rainfall was localized directly above the rain gauge. A dense rain gauge network is desirable for operational flood forecasting of such localized rainfall events; however, as mentioned above, the installation of such a network is for the most part not practical (Zhu et al. 2013). Therefore, rainfall is often mischaracterized during high intensity small spatial-scale events leading to substantial error in predicted stream flows (Golding 2009). Several methodologies have been developed to optimize the location and density of rain gauge networks (see, e.g., Pardo-Iguzquiza 1998; Jung et al. 2014).

Secondly, systematic and calibration errors affect the accuracy of gauges through losses due to evaporation, splash-out, wind effects, valley effect, tree cover, building cover or mis-calibration (WMO 2008). These errors affect the measured depth and the resulting

calculated spatial distribution of the rainfall field. According to the WMO (2008) two types of wind effects hinder the accuracy of rain gauges:

(1) the effect of the wind translating the droplets of rainfall so that they miss the rain gauge; and
(2) the effect of the gauge changing the trajectory of the wind so that the characteristics of the rainfall are different around the gauge than elsewhere in the watershed.

Larson and Peck (1974) examined the results from several studies on the effect of wind-blown rainfall on the accuracy of final depth measurements; a 12% error exists in wind loading of 5 m/s and a 19% error exists in wind loading of 10 m/s with no wind shield present. The data were extrapolated to determine that during the wind loading of an average thunderstorm (10 to 35 m/s) the error would be in the range of 20% to 40% (Larson and Peck 1974). Other environmental effects, such as trees, buildings and valleys, can adversely influence rain gauge measurements with the magnitude of the error dependent on the siting of the gauge. Ideally, gauges should not be situated in valleys or in areas with trees or buildings where measurements can be obstructed (WMO 2008). As seen in basins across Canada, due to economic considerations, gauges tend to be located improperly close to the above obstructions (Volkmann et al. 2010). As an example, operational purposes require the Upper Thames River Conservation Authority (UTRCA), located in southwestern Ontario, to install their rain gauges to correspond with locations of stream gauges. As a result, many rain gauges in the watershed tend to be located in valleys and in close proximity to trees where streams are generally present. Lastly, gauge quality control is of critical importance, as rain gauges are prone to malfunctioning (Steiner et al. 1999). Without proper maintenance and calibration gauges can suffer from errors associated with misreading, an error that is prevalent in many of Canada's automatic recording gauges.

2.2.2 Effect of rain gauge uncertainty on hydrological modelling

Highly variable rainfall fields have a demonstrated effect on runoff modelling (Schilling and Fuchs 1986). The effect of rainfall field variability was investigated by Faures et al.

(1995) who studied the effect of varying gauge density and placement on hydrological modelling results for a 4.4 ha semi-arid watershed in southeastern Arizona, USA. By varying the gauges used to generate the rainfall input for the model they found that the peak runoff and the runoff volume varied substantially with a coefficient of variation which ranged from 9% to 76% and 2% to 65%, respectively. This study indicated that in an environment dominated by high intensity rainfall events with considerable spatial variability, rain gauge density and placement can strongly influence predicted stream flows from hydrological modelling, leading to increased uncertainty in model results. The errors within gauge measurements due to systematic and calibration issues also often lead to considerable error in subsequent modelling efforts. Habib et al. (2008) examined the effect of tipping bucket uncertainty on the accuracy of hydrological models for a mid-sized watershed in southern Louisiana, USA. These authors determined that wind and dynamic calibration effects can cause variations in hydrograph peak runoff estimations on the order of 5% to 15%.

These uncertainty issues can have a detrimental effect on the ability to use rainfall estimates from rain gauges alone for input into hydrological models for accurate flood forecasting purposes. McClure and Howell (2013) outlined the failure of the Alberta Environment River Forecast Centre to provide warning to the residents of High River, Alberta, during the June 2013 flooding event. By the time a flood warning was issued the majority of the town was already inundated with flood waters. Hours before flooding occurred the forecasters updated and ran the hydrological model and found that the flood waters would peak at 650 m^3/s, a flow rate not great enough to fully flood the town. However, hours later the flood flow reached 985 m^3/s which resulted in complete flooding of High River. One of the main reasons attributed to the failure to accurately predict this event is the lack of accurate rainfall estimates and poor or missing gauge readings. The economic consequences of the inaccurate predictions in this example identify the need for re-examination of rainfall inputs used by Canadian flood forecasting centres. The need to improve rainfall estimation has been identified by numerous authors (see e.g., Wilson and Brandes 1979; Kouwen 1988; Borga et al. 2000; Beven 2002; Goudenhoofdt and Delobbe 2009; Looper and Vieux 2012; etc.), leading to the investigation of other methods to increase the accuracy of rainfall estimation.

2.3 Rainfall estimation: radar

Radar (radio detection and ranging) transmits pulses of microwave signals to detect rainfall droplets in the atmosphere. The microwave pulses travel out from the radar tower until they come into contact with particles present in the atmosphere. The reflected energy of the wave off the particles is captured by the radar tower, and the quantity of reflected energy (reflectivity in dbz) is related to raindrop size, type and distribution. In the case of rainfall the raindrop size and distribution is related to the reflectivity using the Marshall-Palmer reflectivity droplet size ratio, *Z-R* (Marshall and Palmer 1948), following:

$$Z = aR^b, \tag{2}$$

where Z is the reflectivity factor measured by the radar station (dbz), R is the rainfall intensity (mm/hr), and a and b are empirical coefficients determined during calibration.

For conventional radar, there exist several different types of radar towers in operational use today, distinguished according to emitted wavelength characteristics as either S-band, C-band or X-band (see Table 1). The typical size of precipitation particles is a determining factor in the size of wavelength used, as there exists an optimal size ratio between the precipitation particle and the radar wavelength (Berne and Krajewski 2013). The optimal size ratio ensures maximum detectability of precipitation while minimizing beam attenuation, as the attenuation by precipitation has a greater effect on smaller wavelengths (Berne and Krajewski 2013). Therefore X-band radar tends to be the most easily attenuated, with S-band radar being the least affected by attenuation of the wavelength. However, the larger S-band wavelength does not detect light rain or snow as well as the smaller wavelengths do (WMO 2008).

Table 1: Weather radar characteristics (modified from Table I.3.3, WMO 2008)

Band	Frequency (GHz)	Wavelength (cm)
S	2-4	5.77 – 19.3
C	4-8	4.84 – 7.69
X	8-12	2.75 – 5.77

The Canadian federal government agency Environment Canada (EC) operates 30 C-band and one S-band radar stations across the country, covering land comprising approximately 90% of the population (Environment Canada 2009). Each radar location has an effective range of 250 km with Doppler capability up to 120 km around the site (Environment Canada 2013d). According to Environment Canada (2009), the purpose of the Canadian Meteorological Radar Network is to provide the country with continuous weather surveillance to enable advanced warning of severe meteorological events. The Canadian C-band radar stations emit 5.6 cm wavelengths. The selection of the optimal radar tower is largely dependent on climate. Accordingly, for the Canadian climate, C-band radar was selected as it is better suited for the detection of solid precipitation (snow) than S-band radar is (Environment Canada 2009). Roughly 80% of the weather radar in use around the world uses C-band radar stations (Environment Canada 2009). Radar networks in Western Europe all rely on C-band radar for meteorological surveillance. The United States have adopted S-band radar for their radar network, which uses a 10 cm wavelength that requires more energy and a larger dish. S-band radar was selected as the southern states experience numerous high intensity rainfall events every year and the larger wavelength is not as easily attenuated during these heavy precipitation events (Xie et al. 2006).

Radar for QPE for use in hydrology began in the early 1960s. Radar was seen to have immense potential in the field of hydrology, as it facilitates the observations of both the location and movement of areas of precipitation within the range of the radar tower, capturing the immense spatial and temporal variability in rainfall fields with a high degree of resolution (Wilson and Brandes 1979). Wilson and Brandes (1979) reported one of the first summaries of weather radar to determine a quantitative measurement of rainfall for use in flood forecasting. For a small catchment in Oklahoma, USA, these authors determined that the spatial distribution of radar had a marked influence on the ability to provide real-time flash flood warning in comparison to rain gauge data. Similarly, Vehvilainen et al. (2004) found that for small catchments in the Baltic Sea region radar estimates substantially increased the accuracy of flood forecasting hydrological models during extreme rainfall events. Collier (1986) compared the accuracy of hourly rainfall estimates made using rain gauge and radar data and

determined that in order for the rain gauge network to provide a spatial distribution of the rainfall field as accurately as radar, a rain gauge network spacing of one gauge every 20 km^2 was needed. Despite these advantages, in the early stages of its application the lack of knowledge and understanding of the inaccuracies associated with radar imagery limited its widespread use for hydrological modelling (Jayakrishnan et al. 2004; Golding 2009).

2.3.1 Uncertainty associated with radar

The lack of confidence in radar QPE is due to the indirect measurement of the intensity of a rainfall event (Environment Canada 2013d), which introduces uncertainty in measured accumulation accuracy (Goudenhoofdt and Delobbe 2009). Even with substantial improvements in radar signal treatment, substantial error still exists in the conversion of raw reflectivity data into QPE (McMillan et al. 2011). Creutin et al. (2000) characterized three major sources of radar error for QPE:

(1) electronic instability and mis-calibration of the radar system and *Z*-*R* relationship;
(2) beam geometry; and
(3) fluctuation in atmospheric conditions.

All three categories of errors can have a considerable effect on the ability to use radar in hydrological modelling applications. According to Golding (2009), it is the above sources of error that limit the widespread use of radar in hydrological modelling.

The first error outlined by Creutin et al. (2000) relates to the use of the Marshall-Palmer relationship introduced in Eq. (2) above. This relationship can be calibrated at each radar location. Once calibrated, the coefficients are generally held constant (Steiner and Smith 2000). Each droplet, however, does not hold true to the same ratio. Furthermore, the ratio does not hold true for each storm event, and consequently will tend to either underestimate or overestimate the rainfall rate. Vieux and Bedient (1998) and Morin et al. (2006) investigated the effect of manipulating the Marshall-Palmer relationship on simulated hydrographs and found that small manipulations in this relationship can cause substantial changes in the simulated hydrograph.

The second and third categories identified by Creutin et al. (2000) are dependent on the radar environment. These errors include beam broadening, clutter, anomalous propagation, visibility effects, variability in time and space of the vertical profile of reflectivity (VPR), beam power attenuation and issues related to the microphysics of precipitation. These errors affect the measurement of reflectivity from the atmosphere and can result in substantial measurement uncertainty. For example, Michelson and Koistinen (2000) demonstrated how beam broadening in a study conducted in the Baltic Sea caused radar accuracy to deteriorate the further the beam traveled. Furthermore, spatio-temporal sampling errors can result from the fact that radar measures rainfall at substantial heights above the ground. Between the measurement location and the ground, the rainfall can move substantial lateral distances or even evaporate before reaching the ground. Errors in reflectivity result in errors in the subsequent rainfall estimation. A full description of radar environmental errors can be found in Environment Canada (2013d).

2.3.2 Effect of radar uncertainty on hydrological modelling

Numerous studies have attempted to assess the various errors in radar QPE to quantify the corresponding effect on the accuracy of hydrological models. These studies have indicated that uncertainties due to the errors related to calibration and processing of radar data can have a detrimental effect on confidence in hydrological modelling results. Borga (2002) studied the effect of errors in radar rainfall estimates on rainfall-runoff modelling in the Brue Catchment in England. Focusing mainly on range-related errors, VPR effects and errors due to mis-calibration of the Marshall-Palmer relationship, Borga (2002) observed that the errors considerably affected stream flow simulations resulting in errors of similar magnitude to those in gauge-only simulations. Kouwen and Garland (1989) examined the effect of radar generated rainfall on a fully-distributed hydrological model in the Grand River watershed in southern Ontario, identifying anomalous propagation, clutter and visibility effects as significant sources of error in the estimated rainfall leading to over-estimation in predicted peak flows by 10%. Krajewski et al. (2010) attempted to determine if there had been substantial improvements in radar processing technology since the study by Wilson and Brandes (1979) that would lead to improvements in the accuracy of radar QPE. Using upgraded radar correction and the same gauge network in

Oklahoma, USA, as Wilson and Brandes (1979), Krajewski et al. (2010) discovered decreased magnitudes of error in QPE compared to the errors Wilson and Brandes (1979) had found 30 years earlier, concluding that improvements in radar hardware and software have substantially improved radar rainfall estimation. However, Jayakrishnan et al. (2004) and Neary et al. (2004), still determined that radar data must undergo correction before they can be used in hydrological modelling.

Uncertainties related to radar are tied to the basin being modelled. Bell and Moore (1998) investigated the effect of using raw radar data for hydrological modelling and determined that raw radar-derived rainfall estimates increased the accuracy of the hydrological model in small catchments, while it had no considerable effect in larger basins. Vehvilainen et al. (2004) observed similar findings, concluding that in small catchments (less than 500 km^2) where response times are on the order of hours, hydrological models can benefit from the high temporal and spatial resolution of radar data. Borga et al. (2000) explored the effect of mountainous topography on radar QPE, comparing the results of stream flows simulated with raw radar against stream flows simulated with rain gauge rainfall. Due to beam blocking in mountainous regions, radar simulations provided the same accuracy in hydrological modelling as gauge only driven results (Borga et al. 2000). Therefore, the use of raw radar for rainfall estimation can potentially increase the accuracy of the rainfall input for specific conditions; however, an understanding of location-specific factors is required in order to determine whether radar will aid in hydrological modelling.

A recent Canadian example of the error associated with radar QPE was observed during an extreme rainfall event occurring on 8 July 2013, where heavy rainfall in the Greater Toronto Area caused widespread flash flooding resulting in approximately $1 billion in damage and affecting approximately 300,000 residents (Environment Canada 2014). During this event, the single polarized product from the EC radar tower at King City, Ontario (just north of Toronto) estimated that approximately 27.2 mm of rain fell on the city (Boodoo et al. 2014), while the rain gauge at Pearson International Airport in Mississauga recorded 126 mm over the same time period (Government of Canada 2014). This discrepancy is suggested to be a result of attenuation of the C-band wavelength and

dome wetting (Boodoo et al. 2014). This example further demonstrates the potential magnitude of radar errors and subsequent consequences caused by using radar QPE operationally for hydrological modelling.

2.4 Gauge-radar merging methods

Neither rain gauges nor radar has demonstrated the ability to provide an accurate depiction of the rainfall field. Rain gauges provide accurate point rainfall estimates, but their spatial resolution is limited by the low-density of a gauge network and the errors associated with interpolation schemes to fill in missing data. Radar, on the other hand, provides accurate spatial and temporal resolution of the rainfall field at significant heights above the surface of the earth, but numerous measurement errors result in inaccuracies in rainfall depths at the ground. The problems associated with each measurement technique have led to numerous attempts to merge rainfall estimates from the two instruments. This merging allows for the extraction of each instrument's strengths while minimizing individual weaknesses (Erdin 2009). According to Wilson (1970, p. 495): "the combined use of radar and rain gauges to measure rainfall is superior to the use of either separately." It has since been recognized that the combination and adjustment of radar rainfall data with rain gauge accumulations can substantially improve the accuracy of rainfall estimates and subsequent hydrological modelling results (see e.g., Kouwen 1988; Vehvilainen et al. 2004; Kalinga and Gan 2006; Kim et al. 2008; Looper and Vieux 2012; etc.). An extensive review of the literature reveals a number of merging methods that have been developed for operational use to address the limitations of each individual measurement instrument. This section summarizes the vast majority of gauge-radar merging methods in operational use today. Two merging methods not discussed in this section are co-kriging (Krajewski 1987) and surface fitting using a multi-quadric surface (Cole and Moore 2008). Co-kriging is not included as its use has decreased due to the approximation methods employed (Todini 2001) and poor suitability for real-time applications (Goudenhoofdt and Delobbe 2009). Surface fitting using a multi-quadric surface is not discussed as its use has been extremely limited. Numerous statistical modifications of the merging methods presented in this section exist (see, e.g., Moore et

al. 1989; James et al. 1993); however, the underlying assumptions of the methods are largely identical to the versions presented in this Chapter.

Gauge-radar merging methods can generally be divided into two categories (Wang et al. 2013): 1) bias reduction techniques; and 2) error variance minimization techniques. Each category follows a similar set of assumptions. In the following sub-sections, the merging methods will be discussed according to these two categories.

2.4.1 Bias reduction techniques

Gauge-radar merging methods categorized as bias reduction techniques attempt to correct the bias present in radar accumulations using rain gauge accumulations as the real rainfall value. The radar field represents a background guess which is subsequently adjusted by the known (rain gauge) information. According to Koistinen and Puhakka (1981), the assumptions for bias correction schemes include:

(1) gauge measurements are accurate for each gauge's respective location;
(2) radar accurately measures relative spatial and temporal variability of precipitation;
(3) gauge and radar measurements are valid for the same location in time and space; and
(4) the relationships based on comparisons between gauges and radar(s) are valid for other locations in time and space.

It is important to note that these assumptions, although necessary for the adjustment of radar using rain gauges, are false and often lead to erroneous correction factors. Four gauge-radar merging methods categorized as bias reduction techniques will be discussed separately below.

2.4.1.1 Mean field bias correction

The mean field bias (MFB) correction was the first merging method proposed for the correction of measurement bias in radar accumulations (Hitschfeld and Bordan 1954). This method attempts to remove the bias introduced in radar rainfall estimates through the uncertainty in the radar calibrated *Z-R* relationship (Borga et al. 2002; Hanchoowong et al. 2012). The correction is, therefore, represented by a single correction factor applied

to the entire radar field. Since rain gauges are assumed to represent the true rainfall accumulation values for bias correction techniques, the mean of the gauge accumulations is assumed to represent the true mean of the rainfall field. Thus, the radar estimates must produce the same mean rainfall accumulation at the gauge locations.

A static, long-term bias correction factor for radar accumulations based on rain gauges was first recommended by Hitschfield and Borden (1954). However, the multiplicative bias in the reflectivity-intensity relationship varies temporally, causing the effect of the static correction factor on the accuracy of the radar rainfall estimates to fluctuate substantially (Smith et al. 2007). A dynamic MFB correction was adopted by Wilson (1970) to continually update the mean correction factor on various temporal scales. The following two steps are taken in order to apply a MFB correction.

(1) The weighted correction factor is calculated using a simple arithmetic mean demonstrated with the following equation according to Wilson and Brandes (1979):

$$C = \frac{\sum_{i=1}^{N} G_i}{\sum_{i=1}^{N} R_i}, \tag{3}$$

where C is the correction factor, G_i is the measured rainfall at gauge i, and R_i is the radar measured rainfall at gauge i. The radar rainfall measured at the gauge is taken as the spatial integration of rainfall for the radar bin above the rain gauge. The correction factors are obtained at a set time step (e.g., hourly, daily, etc.).

(2) The correction factor is then applied to the entire spatial domain of the radar, as it is multiplied with the radar value at each bin location in order to develop the adjusted radar image.

MFB correction has become a widely recognized and applied technique for adjusting radar rainfall grids due to its simplicity and ease in implementation in near-real time. The MFB technique has become a standard merging method for radar images (see e.g., UK Nimrod system; US NEXRAD). Wilson (1970) examined the effect of MFB correction

on estimated rainfall accumulations for extreme rainfall events in Oklahoma, USA. For a catchment of 2590 km^2, Wilson (1970) determined that the root mean square error was reduced by 39% after the radar was adjusted using the MFB approach. Wilson and Brandes (1979) discovered large discrepancies (greater than 60% difference) between rain gauge measurements and radar measurements for severe rainfall events in Oklahoma, and determined that by applying a simple MFB correction scheme this discrepancy decreased by 24%. Borga (2002) used radar corrected with MFB for stream flow predictions in the Brue catchment, England, and found that corrected rainfall increased model efficiency (i.e., Nash-Sutcliffe efficiency) by up to 30% as compared to radar only rainfall. Many further studies have attempted to combine MFB correction with other merging methods to generate rainfall estimates at a greater degree of accuracy (see e.g., Borga et al. 2002; Jayakrishnan et al. 2004; Kalinga and Gan 2006; Krajewski et al. 2010; 2011; Looper and Vieux 2012; etc.).

2.4.1.2 Brandes spatial adjustment

Brandes spatial adjustment (BSA) is part of a broader category of local bias correction schemes. Local bias correction schemes are similar to MFB correction in that the rain gauges represent the true rainfall accumulation. However, where MFB assumes that the radar biases are evenly distributed across the entire spatial domain, BSA assumes that the biases are spatially-dependent. First proposed by Brandes (1975), BSA sought to distribute correction factors across the radar field. Brandes (1975) proposed the use of the Barnes objective analysis scheme (Barnes 1964), a scheme based on the assumption that "the two dimensional distribution of atmospheric variables can be represented by the summation of an infinite number of independent waves" (Barnes 1964, p. 397). BSA uses a distance weighting scheme with a smoothing factor to determine the influence of a known data point on the interpolated value of a specific radar bin. Proximity controls the influence: the closer the known data point is to the unknown data point, the greater the influence of the known data point. The method determines the value at unknown points as a sum of the determined weights. The technique is a combination of a surface fitting and weighted averaging interpolation methods.

Brandes (1975) suggested two iterations through the objective scheme in order to develop appropriate correction factors. The following four steps are taken to determine the correction factors at each radar bin.

(1) The correction factors are calculated at each rain gauge location based on a ratio between the radar estimations and rain gauge accumulations. Similar to the MFB method the radar measured at the gauge is taken as the spatial integration of rainfall for the radar bin above the rain gauge. The correction factors (C) for each rain gauge location are obtained at a set time step (e.g., hourly, daily, etc.) using:

$$C = \frac{G}{R}, \tag{4}$$

(2) The weights (WT) for each radar bin i from each gauge location are determined by:

$$WT_i = \exp\left(\frac{-d^2}{EP}\right), \tag{5}$$

where d is the distance between the gauge and the centroid of bin i, and EP is a smoothing factor based on the rain gauge network density.

(3) The correction factors are interpolated across the radar rainfall grid, using two passes (F_1 *and* F_2) of the multi-pass Barnes interpolation (Barnes 1964), determined by:

$$F_1 = \frac{\sum_{i=1}^{N}(WT_i)(G_i)}{\sum_{i=1}^{N} WT_i}, \tag{6}$$

and

$$F_2 = F_1 + \frac{\sum_{i=1}^{N}(WT_i)(D_i)}{\sum_{i=1}^{N} WT_i}, \tag{7}$$

where D_i is the difference between the initial correction factor and the correction factor following first pass:

$$D_i = C_i - F_{1,i}. \quad (8)$$

(4) The spatially interpolated correction factors at each bin are multiplied by the radar rainfall as:

$$R_{new,i} = (R_{old,i})(F_2), \quad (9)$$

where $R_{new,i}$ is the new corrected precipitation value at bin i, and $R_{old,i}$ is the original rainfall value measured at bin i.

BSA has been demonstrated in numerous studies to reduce estimated rainfall accumulation error. Wilson and Brandes (1979) analyzed the effect of MFB and BSA on the accuracy of radar rainfall estimates in Oklahoma, USA. These authors observed that the root mean square error in radar rainfall estimates was reduced from 43-55% without adjustment to 18-35% with a MFB adjustment and 13-27% with BSA, demonstrating that BSA provided considerable improvement in the accuracy of radar estimates and improved performance over MFB correction. Using the BSA method to correct radar derived rainfall for use in a distributed hydrological model, Kouwen (1988) observed an improvement in the radar-corrected simulated flows against using rain gauge or radar only rainfall accumulations. Looper and Vieux (2012) analyzed the effect of using radar rainfall adjusted with BSA versus rain gauge only rainfall in a fully distributed hydrological model for flood forecasting purposes in San Antonio, Texas, USA, observing that correlation between observed and predicted flows increased with the use of the BSA merging method.

2.4.1.3 Local bias correction with ordinary kriging

Local bias correction with ordinary kriging (LB) applies many of the same concepts identified for the BSA method. This method was first proposed as a technique for spatially distributing gauge-radar correction factors over the entire radar domain. The difference between the LB and BSA techniques lies in the distribution of the correction

factors. Where Brandes (1975) proposed using the Barnes objective analysis scheme (Barnes 1964) to distribute the correction factors in two dimensions for BSA, LB adopts the geostatistical method of ordinary kriging to distribute the correction factors over the radar spatial domain. Kriging is an optimal interpolation technique which applies a weighted moving average to produce the best local estimate of a regionalized variable (Babish 2000). Kriging is able to take into account a model of the covariance of the spatial data structure. In this case, the regionalized variable is the correction factor at the gauge location which describes radar bias at discrete locations across the radar field (Seo and Breidenbach 2002). Babish (2000) provided a simple explanation of kriging with the following two parts: 1) the semivariance calculated between each of the regionalized variables is used to generate the shape of the variogram (which displays the variance between regionalized variables as a function of distance); and 2) the variogram is then used to determine the weights needed to define the effect of the regionalized variables on the interpolation. A full explanation of ordinary kriging can be found in Wackernagel (2003).

The following steps summarize how the correction factors at each radar bin for the LB correction technique are determined.

(1) The correction factors (obtained at a set time step) are calculated at each rain gauge location based on a ratio between the radar estimations and rain gauge accumulations (Eq. 4). Identical to the MFB and the BSA scheme, the radar measured at the gauge is taken as the spatial integration of rainfall for the radar bin above the rain gauge.
(2) A variogram is developed to explain the spatial correlation as a function of the inter-station distances. From this variogram, kriging weights are then determined for each interpolated location. The weights are then used to develop the unknown correction factors at the interpolated bin locations.
(3) The new grid of correction factors are multiplied by the original radar values to obtain the new corrected rainfall field.

James et al. (1993) analyzed the performance of the LB merging method against BSA and rain gauge only data in a hydrological model for the Yockanookany watershed in Mississippi, USA. Their analysis examined the effect of the calibrated radar estimates on modelled hydrograph accuracy. The authors found that the LB and BSA merging methods produced superior results in terms of root mean square error as compared to rain gauge only data. While LB and BSA both produced improved results, neither method proved superior.

2.4.1.4 Range dependent bias correction

The range dependent bias correction method assumes that radar biases are a function of distance from the radar tower (Michelson and Koistinen 2000). As mentioned above, the accuracy of radar estimates deteriorates with distance from the radar tower due to overshooting of the beam, beam broadening, VPR and beam attenuation (Creutin et al. 2000). Michelson et al. (2000) proposed a method which equates the rain gauge to radar ratio as a function of distance, where the relationship is expressed in log-scale and the range is approximated by a second-order polynomial whose coefficients are determined through observation and fitted using least squares fit. The correction factor (C_{RDA}) is determined from:

$$\log[C_{RDA}] = ar^2 + br + c, \tag{10}$$

where r is the distance from the radar tower to the radar bin, and a, b and c are coefficients determined through observation and fitted using least squares fit (Michelson and Koistinen 2000).

The range adjustment scheme has been shown to be best applied in combination with other merging methods (see e.g., Michelson and Koistinen 2000; Todini 2001; Goudenhoofdt and Delobbe 2009). For instance, Michelson and Koistinen (2000) examined the effect of combining range dependent bias correction with BSA in the Baltic Sea Region, finding that correlation with an independent gauge network improved substantially as compared to unadjusted radar. Goudenhoofdt and Delobbe (2009) used the methodology of Michelson and Koistinen (2000) and came to similar conclusions,

observing a substantial decrease in the mean absolute error between adjusted radar and unadjusted radar.

2.4.2 Error variance minimization techniques

Error variance minimization techniques attempt to eliminate the bias present in radar accumulations, while minimizing the variance between the two measurements. With minimization of error variance both radar and rain gauges are assumed to be subject to systematic and random errors that cause the difference between the measurements. Following Wang et al. (2013) error variance minimization techniques are based on the assumption that the error field can be fitted with a mathematical model. Four gauge-radar merging methods categorized as error variance minimization techniques will be discussed separately below.

2.4.2.1 Bayesian data combination

The Bayesian data combination (BDC) is used not only as a method to eliminate the bias found in radar accumulations by forcing it to the rain gauge data, but also to minimize the variance between the two measurements (Todini 2001). It also assumes that a rain gauge cannot be directly compared to the integration of radar pixels of over 1 km^2. Todini (2001) proposed the technique to krige the gauge estimates to fit the same grid as the radar grid. According to Todini (2001), the difference between radar and interpolated rain gauge estimates is assumed to be an intrinsic random field, which can be characterized by an experimental variogram. As outlined by Todini (2001), the following steps are performed to apply the BDC merging method.

(1) The rain gauge estimates are block-kriged to fit the radar grid. The difference between the two measurements at each grid location is taken.
(2) The error field is fitted with an experimental variogram to develop a smoothed error field.
(3) A Kalman filter approach is applied to combine the kriged gauge estimates with the modelled error variogram in a Bayesian framework.

Todini (2001) examined the reduction in bias and variance using the BDC merging method in the Reno catchment of Italy, and observed a substantial reduction in variance from the uncorrected radar accumulations. Wang et al. (2013) tested BDC against both uncorrected radar and radar corrected with MFB for an urban catchment in London, England. These authors determined a substantial reduction in the root mean square error for both correction methods against uncorrected radar, and a further improvement in root mean square error for BDC compared to the MFB merging method.

2.4.2.2 Conditional merging (kriging with radar based error)

Conditional merging (also known as kriging with radar based error) uses kriging to extract the optimal data from each observation set (Pettazzi and Salson 2012). Established by Sinclair and Pegram (2005), the process is based on the assumption that the radar observation produces a true field of unknown values, while the rain gauges produce an unknown field of true values. The spatial structure of the observed field is based on the radar data and the rain gauge data is fitted into this field using ordinary kriging (described above), thus combining the strengths of each technique (Sinclair and Pegram 2005). The corrected field is determined by the following steps.

(1) The radar values interpolated over each of the gauge locations are found and are kriged in order to create the radar kriged field (R_k).

(2) The difference between the kriged radar field and the original radar field is taken to obtain a correction field with the following equation:

$$\varepsilon_R(s_i) = R(s_i) - R_K(s_i). \tag{11}$$

(3) The correction field is added to the kriged rain gauge surface (G_k) to obtain the corrected rainfall estimates (Corr. Precip(s_i)) at location s_i by the following expression due to Sinclair and Pegram (2005):

$$\text{Corr.Precip}(s_i) = G_K(s_i) + \varepsilon_R(s_i). \tag{12}$$

Pettazzi and Salson (2012) compared the accuracy of conditional merging with raw radar on an independent rain gauge network. Conditional merging was tested for a summer 2011 precipitation event over the City of Galicia, Italy, which resulted in extensive

flooding. These authors observed that conditional merging was able to substantially reduce mean absolute error and root mean square error in comparison to raw radar data. Kim et al. (2008) conducted a similar study, examining the effect of conditional merging on the accuracy of generated stream flows from a fully-distributed hydrological model in the Anseong-cheon basin in South Korea. Four approaches of rainfall estimation were used: 1) kriged rain gauge only; 2) radar data alone; 3) radar corrected with MFB; and 4) rainfall corrected using conditional merging. Kim et al. (2008) determined that conditional merging provided predicted stream flows that had the lowest mean absolute error, root mean square error, normalized peak error and peak timing error, in comparison to observed stream flows.

2.4.2.3 Kriging with external drift

Kriging with external drift (KED) belongs to a collection of hybrid non-stationary geostatistical methods that use auxiliary information to improve spatial prediction (Hengl et al. 2003). In this technique the rain gauge data is used as the primary regionalized variable and the radar data is used as the auxiliary information (Erdin 2009). KED is similar to ordinary kriging, except the mean is now a deterministic function of the radar field. The rainfall (*P*) at location *i,j* can then be modelled by:

$$P_{i,j} = \alpha + \beta R_{i,j} + z_{i,j}, \tag{13}$$

where α and β are the intercept and slope of the linear trend based on the radar data and $z_{i,j}$ is the random process approximated locally by the regionalized rain gauge variable. Therefore, $\alpha + \beta_{i,j} R_{i,j}$ is the deterministic part of the kriging scheme (drift parameter) modelled by the radar data. For more information on KED refer to Wackernagel (2003).

Erdin (2009) investigated the accuracy of applying KED for an extreme rainfall event over Switzerland. In comparison with LB and radar only rainfall, Erdin (2009) concluded that both KED and LB outperformed raw radar data alone, with KED exhibiting the greatest accuracy in determining rainfall accumulations. LB, however, outperformed KED at establishing the spatial structure of the rainfall event. Schuurmans et al. (2007) compared KED to ordinary kriging of rain gauge data over the Netherlands and found

that by taking into account radar as secondary information, KED produced more accurate rainfall estimates, particularly over larger areas.

2.4.2.4 Statistical objective analysis

Statistical objective analysis (SOA), first proposed for the combination of rain gauge and radar data by Pereira et al. (1998), takes advantage of the optimal interpolation equations of Gandin (1965) to generate a corrected field of rainfall estimations. The optimal interpolation equations minimize the expected final error variance. SOA is a computationally intensive merging method (Goudenhoofdt and Delobbe 2009) which computes precipitation estimates at a grid point as a weighted linear function of a background guess corrected by observations. For the case of a rainfall field generated by radar and rain gauges, Pereira et al. (1998) proposed the use of radar as the background field to be subsequently corrected using rain gauges as the observations. The final precipitation field is generated following:

$$P_a(x_i,y_i) = P_r(x_i,y_i) + \sum_{k=1}^{K} w_{ik}\left[P_g(x_k,y_k) - P_r(x_k,y_k)\right], \tag{14}$$

where $P_a(x_i,y_i)$ is the final analysed precipitation at the grid point *i*, $P_r(x_i,y_i)$ is the radar rainfall estimate at grid point *i*, w_{ik} is the posteriori weight at grid point *i* based on rain gauge location *k*, $P_g(x_k,y_k)$ is the rain gauge estimate at rain gauge *k*, $P_r(x_k,y_k)$ is the radar rainfall estimate at rain gauge location *k*, and *x* and *y* are coordinates. The SOA scheme generates weights which minimize the expected error variance of the final precipitation field using the following linear system for the generation of the system of weights:

$$\varepsilon_a^2 = 1 - \sum_{l=1}^{K} \rho_{ki} W_l \ , \tag{15}$$

where ρ_{ki} is the background cross correlation between grid point *i* and rain gauge location *k*, ε_a^2 is the normalized background error and W_l is a posteriori weight. For a full review of the derivation of the SOA equations, see Daley (1991).

Gerstner and Heinemann (2008) investigated the effect of using SOA on an hourly temporal resolution to determine the influence of SOA on the accuracy of rainfall estimations in Western Germany. These authors found that in 78% of the comparisons between SOA merged rainfall estimations and raw radar alone, there was a marked improvement in the root mean square error. This improvement resulted in a reduction of 48% in the root mean square error averaged over the 8 month study period. Kalinga and Gan (2006) studied the effect of using SOA to merge rain gauge and radar rainfall estimates on modelled stream flow accuracy from a semi-distributed model in the Blue River basin of south central Oklahoma. These authors concluded that the use of SOA as compared to raw radar alone substantially increased model efficiency (Nash-Sutcliffe efficiency), particularly during stratiform rainfall.

2.5 Selection of appropriate gauge-radar merging methods

The selection of appropriate gauge-radar merging methods is influenced by several location-specific environmental, hydrological and operational factors. These factors can influence the reliability of radar estimates and performance of gauge-radar merging methods and include:

(1) rain gauge network density;
(2) climate and storm characteristics;
(3) proximity of the radar tower;
(4) basin response time; and
(5) time-step of adjustment.

In the selection of an appropriate rainfall estimation technique it is important to understand the influence of the above factors on the uncertainty of the rainfall estimate. These factors are inter-related with each other which makes quantifying the exact numerical uncertainty on the final accuracy a difficult task. Therefore, in the selection of an appropriate estimation technique, all factors need to be considered. Furthermore, the diversity of the geographic locations in studies reported in the literature makes comparison of the merging methods difficult and presents an obstacle for establishing best practices. This section discusses these influencing factors separately, summarizes

previous attempts to compare various merging methods and identifies opportunities for future research.

2.5.1 Influencing factors

Rain gauge density can play a large role in the assessment and accuracy of gauge-radar rainfall estimates. In general, there are three main conclusions determined through a sensitivity analysis of gauge density. First, studies conducted in basins with a high density of rain gauges often conclude that rain gauge estimates alone outperform gauge-adjusted radar. This is due to the ability of the high density rain gauge network to characterize the spatial variability in the rainfall field. For example, Goudenhoofdt and Delobbe (2009) determined that rain gauges alone had greater accuracy than MFB and range dependent bias correction at densities greater than one gauge per 330 km^2 and 250 km^2, respectively. The density in the study was decreased to a minimum of one gauge per 175 km^2, where it was found that even at this density spatial adjustment and error variance minimization methods still provided better accuracy than rain gauges alone. Secondly, changes in density affect individual merging methods differently. Goudenhoofdt and Delobbe (2009) found that the effect of gauge density varied between gauge-radar merging methods, with a decrease in density having the largest effect on spatial adjustment methods and error variance methods, while having a less pronounced influence on MFB reduction and range dependent bias correction. Finally, the increase in accuracy due to increasing the gauge density is not linear. Substantial increases in accuracy occur initially as gauge density increases; however, at a certain gauge density the increase in accuracy asymptotically approaches a finite value. Biggs and Atkinson (2011) observed that while the role of rain gauge density is substantial, the greater accuracy provided due to increases in network density yields at a certain point. In a 2065 km^2 basin of the Severn River, England, these authors observed that the use of six gauges for radar correction provided similar accuracy to using 12 gauges. The accuracy decreased with less than six gauges, demonstrating the influence of gauge network density on the accuracy of gauge-radar merging methods. It is important to note, however, that the results from these studies are not transferable between basins as the effective density is influenced by basin topography, climate, gauge distribution, temporal

time-step of adjustment and merging method selected. Therefore, it is recommended that a sensitivity analysis be conducted in order to identify the effect of gauge density on rainfall estimations for any particular basin.

Numerous studies (see, e.g., Stellman et al. 2001; Kalinga and Gan 2006; Smith et al. 2007; Erdin 2009; etc.) indicate that storm type has a substantial influence on the accuracy of gauge-radar merging methods. These studies reveal that radar tends to under-estimate rainfall during large magnitude convective events and over-estimate stratiform rainfall. Smith et al. (2007) examined the effect of using radar corrected rainfall rates for flash flood forecasting in a small urban catchment in Baltimore, Maryland, USA. The rainfall rates were corrected on an event-basis using the MFB correction method. Individual event biases (gauge to radar ratio) were identified, ranging from 0.41 (over-estimation) to 2.77 (under-estimation). According to these authors, the variation in individual event biases varied as a result of storm type and magnitude, with convective storms producing higher biases at larger magnitudes than during stratiform rainfall. Smith et al. (2007) concluded that correcting based on storm type considerably increased correlation between observed and predicted flood flows. From the analysis of the variation in accuracy due to storm types, it is evident that the addition of radar rainfall estimates is beneficial for the estimation of rainfall from convective cells, and provides little to no added benefit in the estimation of stratiform rainfall from frontal events. This is due to the timing and distribution of the rainfall and its effect on the error of rain gauges alone. Convective cells are characterized by localized high intensity rainfall of short duration, which are often mis-characterized by rain gauges but picked up by radar, whereas, stratiform rainfall is characterized by widespread low intensity rainfall of relatively long duration (National Oceanic and Atmospheric Administration [NOAA] 2015), which rain gauge networks can characterize. Therefore, in basins in which high intensity localized rainfall events are a concern, the addition of radar for rainfall estimation can substantially increase the accuracy of the estimated rainfall field.

The proximity to the radar tower also influences the accuracy of the radar estimate. The accuracy of radar rainfall estimates deteriorate with distance from the radar tower. This is due to a variety of errors including beam broadening, beam overshooting, beam

attenuation and the area of integration. According to Michelson and Koistinen (2000), at distances greater than 50 km from the radar tower, the addition of range dependent bias correction increases the accuracy of the rainfall estimates. Therefore, for basins which extend beyond 50 km from the radar tower a range dependent bias correction scheme should be introduced to mitigate the error due to range related biases.

The need for radar in QPE is dependent on the basin characteristics related to the response time of the basin being modelled. The addition of radar is beneficial in basins with response times on the order of hours (Gjertsen et al. 2004). This is because these basins are greatly affected by high intensity localized events that require rainfall estimation on small spatial and temporal scales. This generally includes basins which are smaller in size with surfaces conducive to generating high volumes of excess runoff in short periods of time (i.e., urban, clays, saturated conditions, etc.). For larger basins with slower response times the addition of radar has been demonstrated to be less beneficial, as flows are shown to be less affected by short-duration high-intensity rainfall. In instances where larger time-steps (greater than 24 hours) can be used to accurately model basin response, rain gauges alone can often accurately quantify the rainfall field (Gjertsen et al. 2004). While the addition of radar has been demonstrated to be beneficial in modelling small basins, larger basins can also benefit from the addition of radar in remote areas where rain gauge density is extremely limited.

The temporal resolution of rainfall estimation plays a substantial role in the accuracy obtained in radar and rain gauge accumulations. Rainfall accumulations with a high temporal resolution are often required for flash flood modelling. According to Berne and Krajewski (2013, p. 357): “because precipitation exhibits a strong spatial and temporal variability over a large range of scales, the hydrological research and operational communities need more reliable precipitation estimates and forecasts with increasingly high resolution (i.e., a few kilometers-minutes and below) to adequately capture the dynamics of precipitation events in space and time.” The time-step required for modelling can affect the use of radar in hydrological modelling for two main reasons. First, altering the time-step of adjustment is important due to the spatio-temporal sampling errors caused by the assumption that gauge and radar measurements are valid for the same

locations in time and space (Kitchen and Blackall 1992). Rain gauges provide point measurements while radar provides a volumetric integration of the atmosphere at significant heights above the rain gauge. The direct comparison between the two data sources at different elevations causes spatio-temporal sampling errors. The magnitude of these errors is affected by the temporal scale at which the accumulation comparison is made, with the comparison naturally becoming stable for longer time-steps, as the error fluctuations are averaged out over time. By increasing the time-steps, however, the comparisons may miss out on the short-term variations due to variable meteorological conditions that may, in turn, affect the accuracy of the adjusted radar estimate. It is important to find a balance between the two error sources (Gjertsen et al. 2004). Spatially dependent bias correction methods are most affected by a change in the time-step. This is due to the fact that at shorter time-steps variations between the gauges and radar are more pronounced, leading to large variations in the correction factors at individual gauge locations. These large variations, however, tend to be averaged out in the MFB method and in error variance methods where more weighting is placed on gauge observations in situations with large error fluctuation between gauge and radar. Secondly, gauge estimates and gauge adjusted radar converge to similar levels of accuracy as the time-step required increases above 24 hours (Gjertsen et al. 2004). As the time-step increases above 24 hours, the spatial and temporal advantages offered by radar decrease in importance as the error due to spatial and temporal variations in gauge estimates are averaged out. The vast majority of the studies presented in this Chapter have identified case studies in which the gauge-radar merging schemes were conducted on daily or event based temporal resolutions. This resolution is often too coarse for operational purposes in basins with quick response times. Further research into the effect of gauge-radar merging methods on hydrological models at an hourly resolution (or less) is still required.

The inclusion of radar data presents an additional issue in terms of data management and computational requirements. In selecting an appropriate merging method it is important to consider computational requirements. Radar data sets are large and efficiency is required in data collection and storage. Manipulation of the data sets with the incorporation of rain gauges can be computationally intensive. More complicated

merging methods such as the error variance methods require greater computational effort than simple MFB and local bias correction methods.

2.5.2 Comparison of gauge-radar merging methods

No previous study has provided an in-depth comparison of all gauge-radar merging methods discussed in this Chapter. Case studies are primarily done to assess the viability of implementing one of the merging methods, comparing the corrected rainfall against rain gauge only data or radar only data. Several studies have compared various merging methods in particular geographic locations (see, e.g., Kim et al. 2008; Goudenhoofdt and Delobbe 2009; Erdin 2009; etc.). The results of these studies tend to be similar to the conclusions of Goudenhoofdt and Delobbe (2009), who compared seven major merging methods in a study conducted in the Netherlands. The mean absolute error and the root mean square error were used as measures of accuracy to compare the daily estimated corrected rainfall values against an independent rain gauge network. Goudenhoofdt and Delobbe (2009) examined: 1) MFB correction; 2) range dependent adjustment; 3) static local bias correction and range dependent adjustment; 4) BSA; 5) ordinary kriging of rain gauge data only; 6) conditional merging (kriging with radar based error correction); and 7) KED. These authors determined that all correction and merging methods outperformed raw radar alone. In terms of the greatest accuracy, KED was determined to provide the best representation of the rainfall based on spatial distribution and accumulated rainfall depths. Goudenhoofdt and Delobbe (2009) concluded that error variance minimization methods outperformed bias correction schemes due to the use of optimal interpolation to combine the two data sets. This took into account the covariance structure of the data, reducing bias and minimizing variance. The variability of results from the studies presented in the literature make drawing general conclusions on gauge-radar merging methods difficult. Furthermore, the factors that influence accuracy (described above) make the selection of an estimation technique for operational purposes challenging. With geographic and operational concerns playing a key role it is important to test each individual merging method to assess which best suits the environment and constraints of a particular location. Few studies examine the wide range of available gauge-radar merging methods for a variety of different scenarios (i.e., temporal resolutions).

Therefore, the effect of each of the influencing factors on different merging methods has not been determined. Due to the variability in rainfall fields, watershed geography, rain gauge networks and radar environment, it is challenging to establish standard practice regarding gauge-radar merging methods. The lack of studies conducted in Canada using EC radar, particularly those conducted at high temporal resolutions (e.g., on an hourly basis), makes further assessment necessary. Accomplishing this would determine whether EC radar merged with rain gauge data can be applied on an hourly basis to generate accurate spatially-distributed rainfall fields for use in hydrological models.

2.6 Opportunities and recommendations

Several radar related challenges persist that, if answered, could considerably improve the quality of radar estimates in hydrological modelling. First, the development of measures to improve radar estimates in mountainous terrain environments is required, as the interaction between this type of terrain and the atmosphere increases rainfall pattern variability (Berne and Krajewski 2013). Second, the incorporation of snow algorithms is required to enable the continual determination of snowpack. This is particularly important for northern regions such as Canada, where spring melt is the dominant source of flooding events. Third, merging methods need improvement at shorter time-steps in heavily urbanized basins where rainfall estimates are required on the order of minutes in order to quantify the predicted flow in the appropriate time frame. Currently, merging methods have been shown to improve accuracy mainly at time-steps of one hour and greater. However, at time-steps less than one hour, accuracy approaches that of raw radar alone due to spatio-temporal sampling errors involved in the direct comparison of radar and gauges. Quantifying the spatio-temporal sampling uncertainties at shorter time-steps will aid in developing greater accuracy in rainfall estimation techniques.

Recently, greater focus has been put on the incorporation of radar and rain gauge data into QPE ensemble products with satellite imagery and numerical weather models. The incorporation of radar-based rainfall estimates as input can make substantial improvements in QPE ensemble products. These products rely on empirically-based modelling of the uncertainties associated with the individual estimation techniques to develop a product in which the uncertainty is known. A recent example is the

development of the Canadian Precipitation Analysis (CaPA) system in Canada. The current operational form of CaPA was released in 2011 and uses the optimal interpolation scheme as outlined in Daley (1991) to adjust rainfall forecasts provided by the Global Environmental Multiscale (GEM) model based on ground observations from rain gauges (Mahfouf et al. 2007). The current operational configuration of the CaPA system does not use radar information as part of the data assimilation process. Initial testing of the CaPA system used radar QPE as observation; however, the inclusion of radar decreased the accuracy of the estimates due to the numerous errors present in radar QPE (Fortin et al. 2014). This led to a significant upgrade to the unified radar processor (URP) software used to convert reflectivity at Canadian radar stations to rainfall. The current experimental version of CaPA includes radar QPE. The experimental version was compared against the operational system during a test period in the summer of 2013. Using two categorical scores (frequency bias indicator and the equitable threat score), substantial increases in accuracy (in locations within 120-125 km of an EC radar tower) of the generated rainfall grid were observed with the addition of radar observations (Fortin et al. 2014). While rainfall ensemble products such as the CaPA system are able to use the available information to provide accurate rainfall estimates, the spatial and temporal resolution are often coarse. This can make implementation into hydrological models at the basin-scale and within "flashy" watersheds challenging. Further research is needed to increase the temporal and spatial resolution of rainfall ensemble products such as CaPA in order to make greater use of such products at the basin-scale.

Although in certain circumstances the use of radar is known to increase the accuracy of rainfall estimates (and corresponding confidence in hydrological modelling output), operational use of radar in hydrological modelling remains limited. This Chapter provides a comprehensive summary of the use of gauge-radar merging methods which will assist in the implementation of radar products in operational circumstances. While numerous studies have revealed that the inclusion of radar in hydrological modelling can improve the accuracy of simulated stream flows, few Canadian studies have been conducted at a basin scale to assess the viability of using gauge-radar rainfall estimates from EC's radar network. Such research is of the utmost importance in order to advance the use of radar-based ensemble products in operational applications.

Chapter 3

3 Description of study area, data and gauge-radar merging methods

The evaluation of gauge-radar merging methods is completed using the Upper Thames River basin, located in southwestern Ontario, Canada, as a case study. The following Chapter provides a description of the study area as well as the data used in the analysis of rainfall accumulations (Chapter 4) and hydrological modeling results (Chapter 5). A description of the four merging methods selected for the analysis is also included.

3.1 Description of study area

The UTRb was selected as the study area for this research (see Fig. 1). Water resources in the UTRb are managed by the Upper Thames River Conservation Authority (UTRCA) in conjunction with provincial and local governments. The UTRCA provides a large variety of services, including provision of information to the public regarding land use planning, flood impacts, drought conditions and water quality. The UTRb, comprised of an area of 3421 km^2, receives an annual average precipitation of 955 mm, of which, approximately 40% is carried downstream by the Thames River (Wilcox et al. 1998). The Thames River is comprised of three main branches, the North, Middle and South Branch. The North Branch begins north of Mitchell and flows south through St. Mary's. The Middle Branch begins southwest of Tavistock and flows through Thamesford before joining the South Branch east of Dorchester. The South Branch starts east of Tavistock and flows southwest through Woodstock. The North and South branches meet at the Forks of the Thames in the City of London. From there the river flows southwest exiting the boundary of the UTRb in Delaware. The Thames River is fed by three main tributaries: the Avon River, Trout Creek and Medway Creek. Three major flood control reservoirs regulate flows along the Thames River, protecting major urban centres from potential flooding impacts. The flows within the Thames River vary substantially both seasonally as well as annually, depending on climatic conditions (Cunderlik and Simonovic 2004). The soil of the UTRb is comprised of mainly silt and clay. These soils exhibit low infiltration and are conducive to ponding and production of excess runoff during rainfall events (Wilcox et

al. 1998). Agriculture dominates the landscape of the UTRb, with 78% of the watershed being cleared for agricultural purposes. Other major land cover includes urban and natural vegetation, which make up 8%, and 13% of the watershed, respectively.

Frontal rainfall patterns generally occur November through April in the UTRb, while high intensity convective cells dominate during the summer months (June through August). The remainder of the year is categorized by a combination of frontal and convective systems. Generally, flooding events in the UTRb result from a combination of frontal rainfall and snowmelt in the months of March and April. However, intensive summer storms (which are difficult to predict and quantify), such as the floods of September 1986, and July 2000, can produce peak flows that exceed those generated by snowmelt (Cunderlik and Simonovic 2004). Currently, the UTRCA relies on a network of rain gauges as input into a semi-distributed hydrological model as well as for quantitative observational purposes. The UTRCA also relies on radar for qualitative purposes. With the vast majority of the watershed being cleared of natural vegetation for agriculture and urban development, extreme localized rainfall events have a tendency to cause localized flooding in the basin (UTRCA 2012).

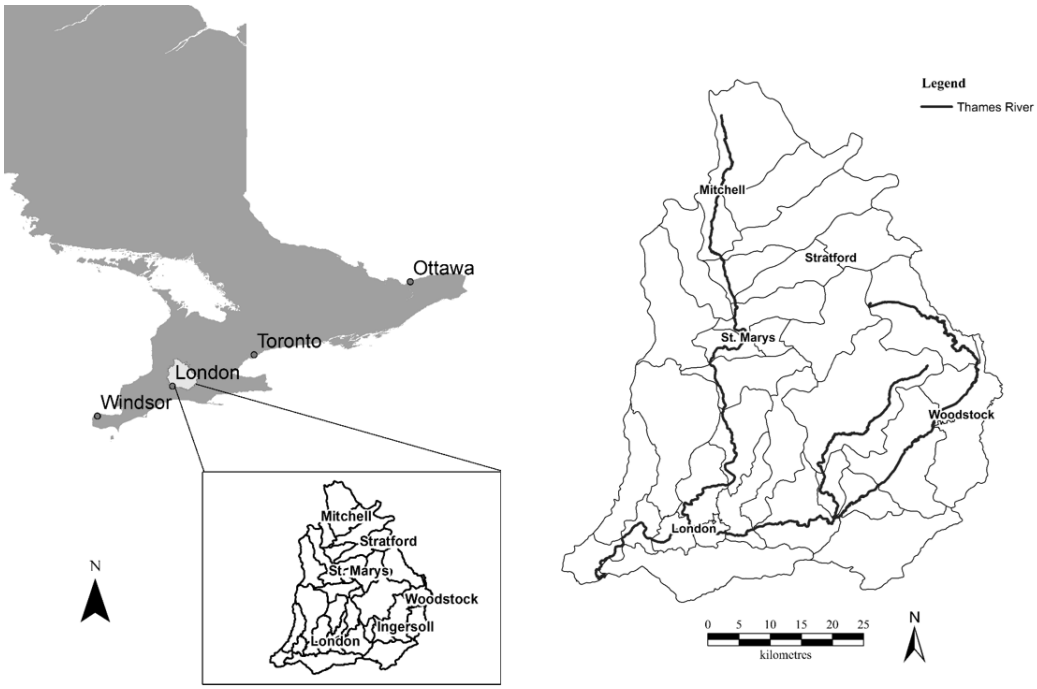

Figure 1: Upper Thames River basin in southwestern Ontario, Canada

3.2 Description of data

3.2.1 Rain gauge network

The UTRCA maintains and operates 20 tipping bucket (TB) rain gauges in the UTRb. Each tip of the bucket is based on rainfall accumulations of either 0.20 mm or 0.25 mm. The majority of the rain gauges record at an hourly resolution with a few gauges recording at resolutions of 15 minutes. The rain gauge network distribution follows no uniform pattern. Due to ease of installation and maintenance rain gauges were installed to be co-located with stream gauges. Therefore, as seen in Fig. 2, there is an increase in density of the rain gauge network around major urban centres, which are primarily located in the southern portion of the watershed (in particular around the City of London). The poor uniformity of the rain gauge network influences the errors observed during the spatial interpolation of the point data. Following Looper and Vieux (2012) the rain gauges undergo quality control before being implemented in the various merging methods, where the bias between the rain gauge and the radar accumulation at the gauge location is calculated for each rain gauge. The rain gauge is removed as an outlier if the bias is outside two standard deviations of the mean bias.

3.2.2 Radar data

Radar data are provided for the Exeter radar station (see Fig. 2) by EC through the Canadian Meteorological Centre (CMC). The radar data are not yet widely available and are provided as part of a collaborative research effort. The radar data are part of EC experiment number 28 of the experimental Canadian Precipitation Analysis (CaPA) system (version 2.4). CaPA is a rainfall estimation program that combines rainfall forecasts, rain gauges and radar to produce six hour estimates of rainfall accumulations on a 10 x 10 km grid across North America. Radar data are processed and corrected using the Unified Radar Processing (URP) software. Before being issued for the study the radar product undergoes substantial correction, including correction for: attenuation, clutter removal, beam blocking and anomalous propagation. The data are provided in a constant altitude plan position indicator (CAPPI) view set in Cartesian coordinates at an altitude of 1.5 km. The radar data have a spatial radial resolution of one km by one degree and a

temporal resolution of one hour. The Exeter radar station has a Doppler range of 120 km covering the entire extent of the UTRb. The data are processed and georeferenced before being applied using ArcGIS (version 10.2). Additional details on the radar tower are displayed in Table 2.

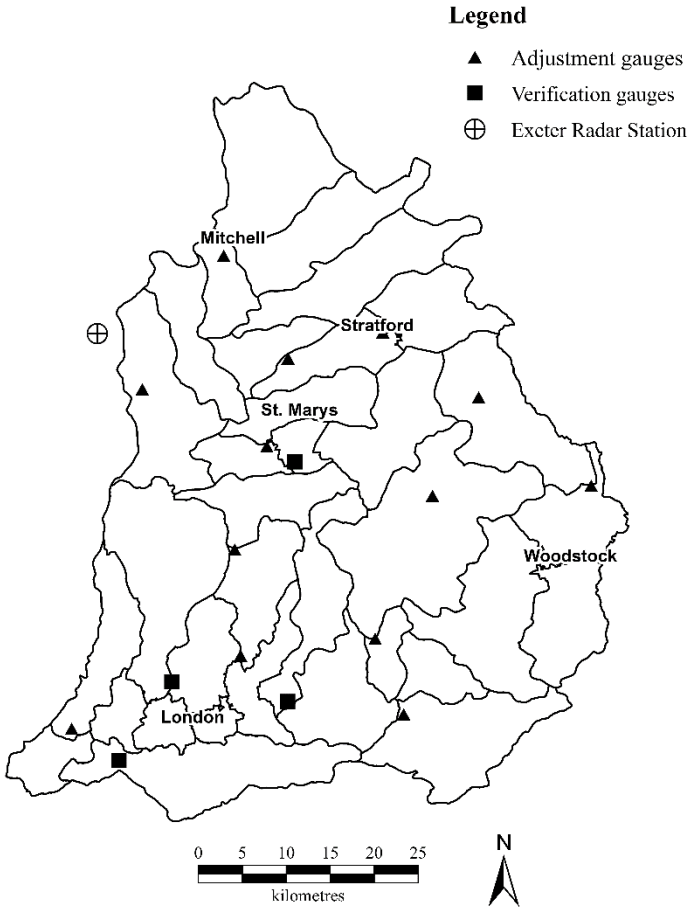

Figure 2: Location of rain gauges and radar station in the Upper Thames River basin

Not all rain gauges in the basin are able to be used in this study. A woodlot located in close proximity to the radar station generates a shadow zone as illustrated in Fig. 3, extending out from the radar station and resulting in a region of unknown radar rainfall. Two rain gauges located within the shadow zone cannot be directly compared to the radar rainfall estimates, and are therefore omitted from this study.

For the remainder of this thesis the term “raw radar” is used to describe the corrected EC radar product unadjusted by ground based rain gauges. This allows for distinction between unadjusted and adjusted radar data.

Table 2: Characteristics of Exeter radar station

Radar station	Exeter
SiteID	WSO
Location	Exeter, Southern Ontario
Latitude	43.3703
Longitude	-81.3842
Ground Height	303 masl
Measurement cycle	10 min
Frequency band	C (5.6 cm)
Doppler mode	Yes

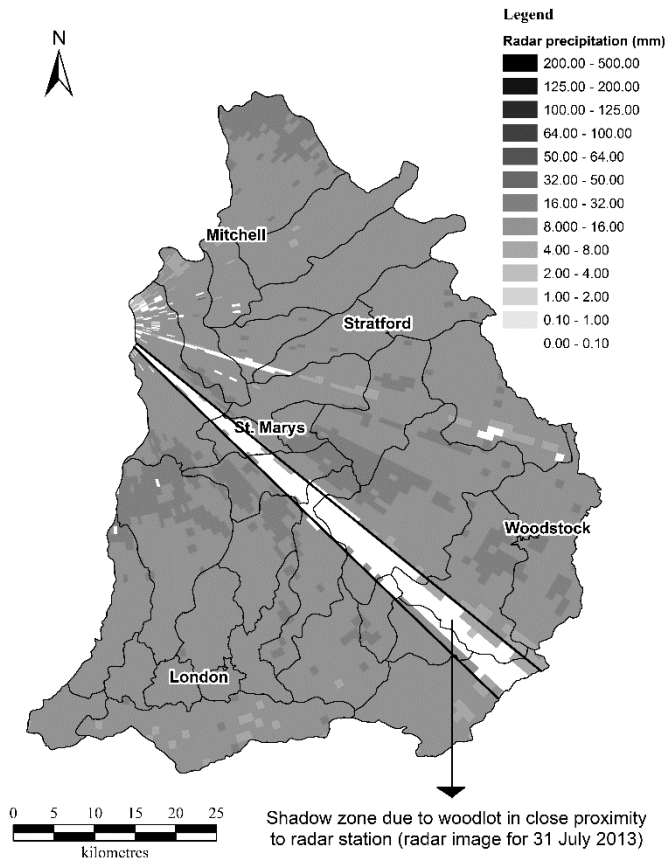

Figure 3: Radar coverage shadow zone over the Upper Thames River basin

3.2.3 Stream flow data

The UTRCA in conjunction with Environment Canada (EC) measures stream flows at 23 locations within the UTRb, as displayed in Fig. 4. The stream gauges (SG) are maintained and operated by EC through the Water Survey of Canada. These stations measure water levels along main channels within the basin, largely in close proximity to damage centres. The measured water levels are converted to flow rates (in cubic meters per second) using EC calibrated rating curves (Lane 1999). Flow rates are determined at an hourly resolution.

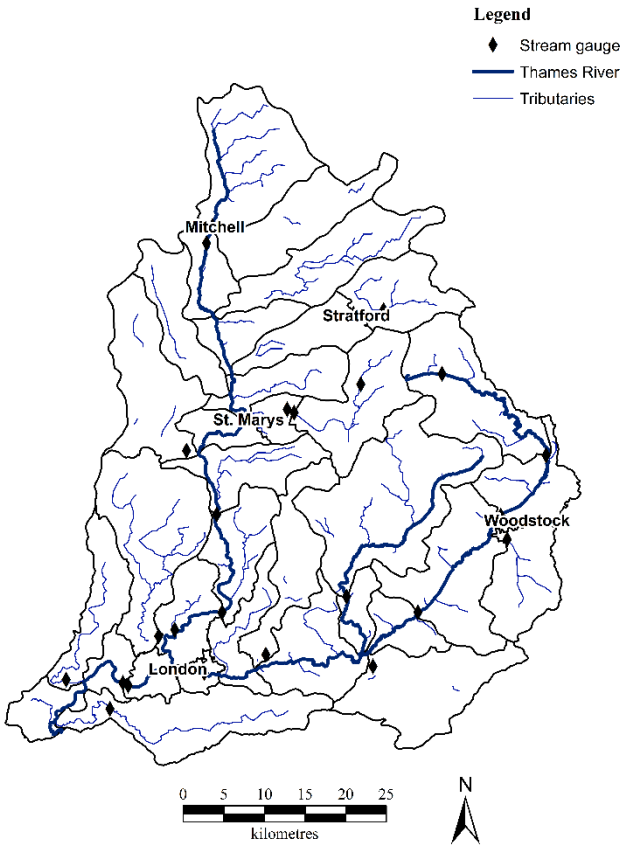

Figure 4: Stream gauge locations in the Upper Thames River basin

3.3 Gauge-radar merging methods

Four merging methods were selected for the analysis in Chapters 4 and 5. These methods applied were selected based on their prominence in literature, their widespread

operational use in other regions and their ability to be implemented in near-real time in the UTRb (Gjertsen et al. 2004; Goudenhoofdt and Delobbe 2009; Berne and Krajewski 2013). For this analysis, a mean field adjustment method (MFB), two spatially-dependent adjustment methods (BSA and LB) and a geostatistical merging method (CM) are evaluated. See Chapter 2 for the comprehensive review and description of these merging methods.

The direct comparison entails comparing the point rain gauge value with the radar pixel located directly above the rain gauge location. For the BSA and LB correction methods rain gauges recording less than 2.5 mm are not used, as minor differences between the observed accumulations can produce excessively large or small calibration factors (Brandes 1975), leading to an erroneous correction field. The LB adjustment method relies on ordinary kriging to distribute the correction factors generated at each rain gauge location. Empirical Bayesian Kriging (EBK) was also explored as an alternative to ordinary kriging, however, EBK was not found to improve the accuracy of the results. In this study a simple spherical variogram is used and the data is assumed to be isotropic. Other variograms explored included circular, exponential, and Gaussian, however, no substantial improvements were observed in accuracy. The parameters of the ordinary kriging spherical model are based on the models recently established by the UTRCA to develop rainfall fields from their rain gauge network. No transformation of the data is conducted and, therefore, the assumption of normality is not upheld.

Chapter 4

4 Evaluation of the effect of gauge-radar merging methods on rainfall accumulation accuracy

The following Chapter analyses the effect of several well-known gauge-radar merging methods on rainfall accumulation accuracy using Environment Canada's (EC) corrected C-band radar product. The analysis in this Chapter addresses four main influencing factors identified in Chapter 2, including rain gauge network density, temporal resolution of adjustment, storm type, and range-related bias, which all have a demonstrated effect on the overall accuracy of gauge-radar merging methods. To accomplish this, the following objectives will be satisfied:

(1) quantify the overall error of each rainfall estimation technique over the entire study period; and
(2) evaluate the effect of several influencing factors (i.e., rain gauge network density, time-step of adjustment, storm type and proximity to the radar station) on the accuracy of estimated rainfall accumulations.

4.1 Rainfall events

Due to the availability of the EC experimental radar product the study period was limited to the periods 1 June 2013 to 31 August 2013, and 1 April 2014 to 31 October 2014. Events are selected based on the magnitude, intensity and distribution of the rainfall field over the UTRb. Based on Krajewski et al. (2010), the duration of a storm event was defined according to the time in which the first rain gauge records a rainfall amount greater than zero, to the time in which all rain gauges again record a value of zero. In the selection of rainfall events the subsequent effect of the rainfall event on flows in the North, Middle and South branches of the Thames River is considered. In order to select the rainfall events for use in the study, the hyetograph and hydrographs (such as the examples displayed in Fig. 5) were analysed. Rainfall events in the watershed have a considerable effect on stream flows in the Thames River due to the basin characteristics described above (Wilcox et al. 1998). For instance, the 5 September 2014 rainfall event depicted in Fig. 5 resulted in an increase in flows approximately 60 times baseflow

conditions. Only storm events that caused an increase in flows in the Thames River and its tributaries were selected since the end purpose of the rainfall estimates is for flood forecasting and warning. In total, eight events and 111 hours of rainfall were analysed in this study. The selected rainfall events are presented in Table 3.

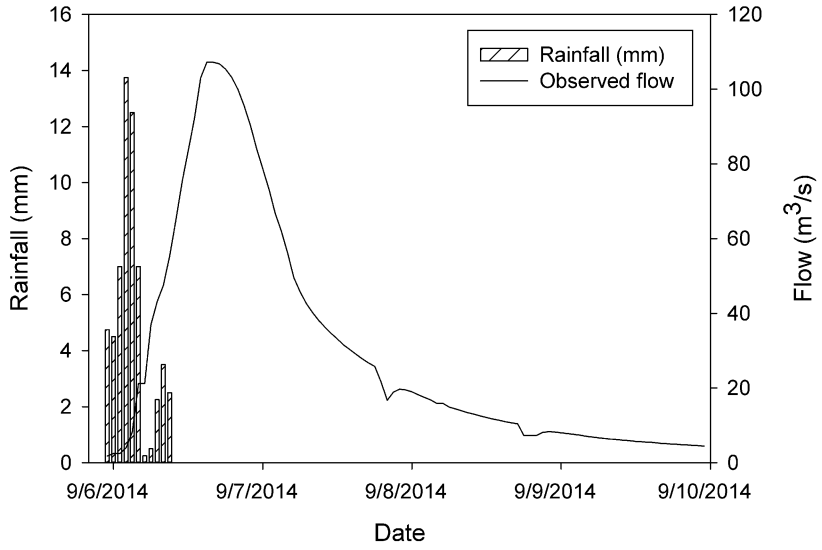

Figure 5: Hydrograph and hyetograph for the rainfall event of 5 September 2014 (Mitchell stream gauge)

Table 3: Characteristics of selected rainfall events

Date	Time (UTC)	Duration (hr)	Maximum rainfall intensity (mm/hr)
28 June 2013	07:00 – 23:00	17	12.0
31 July-August 2013	18:00 – 10:00	17	24.5
20-21 May 2014	16:00 – 07:00	16	13.5
7 July 2014	05:00 – 12:00	8	27.0
8 July 2014	16:00 – 01:00	11	15.5
27-28 July 2014	23:00 – 14:00	16	30.4
5-6 September 2014	23:00 – 10:00	12	43.25
10-11 September 2014	19:00 – 08:00	14	30.6

4.2 Verification methodology

The performance of the gauge-radar merging methods is assessed using hourly rainfall accumulations. The analysis of the rainfall accumulations is conducted using an independent verification network (IN) and verified using cross-validation (CV) in order

to compare the error from each verification methodology. Both methodologies are widely used in rainfall analysis studies (for CV see Shuurmans et al. 2006, Erdin 2009, and Garcia-Pintado et al. 2009; for IN see Seo and Breidenbach 2001, Kim et al. 2008, and Goudenhoofdt and Delobbe 2009). CV is frequently used in geostatistical contexts and situations where no independent gauge network is available to verify the rainfall data. CV involves excluding one of the rain gauge values from the adjustment process. The generated rainfall estimate for the excluded location is then compared against the observed rainfall accumulation, yielding the CV error. The IN methodology uses a series of independent gauges that are not used in the gauge-radar adjustment processes. The estimated rainfall fields from each technique are then compared to the observed rainfall accumulations at the independent gauge locations. Four gauges were selected for the IN. Based on the first assumption identified for gauge-radar merging methods, the excluded gauges in the CV and IN methodologies are assumed to measure the true rainfall accumulations at the rain gauge location.

Following Goudenhoofdt and Delobbe (2009) only rainfall pairs greater than 1 mm were used in the verification. This eliminates large error ratios that may develop due to differences in small accumulations. Furthermore, small accumulations are largely irrelevant in the present work as the study is focused on flood forecasting and warning applications. A brief description of the error statistics used in the error analysis is described below. The individual error statistics were selected to assess different aspects of the rainfall accumulation error.

4.2.1 Mean absolute error

The mean absolute error (MAE) is a common error statistic found in the vast majority of gauge-radar merging literature (see, e.g., Borga et al. 2002; Goudenhoofdt and Delobbe 2009; Looper and Vieux 2012; Zhu et al. 2013). The MAE calculates the average absolute difference between the verification rain gauge and the adjusted radar following:

$$\mathrm{MAE} = \frac{\sum_{i=1}^{N} \left| P_i - G_i \right|}{N}, \tag{16}$$

where G_i is the verification gauge rainfall at gauge i, P_i is the adjusted rainfall measured at gauge i, and N is the total number of gauges. The MAE gives the average magnitude of residuals, placing equal weight on all individual errors.

4.2.2 Root mean square error

The root mean square error (RMSE) is the most common error statistic found in the literature for rainfall verification studies (see, e.g., Seo and Breidenbach 2002; Goudenhoofdt and Delobbe 2009; Biggs and Atkinson 2011; Hanchoowong et al. 2012; etc.). The RMSE determines the square root of the squared residuals following:

$$\mathrm{RMSE} = \sqrt{\frac{\sum_{i=1}^{N}\left(P_i - G_i\right)^2}{N}}\,. \tag{17}$$

Since the residuals are squared before they are averaged the RMSE places greater weight on larger errors. This is useful in the error analysis of rainfall inputs due to the nonlinearity of rainfall to runoff transformations in hydrological models. Large errors in rainfall propagate through hydrological models causing substantial accuracy issues in subsequent modelled stream flows.

4.2.3 Correlation coefficient

The linear correlation coefficient (R) is commonly used in the comparison of rainfall measured by two independent sources (Erdin 2009; Biggs and Atkinson 2010). R is a measure of the linear relationship between two variables, which in this case is the rainfall measured by the verification gauge and the estimated rainfall. The correlation is determined following the expression:

$$\mathrm{R} = \frac{\sum_{i=1}^{n}\left(G_i - \overline{G}\right)\left(P_i - \overline{P}\right)}{\sqrt{\sum_{i=1}^{n}\left(G_i - \overline{G}\right)^2}\sqrt{\sum_{i=1}^{n}\left(P_i - \overline{P}\right)^2}}\,, \tag{18}$$

where $\overline{G}$ is the mean gauge rainfall accumulation and $\overline{P}$ is the mean rainfall accumulation as measured by each estimation technique. The R value lies between +1 and -1, with values greater than zero indicating a positive linear correlation, values equal to zero indicating no correlation, and values less than zero indicating negative linear correlation.

4.2.4 Mean relative error

The mean relative error (MRE) is a common error statistic used in the direct comparison of rainfall accumulations (see, e.g., Michelson and Koistinen 2000; Borga et al. 2002; Kim et al. 2008; Goudenhoofdt and Delobbe 2009; etc.). The MRE describes whether the rainfall accumulation estimates are generally under-estimated or over-estimated as compared to the verification rain gauge. The error statistic is based on the difference between the two measurements normalized to the total true accumulation following:

$$\mathrm{MRE} = \frac{\frac{1}{N}\sum_{i=1}^{N}\left(P_i - G_i\right)}{\frac{1}{N}\sum_{i=1}^{N} G_i}. \tag{19}$$

4.2.5 Coefficient of variation

The coefficient of variation of the root mean square error (CV (RMSE)) is used in this Chapter as a normalized error statistic to assess the difference in accuracy due to alterations in the time-step of accumulation used for correction. This error statistic is used only in the temporal sensitivity analysis in the present work. The CV (RMSE) follows the same derivation as the standard coefficient of variation, except that the standard deviation is replaced with the RMSE. The CV (RMSE) is calculated as the ratio between the RMSE and the average value of true rainfall following:

$$\mathrm{CV}\left(\mathrm{RMSE}\right) = \frac{RMSE}{\overline{G}}. \tag{20}$$

4.3 Results and discussion

Using the error statistics described above, the accuracy of each gauge-radar merging method is assessed and compared to determine whether a mean bias correction, spatially dependent bias correction or a more complicated geostatistical merging method, generates (on average) the best estimate of the rainfall field for an hourly time-step of accumulation using EC radar. The gauge-radar merging methods are also compared against the error calculated using raw radar data alone and rain gauge data alone. The spatial distribution of the rain gauge data alone is generated using ordinary kriging (RGO (OK)). It is important to assess whether the addition of radar provides any further benefit, as rain gauges alone are still used in the vast majority of hydrological modelling applications (Erdin 2009). The comparison of the gauge-radar merging methods against raw radar alone provides an indication of the ability of rain gauges to reduce biases that are observed in radar rainfall fields. The analysis is conducted using the IN methodology and then trends in the observed error are verified using CV. This verification was conducted in order to assess whether biases in the observed error due to the location of the independent gauges in relation to correction gauges alter the trends observed in the overall error. All observed rainfall hours were grouped together for the analysis in order to provide equal weighting to all hours, and to determine (on average) the errors in the rainfall accumulations for each merging method.

The rain gauge network density is altered in this study to quantify the effect of gauge density on the accuracy of select merging methods using EC radar. The analysis will assess: 1) whether a decrease in gauge density affects a particular merging method more than others; and 2) whether the accuracy of the gauge-radar merging methods decrease to the level of accuracy of raw radar alone at lower gauge densities. Addressing these two points will assist in applying the results generated from this study to areas with different gauge densities. The analysis also assesses the effect of the temporal time-step of adjustment on the accumulation error for EC radar, as well as the effect of radar range and storm type errors.

4.3.1 Analysis of merging methods for hourly rainfall accumulations

Fig. 6 presents the error statistics for the hourly rainfall accumulations estimated by each merging method for the 111 hours of analysis (i.e., all events). As shown in Fig. 6a, each merging method reduced the RMSE as compared to the raw radar data alone. The MFB approach provided the greatest reduction in RMSE, reducing the error by approximately 27%. The BSA, LB and CM methods provided reductions in the RMSE of 20%, 16% and 19%, respectively. The MAE of each merging method is presented in Fig. 6b. Again, each method reduced the error compared to raw radar alone. The MFB method provided the greatest reduction in MAE, reducing the error by approximately 20%, while the BSA, LB and CM methods reduced the MAE by 16%, 14% and 14%, respectively. Variations exist between the RMSE values and the MAE values, indicating considerable variability in the individual hourly errors. This suggests that at the hourly time-step large fluctuations in the error exist between the individual hours of rainfall data. This is primarily attributed to the spatio-temporal sampling errors brought on through the direct comparison of radar and rain gauges. Fig. 7 displays the MRE of each of the merging methods. From this figure, it is evident that each estimation technique under-estimated the total rainfall as compared to the verification gauge network.

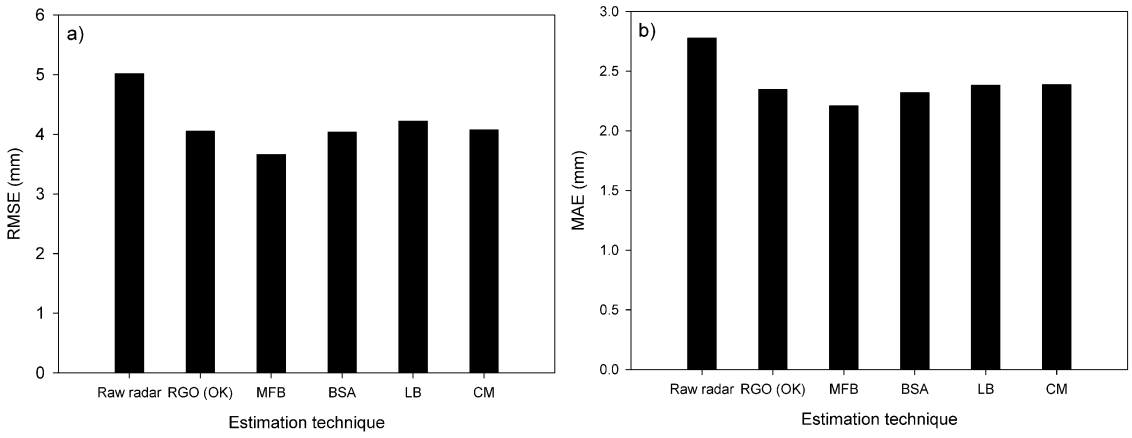

Figure 6: Error of all estimation techniques for hourly rainfall accumulations based on all events analysed: a) RMSE; and b) MAE

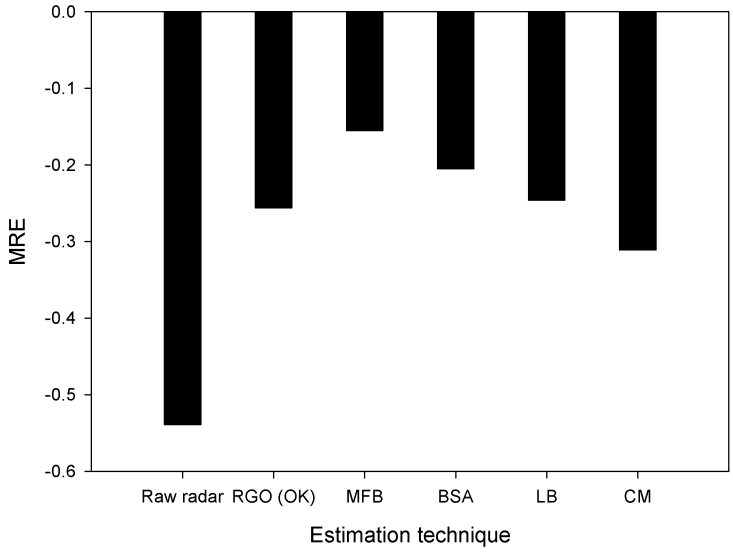

Figure 7: MRE of all estimation techniques for hourly rainfall accumulations based on all events analysed

Rain gauge only estimations were found to display error statistics similar to those of merged estimates, with a 19% reduction in the RMSE compared to raw radar alone. At the hourly time-step only the MFB adjustment method produced rainfall estimates with greater accuracy than the RGO (OK), reducing the RMSE by approximately 10% as compared to RGO (OK). The BSA and CM methods provided rainfall estimates with similar magnitudes of accuracy, with a 0% difference in error as compared to the RGO (OK). The LB method generated an increase in error as compared to RGO (OK), increasing the RMSE by approximately 4%. The comparable accuracy of the RGO (OK) is attributed to two factors: 1) the proximity of the verification gauge to the correction gauge network (distances from verification gauges to correction gauges range from 4 km to 9 km); and 2) the rain gauge network density. The close proximity of the verification gauge network to the correction network limits the effect of rainfall field variability on the end accuracy of the RGO (OK) results.

The comparison in rainfall accumulations between the verification gauges and each estimation technique is shown in Fig. 8. The MFB method provided the largest correlation between the observed and estimated rainfall, with an R value of 0.770, while

the raw radar displayed the lowest correlation, with an R value of 0.707. In general, the raw radar, RGO (OK) and CM methods displayed an under-estimation of the estimated rainfall accumulations, with the magnitude of the error increasing with increase in measured rainfall accumulations. The BSA and LB methods displayed the largest scatter, while the MFB method displayed the smallest scatter in the comparison of measured and estimated rainfall accumulations. An example of the qualitative differences between the rainfall estimation techniques can be found in Appendix A.

Overall, as seen in Table 4 the simple MFB correction method provided the greatest reduction in error compared to the raw radar data and RGO (OK). The success of the MFB method over the spatially dependent correction methods and the more complicated geostatistical merging method is attributed to the temporal resolution of adjustment. As outlined in Gjertsen et al. (2004), at higher temporal resolutions the MFB approach smoothens the fluctuations that can be identified in individual gauges due to spatio-temporal sampling errors, whereas the spatially-dependent correction methods and the geostatistical merging methods are prone to larger errors at smaller time-steps due to the presence of these fluctuations. Of the two spatially-dependent correction methods the BSA method provided slightly greater reductions in error as compared to the LB adjustment method. The geostatistical merging method provided reductions in error similar to those of the spatially-dependent bias correction methods. These results suggest that a simple mean field bias adjustment method outperforms more complicated spatial adjustment methods at the hourly time-step in the UTRb, indicating that increased complexity in gauge-radar merging methods is not warranted under these conditions. In general, the reduction in error observed through the adjustment of radar in this study is similar in magnitude to the error reduction observed by other authors using similar methodology but different radar products in different geographical locations (see, e.g., Borga et al. 2002; Kalinga and Gan 2006; Kim et al. 2008; Goudenhoofdt and Delobbe 2009).

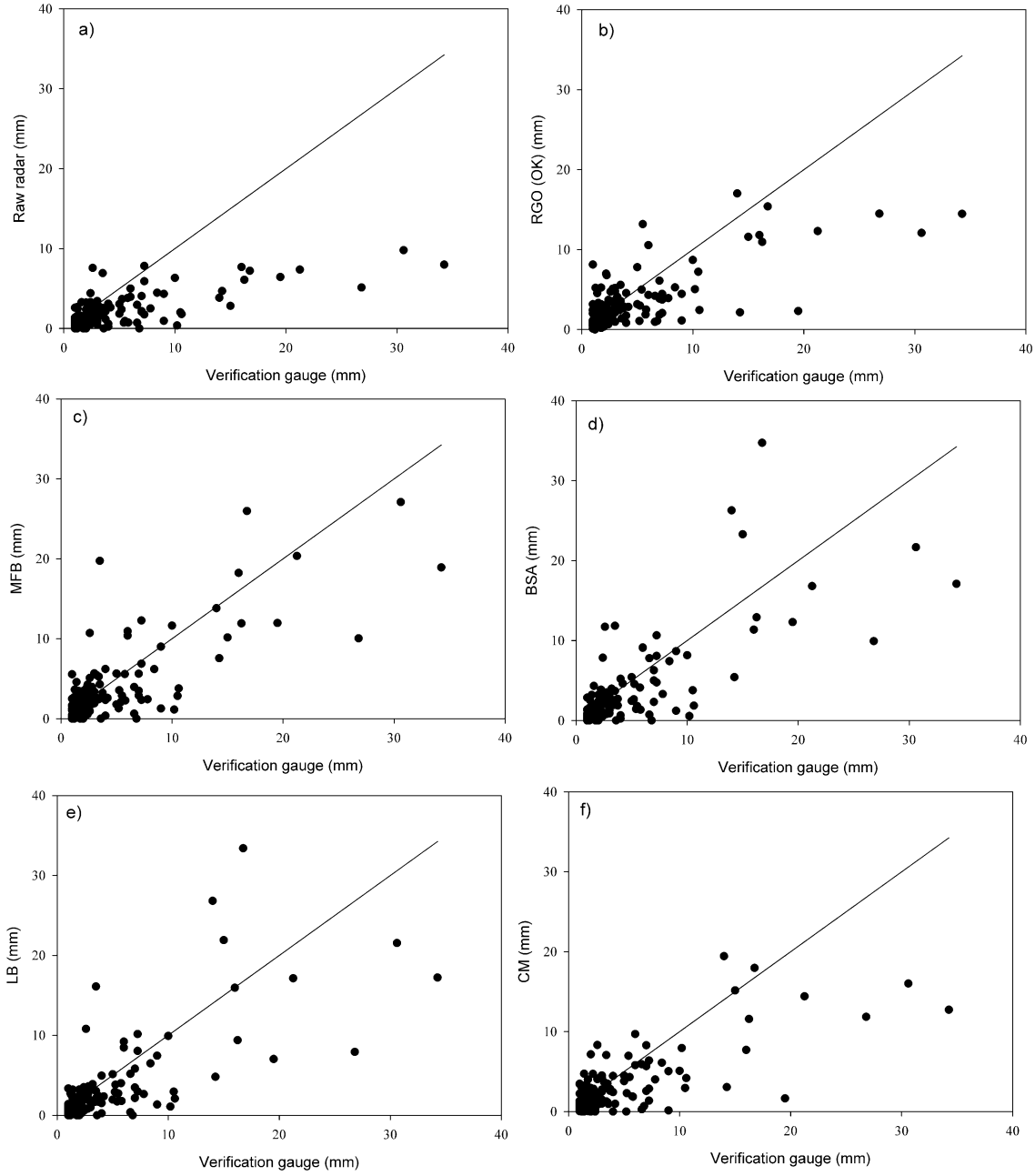

Figure 8: A comparison of hourly rainfall accumulations from the verification gauges and: a) raw radar; b) RGO (OK); c) MFB; d) BSA; e) LB; and f) CM

Table 4: Error statistics of all estimation techniques for hourly rainfall accumulations based on all events analysed

Estimation technique	RMSE	MAE	MRE	R
Raw radar	5.019	2.779	-0.539	0.707
RGO (OK)	4.050	2.347	-0.256	0.726
MFB	3.663	2.211	-0.155	0.770
BSA	4.039	2.321	-0.205	0.738
LB	4.221	2.383	-0.246	0.715
CM	4.071	2.388	-0.311	0.732

4.3.2 Error trend analysis

The RMSE and the MAE were compared for the two verification methodologies (IN and CV methods) as seen in Table 5. Both methodologies presented similar trends in error in which the MFB method provided the greatest reduction in error as compared to raw radar and RGO (OK), and the BSA, LB and CM merging methods provided similar magnitudes of error as compared to RGO (OK). The magnitudes of error vary (between 1% and 16%) from the IN to the CV methods, with the CV method resulting in higher magnitudes in both the RMSE and MAE. The increased levels of error in the CV technique is attributed to the removal of gauges, as CV calculates the error by omitting a gauge from the correction network. Since the gauge network is not evenly distributed throughout the watershed, the removal of certain gauges within the network may increase the overall observed error. Overall, the trends observed in the error between the two methodologies are similar.

Table 5: Error statistics for CV and IN for each estimation technique for hourly rainfall accumulations based on all events analysed

Estimation technique	RMSE (mm)			MAE (mm)		
	CV	IN	Percent diff.	CV	IN	Percent diff.
Raw radar	4.776	5.019	4.8	2.730	2.779	1.8
RGO (OK)	4.486	4.050	10.2	2.518	2.347	7.0
MFB	4.322	3.663	16.6	2.426	2.211	9.3
BSA	4.446	4.039	9.6	2.485	2.321	6.8
LB	4.467	4.221	5.7	2.554	2.383	6.9
CM	4.448	4.071	8.9	2.529	2.388	5.7

4.3.3 Gauge sensitivity analysis

The accuracy of the gauge-radar merging methods depends on the density of the rain gauge network used in the adjustment. The only method selected in this study that directly takes into account rain gauge network density in the formulation of the final estimate is the BSA, which takes into account the rain gauge network density in the smoothing factor, *EP*. As determined above, the error for the CV and IN follow similar trends. Since both methodologies produced similar trends in error, the IN verification methodology was carried through for the gauge sensitivity analysis.

Ideally, rain gauges would have been situated in a manner that provided a uniform spatial coverage of the river basin. However, as shown in Fig. 2 the spacing of the rain gauges within the UTRb is not uniform. Therefore, the effect of the removal of a particular gauge on the spatial coverage within the basin depends on the location of the removed gauge. Clearly, the removal of certain gauges would have a greater effect on the spatial coverage of the network. Considering this, gauges were removed in a manner in which the spatial coverage of the remaining gauge network would be least affected. To accomplish this, a script written in MATLAB and verified using ArcGIS (version 10.2) was used to remove the gauges in a manner that sought to maintain the mean centre of the rain gauge network. In this method the mean centre of the rain gauge network is first determined. Each rain gauge is then removed separately and the new mean centre of the remaining rain gauge network is calculated for each case. The removed gauge that results in the smallest change in the mean centre is selected for removal. The rain gauges used at each gauge density are identified in Table 6 and the rain gauge locations for the highest gauge density (one gauge per 244 km^2) and the lowest gauge density (one gauge per 684 km^2) are displayed in Figs. 9a and 9b, respectively.

Table 6: Gauges used for each gauge density

# of gauges used	Gauge density (gauge per km^2)	Gauges													
		Tavistock	Highland Garage	Woodham/Kirkton	Pittock Dam	Fanshawe Dam	Orr Dam	Mitchell	St. Mary's	Reynolds	Oxbow Creek	Plover Mills	Innerkip	Thamesford	Avon
14	244	✓	✓	✓	✓	✓	✓	✓	✓	✓	✓	✓	✓	✓	✓
13	263	✓	✓		✓	✓	✓	✓	✓	✓	✓	✓	✓	✓	✓
12	285	✓			✓	✓	✓	✓	✓	✓	✓	✓	✓	✓	✓
11	311	✓			✓	✓	✓	✓		✓	✓	✓	✓	✓	✓
10	342	✓			✓	✓	✓	✓		✓	✓		✓	✓	✓
8	427	✓			✓	✓	✓	✓		✓	✓		✓		
5	684						✓	✓		✓	✓		✓		

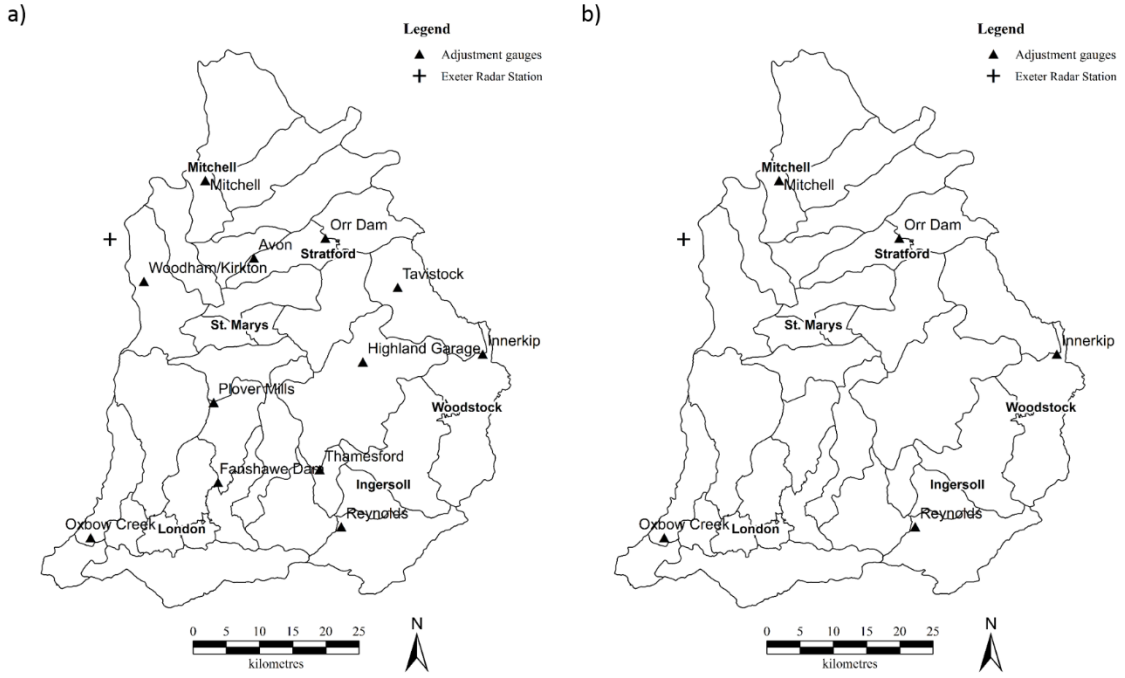

Figure 9: Gauges used for: a) highest gauge network density; and b) lowest gauge network density

Fig. 10 displays the RMSE of the selected estimation techniques for each rain gauge network density. As expected, the error increased as the rain gauge network density decreased. Reductions in the RMSE as compared to raw radar alone decreased from 19%,

27%, 20%, 16% and 19% to 10%, 13%, 4%, 3% and 16% for RGO (OK), MFB, BSA, LB and CM methods, respectively, while decreasing the gauge density from one gauge per 244 km^2 to one gauge per 684 km^2. These results indicate that gauge density has an effect on the accuracy of the individual estimation techniques. All merging methods displayed a lower RMSE compared to raw radar alone at all gauge densities analysed, indicating that merging schemes are still beneficial and provide a reduction in error even at lower rain gauge network densities. As the rain gauge network density decreased, a gradual increase in error was observed for the MFB, BSA and LB methods, with an overall increase in error of 19%, 17% and 16%, respectively. The similar magnitude of increase in error and trend in which the error increases for the MFB, BSA and LB methods suggest that a decrease in gauge density has a similar effect on all three merging methods. The CM and RGO (OK) methods, however, follow a different trend with no noticeable increase in error until a gauge density below one gauge per 427 km^2 is reached. Subsequently, a decrease in gauge density from one gauge per 427 km^2 to one gauge per 684 km^2 produced an increase in the RMSE of 16% and 9% for RGO (OK) and CM methods, respectively. Overall, the CM method was least affected by a change in gauge density. At the highest gauge density the MFB method generated rainfall estimates with the highest degree of accuracy, while at the lowest gauge density the CM method provided the best estimate of rainfall followed by the MFB method.

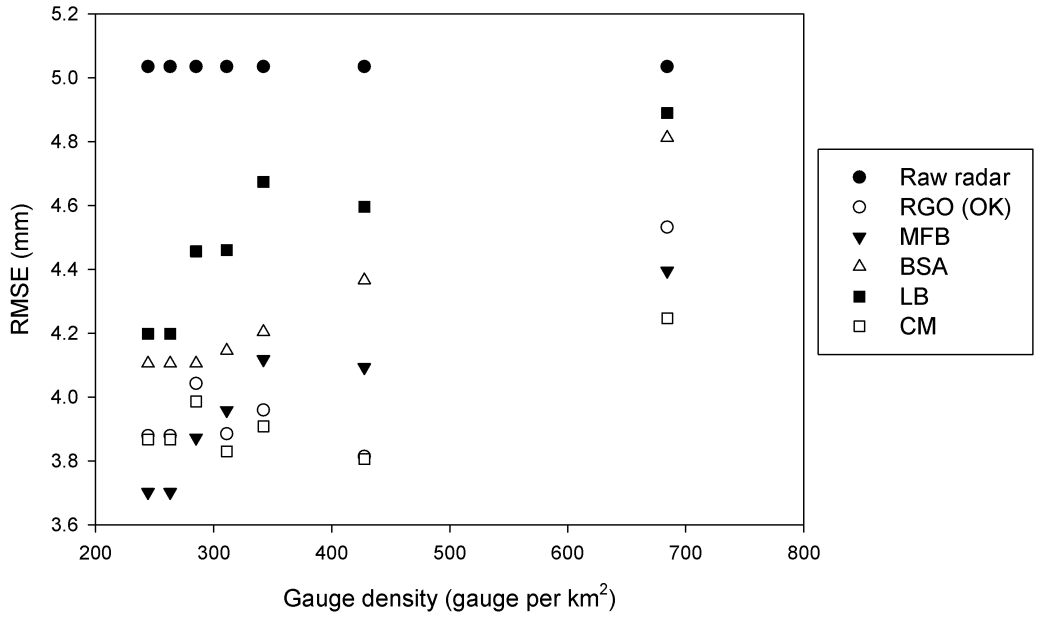

Figure 10: RMSE for each gauge density examined for all estimation techniques for all events analysed

4.3.4 Temporal sensitivity

In order to analyse the effect of the time-step of adjustment on the accuracy of each estimation technique, the methods are applied based on temporal resolutions of accumulation of 1, 3, 6, 12 and 24 hours. These time-steps were selected so as to assess the effect of changing the time-step over a range of values from an hourly time-step to a time-step of 24 hours. The accumulation periods all begin at 00:00 UTC. Accuracy was assessed based on the non-dimensional CV (RMSE).

Fig. 11 displays the CV (RMSE) for each estimation technique based on each accumulation time-step. As expected, there is a decrease in observed error as the temporal time-step of adjustment increases. As the time-step increases the gauge-radar adjustment factors become more stable and large variations that are evident at the hourly time-step are smoothed out, thus decreasing the overall error. The smoothing of individual correction factors has the largest effect on the spatially dependent correction methods, with the BSA and LB methods exhibiting the largest decrease in error from adjustments based on hourly accumulations to 24 hr accumulations. As indicated at the hourly time-

step, the MFB method displayed the lowest error. However, at the 24 hr time-step the BSA method displayed the lowest error. This further affirms the conclusions stated above, where, at smaller time-steps the MFB method outperforms spatially dependent correction methods due to the smoothing of individual rain gauge errors. However, at larger time-steps (greater than 12 hr) the spatio-temporal sampling errors are averaged out, thus reducing the effect of error fluctuations on individual rain gauges. This leads to spatially-dependent correction methods providing the greatest reduction in error in comparison to raw radar alone at larger time-steps of adjustment. At time-steps greater than 12 hrs the decrease in error is relatively minimal.

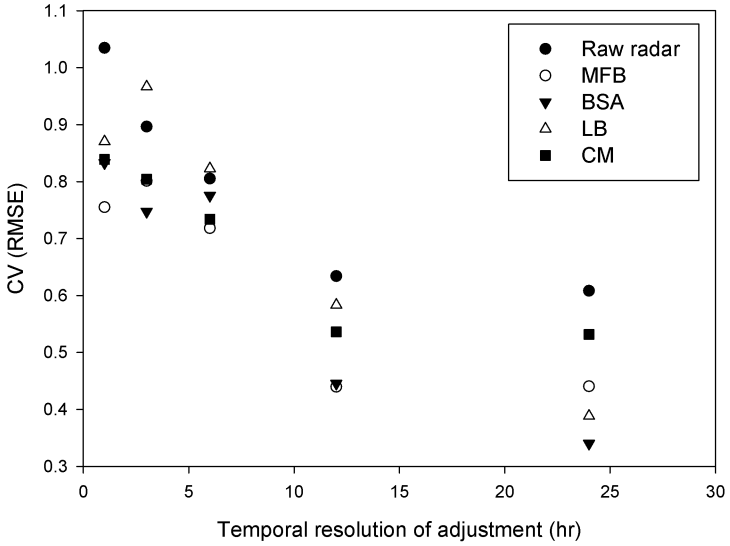

Figure 11: RMSE for each time-step examined for all merging methods for all events analysed

4.3.5 Storm variation

In the above analysis the error was determined by grouping all rainfall hours together in order to obtain the average error of each technique over the entire study period (placing equal weight to each hour). Fig. 12 presents the variation in error between the eight different storm events considered in this study. As shown in Fig. 12, there does exist a variation in error between each estimation technique during the different storm events. In particular the 5 September 2014 event displayed a considerable increase in the RMSE for

all estimation techniques as compared to the other events. Storm type and magnitude can have a substantial effect on the accuracy of the radar rainfall estimates and subsequently on each of the gauge-radar merging methods (Smith et al. 2007). The storm-to-storm variations in accuracy is attributed to the possible difference in storm type (i.e., convective or frontal) and magnitude. Due to the limited study duration, detailed analysis of different storm types and their effect on overall gauge-radar merging accuracy was not possible. Refer to Appendix B for the error values based on each estimation technique for the individual storm events.

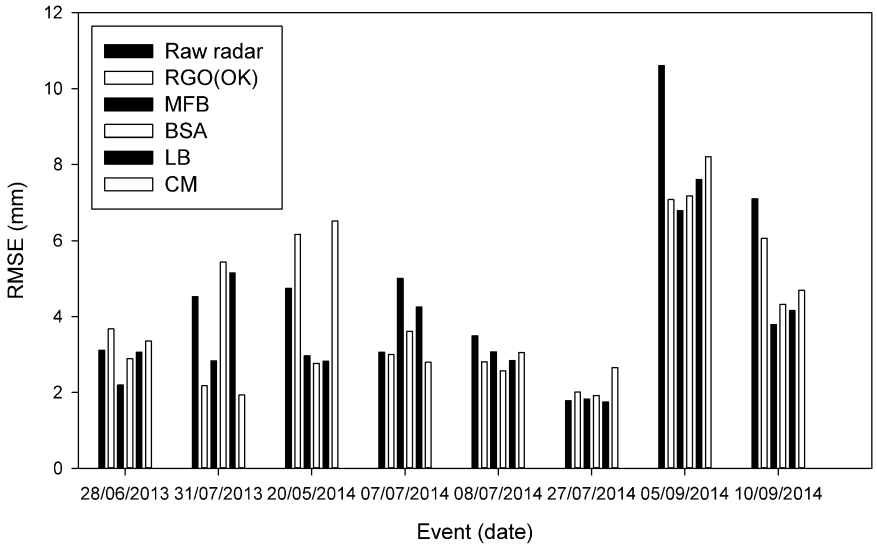

Figure 12: Variation in RMSE between storm events

4.3.6 Range related biases

In order to determine if radar range related biases affected rainfall estimates in the present study, rain gauges were grouped according to distance from the radar tower following the methodology of Goudenhoofdt and Delobbe (2009). Groupings were based on 10 km rings extending outward from the radar tower. The range from the radar tower of the Exeter radar station varies from approximately 10 km to 70 km. As shown in Fig. 13, analysis of the radar error based on these groupings deemed that range related biases do not play a role in the UTRb. This is attributed to the relative close proximity of all points in the UTRb to the Exeter radar station. These results support the assumptions outlined in

Kneble et al. (2005) in which for distances under 80 km from the radar tower range related biases are assumed to be negligible.

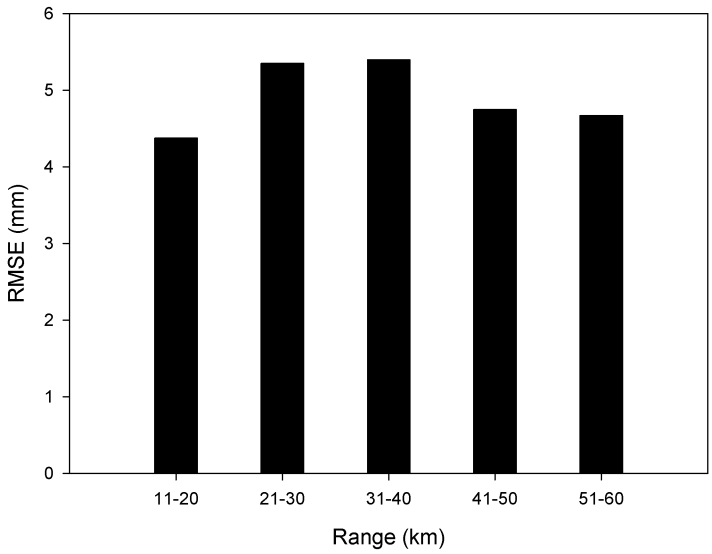

Figure 13: RMSE for gauges within grouped distances from radar station

Chapter 5

5 Application of gauge-radar merging methods in a semi-distributed hydrological model

Although hydrological models have the potential to play a vital role in flood damage mitigation, a lack of confidence in model output often leads to under-utilization of this tool (Takeuchi 2001; McMillan et al. 2011). According to Xiaoli et al. (2010) and McMillan et al. (2011), hydrological model uncertainty is dominated by three main factors:

(1) improper model structure;
(2) parameter uncertainty; and
(3) precipitation uncertainty.

Each factor can substantially affect the hydrological model output leading to increased model uncertainty. Due to the uncertainty involved it is important to understand that the unique output of a hydrological model cannot be fully relied upon (Xiaoli et al. 2010). As discussed in Chapter 2, precipitation inputs play a key role in the accuracy of hydrological models. The uncertainty associated with parameter sets is also inter-related with the uncertainty associated with precipitation, as the calibration of parameter values is based on the assumption of accurate precipitation input (Xu et al. 2006). Therefore, with widespread use of hydrological models there exists a significant demand for precipitation estimates with a high degree of confidence (see, e.g., Wilson and Brandes 1979; Beven and Hornberger 1982; Cole and Moore 2008; Berne and Krajewski 2013).

The following Chapter investigates the effect of gauge-radar merging methods on the accuracy of modelled flows using a semi-distributed hydrological model. Several factors, identified in Chapter 2, have a demonstrated effect on the final accuracy of the incorporation of gauge-radar merging methods as input into a hydrological model. These include: storm type, basin characteristics and rain gauge network density. This Chapter will further assess the effect of these factors on the accuracy of selected gauge-radar merging methods. To accomplish this, the following objectives will be satisfied:

(1) calibrate the hydrological model for incorporation of gauge-radar merged rainfall as input;
(2) evaluate the error of each rainfall estimation technique for three distinct rainfall events in 2014;
(3) quantify the overall error of each rainfall estimation technique over the entire study period; and
(4) evaluate the effect of several influencing factors (i.e., storm type, basin characteristics, and rain gauge network density) on the accuracy of hydrological modelling output based on the selected rainfall estimation techniques.

5.1 Hydrological model

The hydrological model selected for the present research in the UTRb is based on a model selection study conducted by Cunderlik (2003). The model selection methodology outlined in Cunderlik (2003) was based on the following criteria:

(1) data requirements;
(2) temporal scale;
(3) spatial scale;
(4) processes modelled; and
(5) documentation and technical support.

Based on the above criteria, Cunderlik (2003) determined that the Hydrologic Modeling System (HEC-HMS), produced by the U.S. Army Corps of Engineers (USACE) Hydrologic Engineering Center, is best suited for the prediction of flows in the UTRb. Considering this, HEC-HMS, version 4.0, is adopted for use in the present research.

The HEC-HMS model used in the present research was initially developed by Cunderlik and Simonovic (2004) and the Upper Thames River Conservation Authority (UTRCA). For the present purposes, the HEC-HMS model is set-up in a semi-distributed fashion to model flows on an event basis. The selection of a semi-distributed model was based on the results of previous research examining the effect of model spatial resolution on hydrograph accuracy. These studies (see, e.g., Cole and Moore 2008; Berne and

Krajewski 2013; Zhu et al. 2013) found little difference in accuracy between semi-distributed models using basin averaged rainfall and data intensive fully distributed models. An event based model is selected since the objectives of the present research are to model stream flows from single rainfall events for flood forecasting and warning purposes. Based on the selection of a semi-distributed model, the UTRb was subdivided into 33 subbasins through the use of HEC-GeoHMS software following Cunderlik and Simonovic (2004). The delineated subbasins in the UTRb are shown in Fig. 14.

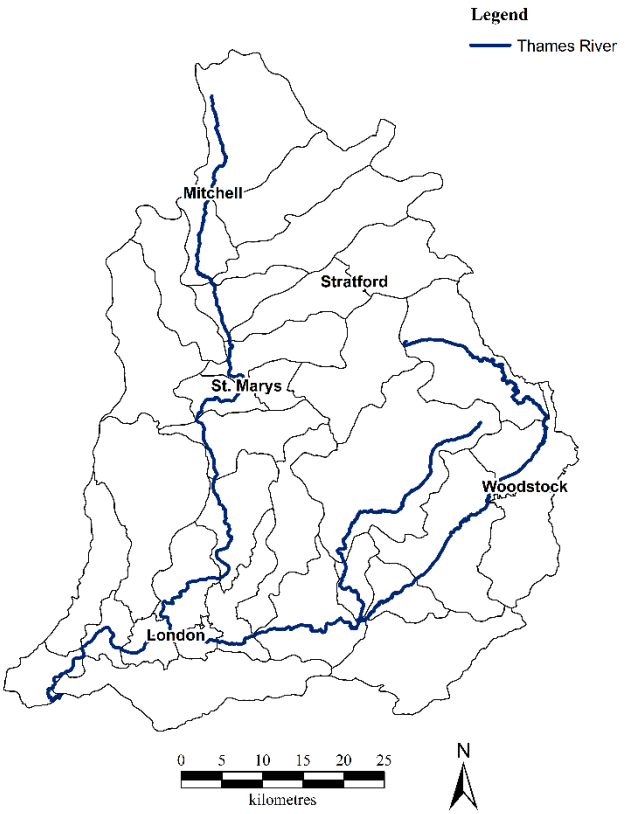

Figure 14: Delineation of the 33 subbasins in the Upper Thames River basin for use in the semi-distributed HEC-HMS model

5.1.1 Selected model components

HEC-HMS is divided into six separate model components. The six model components consist of: meteorological model, runoff volume model, direct runoff model, routing

model, baseflow model and reservoir model (USACE 2013). The selected model components used within HEC-HMS in this analysis were based on the constraints and objectives of the present research and the model component selection identified in Cunderlik and Simonovic (2004).

The meteorological model selected for this analysis is based on the rainfall data considered in this study and the semi-distributed nature of the model. Six different rainfall data sets are used as rainfall input, including: raw radar, rain gauge only distributed using ordinary kriging (RGO (OK)), mean field bias correction (MFB), Brandes spatial adjustment (BSA), local bias correction using ordinary kriging (LB), and conditional merging (CM). Full descriptions of these rainfall estimation techniques are found in Chapter 2. Site-specific operational implementation of these rainfall estimation techniques is discussed in Section 3.3. Each rainfall estimation technique is estimated in a gridded framework. In order to organize the distributed rainfall data in a format that is easily implemented in the semi-distributed hydrological model, the user gauge weighting methodology was employed (USACE 2013). The basin averaged rainfall is inputted into HEC-HMS as the single user defined gauge for each of the 33 subbasins.

The selection of the remaining five model components is based on the model component selection of Cunderlik and Simonovic (2004) who calibrated, verified and conducted a sensitivity analysis of the application of the HEC-HMS model in the UTRb. Following these authors: the Initial and Constant-rate Loss Model is selected as the runoff-volume model; the Clark unit hydrograph (UH) method is selected as the transformation methodology in the model (direct runoff model); the Modified Puls method (also known as storage routing or level-pool routing) is selected as the routing function; and the recession model is selected for modelling the baseflow component of the total stream flow. The Clark UH method is selected as it is frequently used for modelling direct runoff resulting from individual storm events (USACE 2013). The modified Puls method is selected as it is the only technique to take into account backwater effects (e.g., such as those caused by dams) and floodplain storage (USACE 2013), as backwater effects have a large influence in the UTRb due to the presence of three major flood control dams (Cunderlik and Simonovic 2004). The recession model is selected as this method is

suitable for basins where the volume and timing of baseflow is strongly influenced by precipitation events, as it is in the UTRb (Cunderlik and Simonovic 2004). Lastly, a set of source and sink components were substituted for the typical elevation-storage-outflow relationship used by HEC-HMS as a reservoir model. This is required since the UTRb contains three major gate controlled reservoirs and the typical elevation-storage-outflow relationship assumes the reservoir component is a free flowing uncontrolled reservoir. Since the three main reservoirs within the UTRb are gate controlled, the simple elevation storage-outflow relationship cannot capture actual water releases that may reflect specific water management practices or operational rules. Replacing the reservoir components with a set of source and sink components allows for calibration of parameters downstream of the reservoir and verification of the individual rainfall estimation techniques (Cunderlik and Simonovic 2004).

5.2 Rainfall events

Due to the availability of the EC radar product, the study period was limited to the periods 1 June 2013 to 31 August 2013 and 1 April 2014 to 31 October 2014. Events for hydrological modelling were selected based on the magnitude and intensity of the rainfall field over the UTRb, as well as the subsequent effect on flows in the North, Middle and South branches of the Thames River. Only events that caused an increase in flows in all branches of the Thames River were selected for analysis. Based on this criteria three events were selected for the modelling analysis. The characteristics of these events are summarized in Table 7. HEC-HMS is simulated on an event-basis for 96 hours starting from the hour the first rain gauge records a rainfall value greater than zero (Krajewski et al. 2010). The 96 hour timeframe is selected as the extent of the modelling since this is the average length of time until the flow at the UTRb outlet (Byron SG) returns to baseflow conditions for the selected storm events.

Table 7: Characteristics of the selected events for hydrological modelling analysis

Date	Time (UTC)	Rainfall duration (hr)	[+]Maximum rainfall intensity (mm/hr)	[*]Peak flow (m^3/s)
8 July 2014	16:00 – 01:00	11	15.5	138.5
5-6 September 2014	23:00 – 10:00	12	43.25	120.0
10-11 September 2014	19:00 – 08:00	14	30.6	240.6

[+] Maximum rainfall based on rain gauge values only
[*] Peak flow is based on the peak flow at the watershed outlet which is assumed to be the flow at the Byron SG

Based on a qualitative analysis of the radar rainfall images and rainfall intensities recorded by the rain gauges and radar, the 8 July 2014 and 5 September 2014 rainfall events were characterized as localized high intensity rainfall, more representative of convective events. The 10 September 2014 event, however, was more uniform in nature with several localized instances of high intensity rainfall, representative of stratiform rainfall with convective cells. The flooding extent due to the 8 July 2014 and 5 September 2014 rainfall events was smaller in nature relative to the 10 September 2014 event, with peak flows at the Byron SG approximately half of that observed during the 10 September 2014 rainfall event. The flooding due to the 8 July 2014 and 10 September 2014 rainfall events was exacerbated by saturated antecedent soil conditions in the watershed, due to previous rainfall that occurred in the days preceding the events. Conversely, the rainfall of the 5 September 2014 event occurred after a relatively long dry period, leading to dry antecedent soil conditions. The different antecedent soil conditions for the storm events analysed were taken into account in selection of initial losses for the Initial and Constant-rate Loss Model.

5.3 Selected stream gauges

Evaluation of the model performance at all SG locations in the UTRb involves extensive data processing. Therefore, based on the methodology of Cunderlik and Simonovic (2004), the performance of the model is evaluated at five SG locations within the UTRb as identified in Table 8. As seen in Fig. 15, the SG locations were selected so as to represent the different physiographic sub-regions of the UTRb, as well as to reflect different subbasin areas and stream flow regimes (Cunderlik and Simonovic 2004).

As described in UTRCA (2012), the SGs of Innerkip and Waubuno represent runoff from single subbasins along the South Branch of the Thames River. The Innerkip SG measures stream flow for the headwater regions of the South Branch, while the Waubuno SG measures stream flow for the Waubuno Creek (a major tributary along the South Branch). Both subbasins are mainly agricultural, with 81% and 83% being cleared for agriculture, respectively. The soil of the Waubuno subbasin is comprised primarily of silty loam (58%) and clay loam (13%). The soil of the Innerkip subbasin is comprised primarily of silty loam (48%), sandy loam (22%) and clay loam (12%). The Waubuno and Innerkip SGs measure lower flows relative to the other SGs used in this study, with mean annual flows of 1.2 m^3/s and 2.2 m^3/s, respectively. The Mitchell SG represents runoff from a single subbasin at the headwaters for the North Branch of the Thames River. The subbasin is heavily agricultural, with 93% of the land being cleared for agricultural purposes. The soil is comprised mainly of a clay loam (93%). As a result of these characteristics, the Mitchell subbasin is prone to localized flooding. The Mitchell SG has a mean annual flow of 4.5 m^3/s. The St. Mary's SG represents flow from 11 subbasins along the North Branch of the Thames River. The town of St. Mary's represents one of the major damage centres in the UTRb and contains a flood wall constructed along the Thames River to protect the city from flooding. The St. Mary's SG represents the flow at the middle of the North Branch of the Thames River, with a mean annual flow of 20.0 m^3/s. The Byron SG represents the outlet of the watershed in this analysis, and encompasses runoff from 91% of the watershed. The Byron SG lies downstream of the forks of the Thames River, where the North and South branches meet in the City of London. The Byron SG represents an area along the channel in which the slope of the channel begins to decrease, and there is a change from a relatively narrow channel to a wider, shallower channel (Wilcox et al. 1998). The mean annual flow at the Byron SG is 46.0 m^3/s.

Table 8: Characteristics of selected stream gauges

Name	Area (km^2)	Mean annual flow (m^3/s)
Mitchell SG	319	4.5
St. Mary's SG	1062	20.0
Innerkip SG	149	2.2
Waubuno SG	105	1.2
Byron SG	3110	46.0

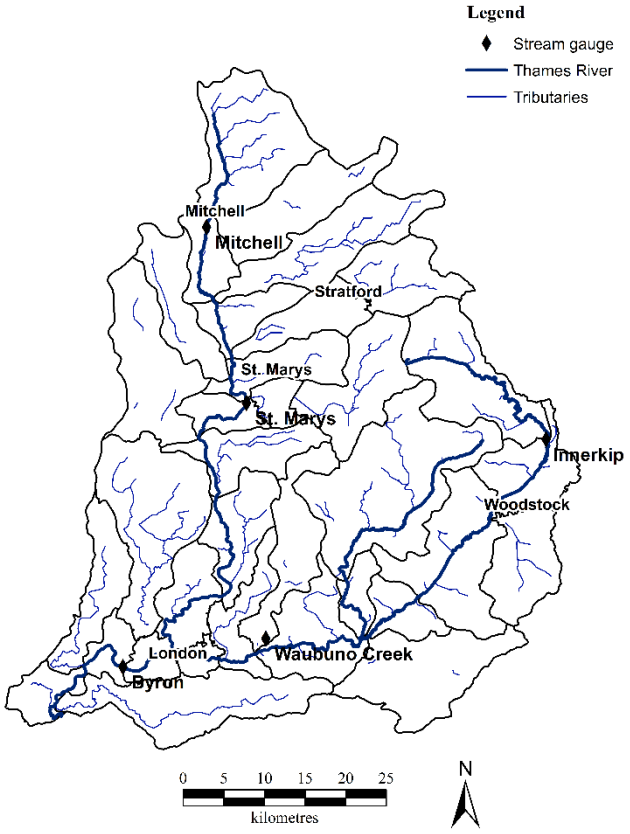

Figure 15: Location of selected stream gauges

5.4 Verification methodology

In order to assess the accuracy of the predicted hydrographs (and subsequently, the accuracy of each rainfall estimation technique), hourly flows predicted by the model are compared to hourly observed flows at the five SG locations identified in Section 5.3. Four statistical measures were used to evaluate the performance of the model. A brief description of the error statistics used in the analysis of the predicted flows is included in the following sub-sections.

5.4.1 Nash-Sutcliffe efficiency

The Nash-Sutcliffe efficiency (NSE) is used to evaluate the performance of each rainfall input in HEC-HMS. As defined by Nash and Sutcliffe (1970):

$$\mathrm{NSE} = 1 - \left[\frac{\sum (Q_O - Q_M)^2}{\sum (Q_O - Q_A)^2} \right]. \tag{22}$$

The NSE is a widely used measure in the evaluation of the performance of a model (Krause et al. 2005). Due to the squaring of residuals the NSE is sensitive to errors during higher peak flow conditions and less affected by errors within baseflow or low flow conditions. This is important for the present research as the primary interest is in the ability of the model to predict flood flows. The NSE value lies between 1 and -∞, with values greater than zero indicating that the model is a better predictor than the mean of the observed data, zero indicating that the model predictions are as accurate as the mean of the observed data, and less than zero indicating that the observed mean is a better predictor than the model.

5.4.2 Percent error in peak flow

The percent error in peak flow (PEPF) is used to evaluate the ability of the model to determine the magnitude of the peak flow and is evaluated following:

$$\mathrm{PEPF} = \left| \frac{Q_M(peak) - Q_O(peak)}{Q_O(peak)} \right| * 100. \tag{23}$$

Again, the magnitude of the peak flow is important in quantifying the extent of flooding, and is an important statistical measure to consider in the present research. Positive (negative) values indicate over-prediction (under-prediction) of the peak flow by the model as compared to the observed peak flow.

5.4.3 Percent error in volume

The percent error in volume (PEV) is used to evaluate the runoff volume generated by the model, as defined by:

$$\mathrm{PEV} = \left| \frac{V_M - V_O}{V_O} \right| * 100 , \tag{24}$$

where V_O is the observed volume of water passing during the storm event and V_M is the modelled volume of water passing during the storm event. The volume of flow is important in understanding the conditions within the basin (saturated or unsaturated) and the possible under- or over-estimation of rainfall. Understanding the PEV will assist in identifying error in the depth of rainfall as well as the initial conditions used in the runoff volume model. Positive (negative) values indicate over-estimation (under-estimation) of the volume by the model as compared to the observed volume.

5.4.4 Peak timing error

The peak timing error (PTE) is used to assess the ability of the model to accurately predict the timing of the peak flow, as determined by:

$$\mathrm{PTE} = \left| T_O - T_M \right| , \tag{25}$$

where T_O is the timing of the peak of the observed hydrograph and T_M is the timing of the peak of the modelled hydrograph. The analysis of the timing of the maximum flow is important in determining when issues due to flooding may occur and when the extent of flooding will begin to subside.

5.4.5 Wilcoxon rank sum test

The Wilcoxon rank sum test (WRST) is used in this study to investigate whether the differences in results from the investigated merging methods are statistically significant. Previous studies have demonstrated the suitability of the WRST in the analysis of various precipitation estimations (see, e.g., Shabbar et al. 1997; Hamill 1998; Kampata et al. 2008). The WRST, based on the work of Wilcoxon (1945) and Mann and Whitney

(1947), is used as a non-parametric alternative to the standard statistical hypothesis t-test (Hayter 2007). The WRST is used in this analysis since the assumption of a normal distribution required for the standard t-test is not upheld in the observed results, with the distribution being skewed by individual SG outliers. The WRST uses a non-parametric statistical hypothesis test to analyse whether the difference in mean ranks of two populations is statistically significant (Hayter 2007). The analysis in this study is completed using the NSE as the target variable. The P-value is examined in order to determine statistical significance. A P-value less than 0.05 indicates that the difference between the two populations is statistically significant, while a P-value greater than 0.05 indicates that the difference between the two populations is not statistically significant. Refer to Hayter (2007) for a full explanation of the WRST.

5.5 HEC-HMS calibration

Calibration is the process of systematically adjusting the values of model parameters until the model results achieve a tolerable level of error in comparison to the observed data (Hossain et al. 2004). The model calibration conducted in this analysis is completed following the methodology of Cunderlik and Simonovic (2004), which consists of a combination of manual and automated parameter calibration. The manual calibration involves setting initial parameter values based on available physical data from the study site. The physical data used in the development of the HEC-HMS model is based on information provided in Cunderlik and Simonovic (2004) and UTRCA (2012). The automated calibration is subsequently used to optimize the user-defined parameter values. Based on the model components selected in HEC-HMS, the parameters identified in Table 9 were required for development of the model.

Table 9: Selected HEC-HMS model components and subsequent required parameters

Component	Parameter	Measured or calibrated
Basin characteristics	Area (km^2)	Measured
Runoff-volume model (Initial and Constant)	Initial abstractions (mm)	Storm dependent (Calibrated/measured)
	Constant loss rate (mm/hr)	Calibrated
	Impervious surface (%)	Measured
Direct runoff model (Clark's unit hydrograph)	Time of concentration (hr)	Calibrated
	Storage coefficient (hr)	Calibrated
Baseflow model (Recession)	Initial discharge ($m^3/s/km^2$)	Measured
	Recession constant	Calibrated
	ratio	Calibrated
Routing model (Modified Puls)	Storage-outflow curve	Calibrated
	Number of subreaches	Measured
	Initial condition	Calibrated

The present study seeks to examine flows as a result of heavy rainfall, therefore, generating peak flows with a high degree of confidence is critically important. Considering this, the peak weighted root mean square error (PWRMSE) was selected as the objective function. The PWRMSE is determined by:

$$\text{PWRMSE} = \sqrt{\frac{\sum_{t=1}^{N}\left(Q_O(t) - Q_M(t)\right)^2 \frac{Q_O(t)+Q_A}{2Q_A}}{N}}; Q_A = \frac{1}{N}\sum_{t=1}^{N} Q_O(t), \tag{21}$$

where Q_0 is the observed flow and Q_M is the modelled flow at time t_1 and Q_A is the average observed flow.

The calibration process begins at SG stations that represent outlets of single subbasins. Once these stations are calibrated, SG stations with more than one contributing subbasin are calibrated. At this stage the parameters of un-gauged contributing subbasins are also calibrated. In the final stage of calibration, individually calibrated subbasins are linked into one model and the parameter calibration is finalized. The 33 subbasins are calibrated based on the order outlined in Table 10. A list of basin names and corresponding basin numbers can be found in Appendix C.

Table 10: Order of calibration for the 33 modelled subbasins

Stream gauge	Basin number calibrated	Calibration order
Mitchell	1,2	1
Avon	7	1
Innerkip	18	1
Cedar Creek	20	1
Reynolds	25	1
Thamesford	23	1
Medway	17	1
Waubuno	27	1
Oxbow Creek	32	1
Dingman Creek	34	1
St. Mary's	3,4,5,8,9,10,11	2
Fanshawe Dam	15,16	2
Pittock Dam	19	2
Plover Mills	12,13,14	3
Ingersoll	21	3
Byron	22,24,26,28,29,30	4
Dutton	31,33	5

Parameters are calibrated based on observed hourly flows. Due to a lack of availability of radar data the calibration is first conducted using rain gauge data alone for an event that began on 9 July 2000. This event represents one of the largest events on record in the UTRb and consisted of a convective rainfall event that resulted in widespread flooding (Cunderlik and Simonovic 2004). The model was then recalibrated using each individual rainfall technique for the 10 September 2014 event in order to examine the effect of recalibrating the model for each rainfall input. The 10 September 2014 event is well-suited for rainfall-runoff calibration both in terms of magnitude and spatial extent. This event represented the largest rainfall event in terms of magnitude of flood flows observed during the study period. Only the model recalibrated using BSA is presented in this Chapter. The verification results for the model calibrated with rain gauge only rainfall is compared to the model calibrated with BSA rainfall in order to assess the effect of recalibrating the model.

5.5.1 Calibration results

The following section outlines the results of the calibration of the RGO (OK) model as well as the calibration of the BSA model. The RGO (OK) model was calibrated for the 9 July 2000 event, and the BSA model was calibrated for the 10 September 2014 event (as

described in Section 5.2). For a summary of the RGO (OK) and BSA calibrated model parameter values see Appendix C and D, respectively.

5.5.1.1 RGO (OK) model

Fig. 16 displays the comparison between the observed and modelled hydrographs for the selected SG locations for the 9 July 2000 rainfall event using the RGO (OK) data in the RGO (OK) calibrated model. Overall, the model simulated the stream flows with a high degree of accuracy, with a NSE ranging from 0.81 at the Innerkip SG (Fig. 16c) to 0.99 at the Byron SG (Fig. 16e) for the various SG locations. The model accurately recreated the rising and falling limbs as well as the peak flow at all SG locations with the exception of the Innerkip SG. As seen in Fig 16c, a bi-modal peak was observed but not predicted by the model at the Innerkip SG. Since the model did not simulate a double peaked hydrograph, the PEV was higher at the Innerkip SG relative to the other SGs in the analysis, with a PEV of -21%. Table 11 displays the calculated error statistics at the selected SGs.

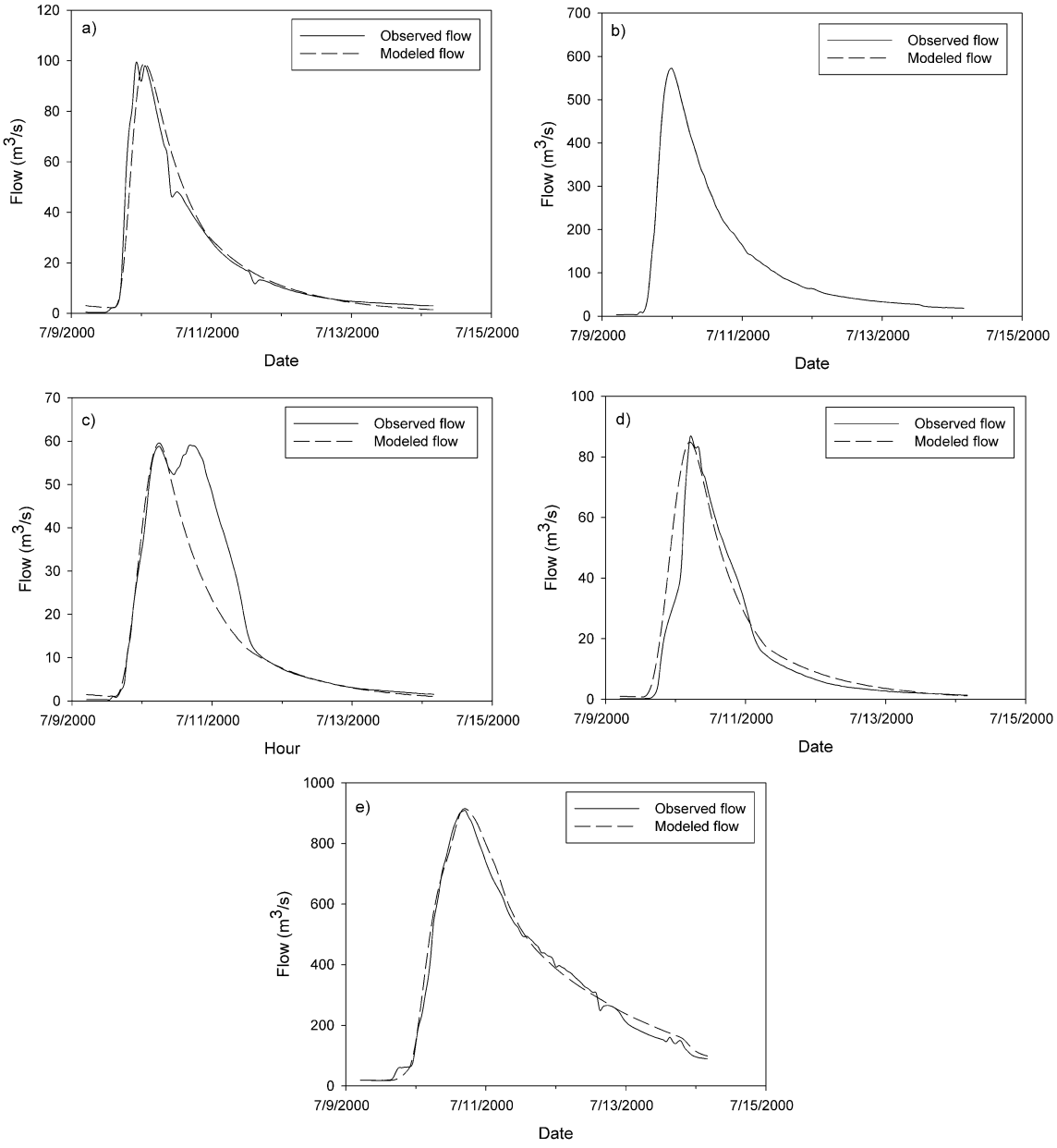

Figure 16: Observed and modelled hydrographs for the July 2000 event using RGO (OK) rainfall as input into the RGO (OK) calibrated model at the: a) Mitchell SG; b) St. Mary's SG; c) Innerkip SG; d) Waubuno SG; and e) Byron SG

Table 11: Error statistics between observed and modelled flows for the July 2000 event at selected stream gauges using the RGO (OK) rainfall data as input into the RGO (OK) calibrated model

Gauge	NSE	PEPF (%)	PEV (%)	PTE (hr)
Mitchell	0.96	0	2	0
St. Mary's	0.98	-3	-4	1
Innerkip	0.81	0	-21	0
Waubuno	0.91	-2	13	0
Byron	0.99	0	3	0

5.5.1.2 BSA model

Fig. 17 presents the comparison between the observed and modelled hydrographs for the selected SG locations for the 10 September 2014 rainfall event using the BSA rainfall data as input into the BSA calibrated model. Overall, the hydrographs indicate a good fit between the predicted flows and the observed flows, with a NSE ranging from 0.85 at the Waubuno SG (Fig. 17d) to 0.97 at the Mitchell SG (Fig. 17a) for the selected SG locations. Despite these overall results, as observed in Fig. 17d, the BSA model did not accurately predict the peak flow magnitude at the Waubuno SG. The model under-estimated the observed peak flow, with a PEPF of -25%. As seen in Fig. 17c, the BSA calibrated model also improperly modelled the falling limb of the hydrograph at the Innerkip SG. Table 12 displays the error statistics for the selected SGs. In general, the performance of the BSA model during the selected calibration period was poor compared to the results of the RGO (OK) calibrated model, displaying greater magnitudes of error in the PEPF, PEV and PTE values.

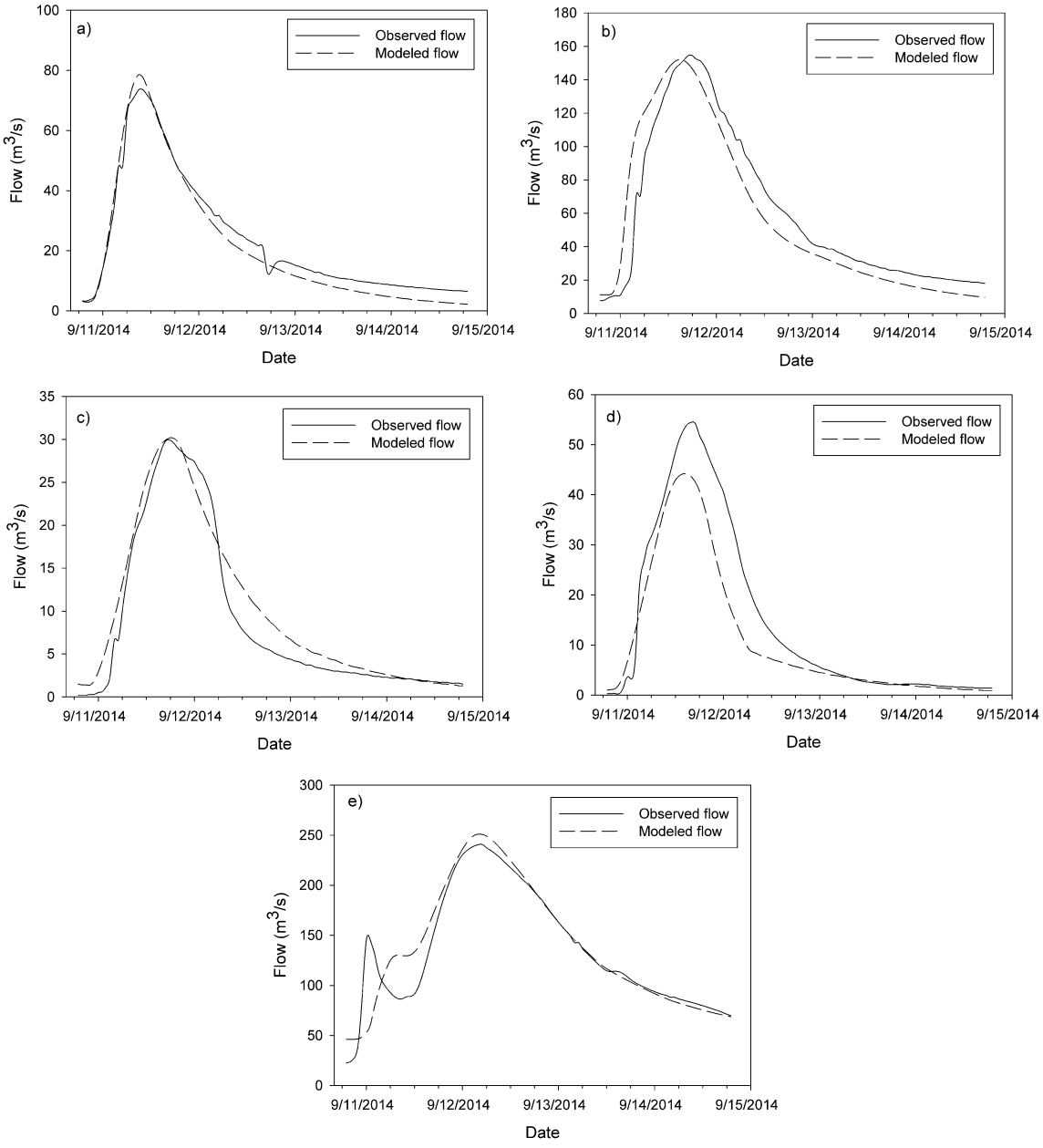

Figure 17: Observed and modelled hydrographs for the 10 September 2014 event using BSA rainfall as input into the BSA calibrated model at the: a) Mitchell SG; b) St. Mary's SG; c) Innerkip SG; d) Waubuno SG; and e) Byron SG

Table 12: Error statistics between observed and modelled flows for the 10 September 2014 event at selected stream gauges using BSA rainfall data as input into the BSA calibrated model

Gauge	NSE	PEPF (%)	PEV (%)	PTE (hr)
Mitchell	0.97	7	-10	0
St. Mary's	0.88	-2	-6	2
Innerkip	0.94	1	14	1
Waubuno	0.85	-19	-25	2
Byron	0.87	4	3	1

5.5.1.3 Calibration sensitivity

To compare the effect on the accuracy of using the BSA rainfall data as input into both the BSA calibrated model and the RGO (OK) calibrated model, both models were simulated using BSA rainfall data for the 5 September 2014 and the 8 July 2014 rainfall events. Table 13 displays the error statistics for these two models for both events. Overall, the verification results between the two models are similar, with a median NSE difference of 0.01 between the two model simulations. The WRST was used to determine whether the difference observed between the two model results was statistically significant. A P-value of 0.727 indicated that significant improvement is not achieved by recalibrating the model using the BSA rainfall as input. Considering this, the model calibrated using RGO (OK) rainfall data for the July 2000 rainfall event was used for the remainder of the analysis presented in this Chapter.

The above sensitivity analysis was conducted for each rainfall estimation technique. The comparison for each individually recalibrated model against the RGO (OK) calibrated model is displayed in Table 14. In general, the results from each recalibration based on the individual rainfall estimation techniques displayed a similar trend in error to the results of the BSA recalibration described above.

Table 13: Model comparison for the 5 September 2014 and 8 July 2014 rainfall events for the BSA calibrated and RGO (OK) calibrated models using BSA rainfall data as input

Event	Station	NSE	
		RGO-Cal BSA	BSA-Cal BSA
8 July 2014	Mitchell	0.53	0.50
	St. Mary's	-0.18	-0.25
	Innerkip	0.75	-0.70
	Waubuno	0.81	0.75
	Byron	0.93	0.93
5 September 2014	Mitchell	0.72	0.73
	St. Mary's	0.58	0.61
	Innerkip	0.90	0.80
	Waubuno	0.58	0.72
	Byron	0.02	-0.14
Median		0.65	0.66
WRST P-Value		0.727	

Table 14: Model comparison for the 5 September 2014 and 8 July 2014 rainfall events for the calibrated models using each rainfall technique as input

Event	Stream gauge	NSE							
		RGO-Cal Raw radar	Radar-Cal Raw radar	RGO-Cal MFB	MFB-Cal MFB	RGO-Cal LB	LB-Cal LB	RGO-Cal CM	CM-Cal CM
8 July 2014	Mitchell	-0.57	-0.19	0.8	0.86	0.7	0.61	0.14	0.17
	Mary's	-1.06	-1.00	0.83	0.83	-0.24	-0.35	-0.71	-0.71
	Innerkip	-0.7	-0.70	0.32	0.25	0.8	0.76	0.37	0.31
	Waubuno	-0.13	-0.13	0.82	0.82	0.66	0.70	0.8	0.76
	Byron	0.9	0.91	0.61	0.79	0.93	0.96	0.94	0.95
5 September 2014	Mitchell	-0.61	-0.53	0.92	0.99	0.72	0.68	0.36	0.42
	Mary's	-0.78	-0.71	0.97	0.88	0.66	0.64	0.08	0.13
	Innerkip	-0.04	-0.28	0.92	-2.08	0.73	0.55	0.89	-0.09
	Waubuno	-0.38	-0.38	0.79	0.79	0.49	0.63	0.11	0.20
	Byron	0.64	0.75	-0.73	-1.20	-0.04	-0.12	0.55	0.27
Median		-0.48	-0.33	0.81	0.81	0.68	0.63	0.37	0.24
WRST P-value		0.440		0.752		0.752		0.703	

5.6 Results and discussion

Each of the rainfall estimation techniques investigated in this Chapter were used as rainfall input into the RGO (OK) calibrated semi-distributed HEC-HMS described in

Section 5.1. The model was simulated for the three flow events identified in Section 5.2, and the modelled hydrographs were compared to the observed hydrographs for the SG locations identified in Section 5.3. The error statistics described in Section 5.4 were used to analyse the accuracy of each individual gauge-radar merging method as input into the calibrated model. The analysis will evaluate (at the hourly time-step) the difference between using a mean bias correction, spatially dependent bias correction or a more complicated geostatistical merging method as input into a hydrological model over the study period analysed. In addition, the gauge-radar merging methods are compared against the hydrographs generated using raw radar data alone and rain gauge data alone. The comparison against rain gauge data alone is important as rain gauges alone are used in the vast majority of hydrological modelling applications today, and it is important to assess whether the addition of radar provides any additional benefit in the modelling of flows in the UTRb. The comparison of the performance of gauge-radar merging methods against raw radar alone provides an indication of the ability of rain gauges to reduce biases often observed in radar rainfall fields. As discussed in Section 2.5.1, rain gauge density can have a considerable effect on the accuracy of the rainfall estimation technique. The rain gauge network density is altered and the model is simulated using the altered rainfall fields in order to investigate and quantify this effect. This is an important consideration in order to extend the results from this study to other watersheds where the rain gauge network density is different. As discussed in Section 2.5.1 both storm type and basin characteristics can also affect the accuracy of rainfall estimation techniques. Both of these influencing factors are further investigated in this Chapter.

Considering this, the results are organized into three main sections:

(1) analysis of the effect of each rainfall estimation technique on the accuracy of predicted stream flows for each rainfall event;
(2) determination of the overall median error for each rainfall estimation technique over the entire study period; and
(3) analysis of the effect of storm type, basin characteristics and rain gauge network density on the accuracy of the predicted flows for each rainfall estimation technique.

The median is used as the descriptive statistic due to the distribution of results based on the variation in the SG locations. Using the median over the mean limits the effect of outliers due to poor modelling at a single SG location.

5.6.1 8 July 2014

Fig. 18 presents the comparison between the observed and modelled hydrographs for each rainfall estimation technique for the 8 July 2014 rainfall event. Through qualitative observation of the various hydrographs it is clear that some discrepancies exist between the modelled and observed flows at each SG location. Fig. 18a displays the modelled and observed hydrographs at the Mitchell SG. Overall, each model was able to successfully capture the general shape of the observed Mitchell hydrograph. One noticeable difference between the modelled and observed hydrographs was in the minor sharp decreases in flow in the falling limb of the observed hydrograph. This was determined to be a result of gate operations of a small reservoir upstream of the Mitchell SG. As described previously in this Chapter, this reservoir was not included in the model and, therefore, the minor variations due to reservoir operations were not present in any of the modelled hydrographs. In general, the modelled flows for the models driven by each rainfall estimation technique under-estimated the peak flows at all SG locations analysed. The only exception was the model driven by the MFB method at both the St. Mary's SG (Fig. 18b) and the Byron SG (Fig. 18e). The under-estimation in peak flows was most notable in the raw radar driven model resulting in a median PEPF of -84%. The MFB driven model provided the best comparison in peak flows to the observed hydrograph reducing the median PEPF to -5%. The hydrographs at the Innerkip (Fig. 18c) and Waubuno (Fig 18d) SGs demonstrated that raw radar produced rainfall estimations that were unable to overcome the initial abstractions (I_a) of the upstream subbasins and, therefore, the raw radar driven model was only able to recreate the falling limb of the hydrograph. At the Waubuno SG (Fig. 18d) each model was unable to accurately capture the steep slope of the rising limb seen in the observed hydrograph. This is attributed to potential errors in the *Tc*. At the Byron SG (Fig. 18e) all estimation techniques provided relatively accurate predictions of flow with the exception of the MFB driven model, which considerably over-estimated the initial peak. Each model at the Byron SG had difficulty generating the

correct timing of the initial peak. The initial peak at the Byron SG is a result of runoff from the heavily urbanized London area. Each model was delayed in the timing of this initial urban peak at the Byron SG. This is attributed to the temporal resolution of the rainfall data and the spatial resolution of the model, as the hourly time-step is too coarse to capture urban runoff scenarios in the HEC-HMS model.

As shown in Table 15, each gauge-radar merging method produced models which predicted flows with higher median efficiency than the raw radar and RGO (OK) driven models for the 8 July 2014 rainfall event. The median NSE was increased from -0.57 and 0.31 for the raw radar and RGO (OK) driven models to 0.80, 0.75, 0.75 and 0.37 for the MFB, BSA, LB and CM models, respectively. The MFB driven model produced predicted flows with the highest median efficiency. The success of the MFB method during the 8 July 2014 event is attributed to the greater depth of rainfall estimated as compared to the other gauge-radar merging methods. The MFB method was able to reduce the median PEV by 78% and 49% over raw radar and RGO (OK), respectively. The raw radar produced the largest PTE with a median of 5 hours due to the poor modelling of the hydrographs at the Innerkip (Fig. 18c) and Waubuno (Fig 18d) SGs, which produced PTE values of 9 and 11 hours, respectively. The other models produced values of PTE with similar magnitudes, which is expected due to using identical values in the rainfall-runoff and routing model parameters.

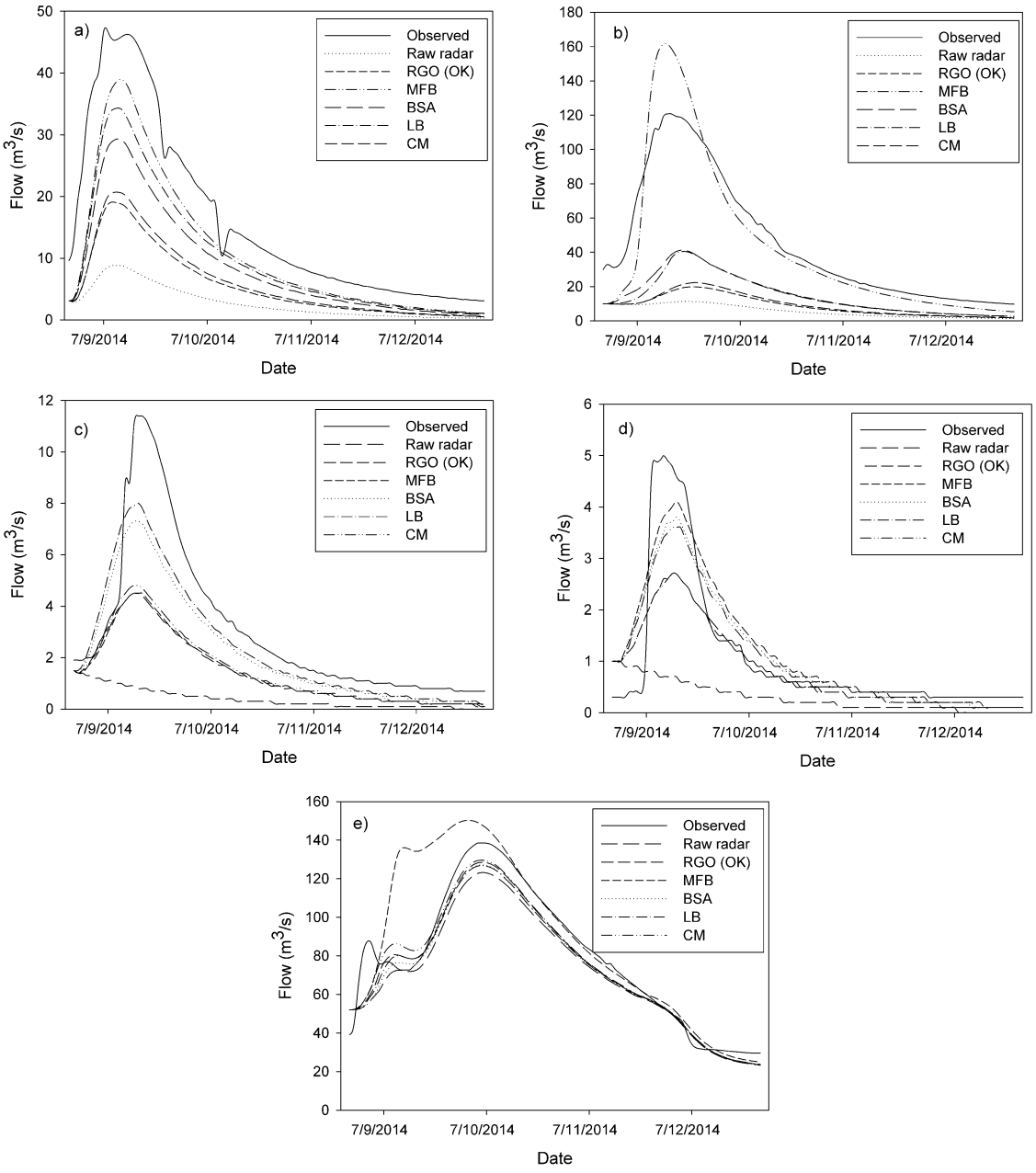

Figure 18: Observed and modelled hydrographs for the 8 July 2014 event for each model driven by each rainfall estimation technique at the: a) Mitchell SG; b) St. Mary's SG; c) Innerkip SG; d) Waubuno SG; and e) Byron SG

Table 15: Error statistics between observed and modelled flows for the 8 July 2014 event at selected stream gauges for all rainfall estimation techniques

Gauge	Raw radar	RGO (OK)	MFB	BSA	LB	CM
			NSE			
Mitchell	-0.57	0.40	0.80	0.53	0.70	0.14
St. Mary's	-1.06	-0.55	0.83	-0.18	-0.24	-0.71
Innerkip	-0.70	0.31	0.32	0.75	0.80	0.37
Waubuno	-0.13	0.67	0.82	0.81	0.66	0.80
Byron	0.90	0.94	0.61	0.93	0.93	0.94
Median	-0.57	0.31	0.80	0.75	0.75	0.37
			PEPF (%)			
Mitchell	-81	-59	-16	-37	-27	-56
St. Mary's	-91	-84	34	-66	-66	-82
Innerkip	-87	-61	-61	-61	-30	-58
Waubuno	-80	-46	-18	-24	-46	-28
Byron	-11	-7	8	-8	-8	-6
Median	-84	-54	-5	-43	-38	-43
			PEV (%)			
Mitchell	-83	-66	-16	-46	-38	-62
St. Mary's	-87	-81	-5	-66	-67	-79
Innerkip	-87	-54	-54	-54	-22	-51
Waubuno	-72	-23	11	3	-23	0
Byron	-10	-6	11	-8	-7	-5
Median	-83	-54	-5	-46	-23	-51
			PTE (HR)			
Mitchell	3	2	4	3	3	3
St. Mary's	5	6	0	4	4	6
Innerkip	9	0	0	0	0	0
Waubuno	11	3	3	3	3	3
Byron	1	1	2	1	1	1
Median	5	2	2	3	3	3

5.6.2 5 September 2014

Fig. 19 presents the comparison between the observed and modelled hydrographs for the model driven by each rainfall estimation technique for the 5 September 2014 rainfall event. In general, each model was able to replicate the shape of the observed

hydrographs, with the exception of the inability of each model to replicate the steep slope of the rising limb in the observed hydrograph at the Waubuno SG (Fig. 19d). At the Innerkip SG (Fig. 19c) the raw radar alone substantially underestimated the peak flow. At the Mitchell SG (Fig. 19a), St. Mary's SG (Fig. 19b) and the Innerkip SG (Fig. 19d) each model under-estimated the peak flow. Again, the MFB driven model provided the closest match in peak flow with a median PEPF of -20%. At the Byron SG (Fig. 19e) each model, with the exception of the raw radar, over-estimated the peak flow.

Overall, as shown in Table 16 each gauge-radar merging method produced models with predicted flows at a higher median efficiency than both the raw radar and RGO (OK) driven models. The NSE was increased from a median of -0.38 and 0.21 for the raw radar and RGO (OK) driven models, respectively, to 0.92, 0.58, 0.66 and 0.36 for the MFB, BSA, LB and CM models, respectively. Again, the MFB model produce predicted flows with the highest median efficiency. This was attributed to the greater depth of rainfall estimated in comparison to the other merging methods, with a reduction in the median PEV of 72% and 48% over raw radar and RGO (OK), respectively. Again, each model displayed PTE values of similar magnitudes, with the MFB driven model presenting a slightly higher PTE due to poor modelling at the Waubuno SG and Byron SG.

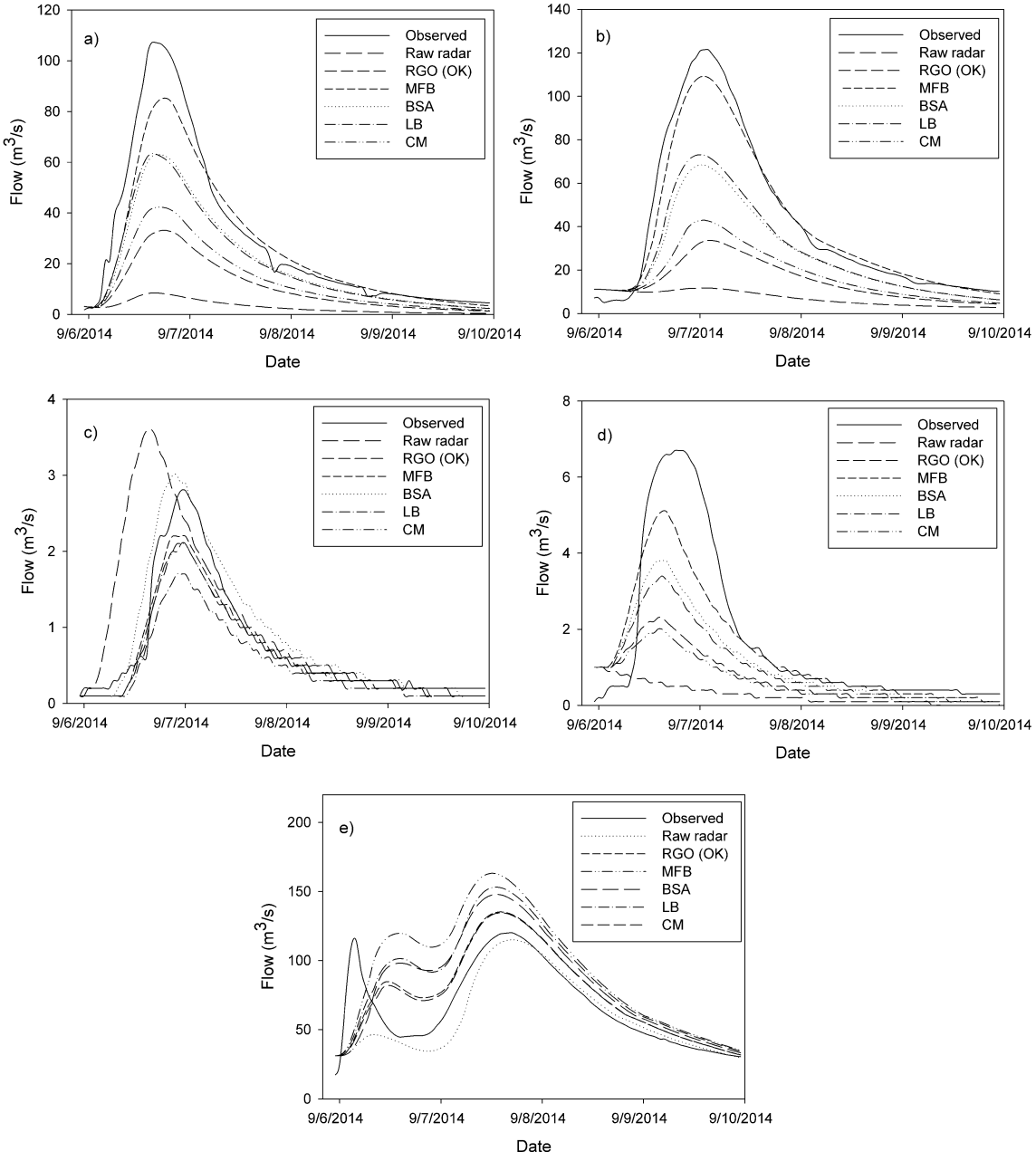

Figure 19: Observed and modelled hydrographs for the 5 September 2014 event for each model driven by each rainfall estimation technique at the: a) Mitchell SG; b) St. Mary's SG; c) Innerkip SG; d) Waubuno SG; and e) Byron SG

Table 16: Error statistics between observed and modelled flows for the 5 September 2014 event at selected stream gauges for all rainfall estimation techniques

Gauge	Raw radar	RGO (OK)	MFB	BSA	LB	CM
			NSE			
Mitchell	-0.61	0.14	0.92	0.72	0.72	0.36
St. Mary's	-0.78	-0.14	0.97	0.58	0.66	0.08
Innerkip	-0.04	0.89	0.92	0.90	0.73	0.89
Waubuno	-0.38	0.21	0.79	0.58	0.49	0.11
Byron	0.64	0.53	-0.73	0.02	-0.04	0.55
Median	-0.38	0.21	0.92	0.58	0.66	0.36
			PEPF (%)			
Mitchell	-92	-69	-20	-41	-41	-61
St. Mary's	-90	-72	-10	-44	-40	-65
Innerkip	29	-25	-21	7	-39	-25
Waubuno	-85	-66	-24	-43	-49	-70
Byron	-4	13	36	23	28	12
Median	-85	-66	-20	-41	-40	-61
			PEV (%)			
Mitchell	-90	-64	-11	-33	-34	-54
St. Mary's	-83	-64	-4	-37	-34	-57
Innerkip	36	-20	-15	16	-35	-20
Waubuno	-84	-59	-17	-36	-43	-63
Byron	-10	14	40	25	29	13
Median	-83	-59	-11	-33	-34	-54
			PTE (HR)			
Mitchell	1	3	3	2	0	2
St. Mary's	0	1	0	1	1	0
Innerkip	7	0	0	0	0	0
Waubuno	4	4	4	4	4	5
Byron	1	2	4	3	3	2
Median	1	2	3	2	1	2

5.6.3 10 September 2014

Fig. 20 presents the flow comparison between the observed and modelled hydrographs for each rainfall estimation technique for the 10 September 2014 rainfall event. As seen in Fig. 20a, each model produced hydrographs with the correct general shape at the

Mitchell SG, however, the raw radar and MFB model considerably under-estimated the peak flow by -85% and -40%, respectively. Each model was unable to capture the general shape of the observed hydrograph at the St. Mary's SG (Fig. 20b) and the Innerkip SG (Fig. 20c), producing a much steeper increase in the rising limb leading to large PTE values at both SG locations. There is a considerable under-estimation in the peak flows for each model at the Waubuno SG (Fig. 20d), with the raw radar, RGO (OK), MFB, BSA, LB and CM driven models all under-estimating the peak flow by -98%, -86%, -68%, -79%, -81% and -86%, respectively. At the Byron SG (Fig. 20e) each model with the exception of the MFB driven model under-estimated the peak flows.

Overall, as shown in Table 17 each gauge-radar driven model produced predicted flows with a higher efficiency than the raw radar driven model, increasing the NSE from a median of -0.68 for raw radar to 0.39, 0.57, 0.59 and 0.62 for the MFB, BSA, LB and CM models, respectively. In comparison against the RGO (OK) driven model, none of the gauge-radar driven models were able to generate an increase in median efficiency. The addition of radar did not add any additional benefit in the modelling of the 10 September 2014 event. In general, the model efficiencies of the gauge-radar driven models for the 10 September 2014 event were lower than the 8 July 2014 and the 5 September 2014 event. This is attributed to incorrect modelling of the rising limb at the St. Mary's and Innerkip SG as well as considerable under-estimation of the peak flows at the Waubuno SG. The errors at the St. Mary's SG and Innerkip SG are attributed to the potential mis-timing of rainfall and the effect of small reservoirs not included in the model evident in the attenuation observed in the rising limb of the observed hydrograph. The error at the Waubuno SG is due to considerable under-estimation of the total rainfall by all estimation techniques over the Waubuno subbasin.

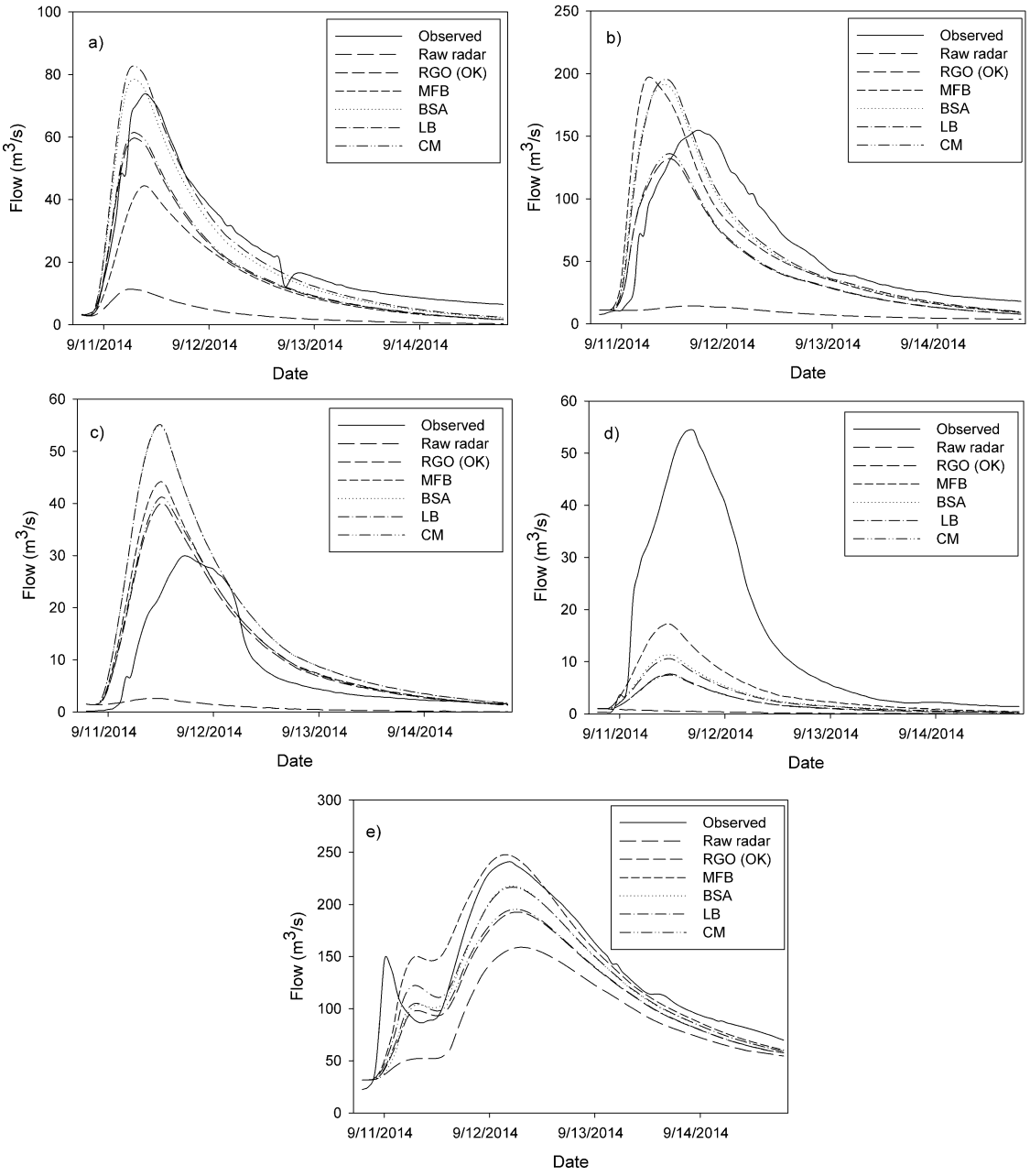

Figure 20: Observed and modelled hydrographs for the 10 September 2014 event for each model driven by each rainfall estimation technique at the: a) Mitchell SG; b) St. Mary's SG; c) Innerkip SG; d) Waubuno SG; and e) Byron SG

Table 17: Error statistics between observed and modelled flows for the 10 September 2014 event at selected stream gauges for all rainfall estimation techniques

Gauge	Raw radar	RGO (OK)	MFB	BSA	LB	CM
			NSE			
Mitchell	-0.75	0.81	0.61	0.91	0.89	0.83
St. Mary's	-1.14	0.61	0.37	0.57	0.59	0.62
Innerkip	-0.57	0.60	0.39	-0.37	-0.39	0.55
Waubuno	-0.68	-0.32	0.10	-0.14	-0.18	-0.32
Byron	0.23	0.70	0.81	0.83	0.84	0.73
Median	-0.68	0.61	0.39	0.57	0.59	0.62
			PEPF (%)			
Mitchell	-85	-19	-40	7	13	-16
St. Mary's	-91	-14	28	24	27	-12
Innerkip	-91	34	48	84	84	38
Waubuno	-98	-86	-68	-79	-81	-86
Byron	34	-20	3	-10	-10	-19
Median	-91	-19	3	7	13	-16
			PEV (%)			
Mitchell	-86	-30	-42	-9	-3	-28
St. Mary's	-86	-29	-5	-3	-2	-28
Innerkip	-90	36	46	78	78	41
Waubuno	-98	-86	-69	-79	-81	-86
Byron	-32	-18	1	-11	-9	-17
Median	-86	-29	-5	-9	-3	-28
			PTE (HR)			
Mitchell	3	2	0	2	2	2
St. Mary's	1	6	10	7	7	6
Innerkip	6	5	5	5	5	5
Waubuno	3	5	5	5	5	5
Byron	1	1	1	0	0	0
Median	3	5	5	5	5	5

5.6.4 Analysis of rainfall events combined

Fig. 21 presents the box-plot of the NSE for the hourly flows predicted by each model driven by the individual rainfall estimation techniques for the three rainfall events

analysed combined. Table 18 displays the P-values based on the WRST used to determine whether the difference between model performances based on each rainfall estimation technique is statistically significant. In comparison with the use of raw radar alone as rainfall input, each of the gauge-radar merging methods provided significant increases in the accuracy of the predicted flows over all three events analysed combined (with P-values for each estimation technique less than the 0.05 threshold). The gauge-radar driven models increased the median accuracy over the raw radar alone driven model, increasing the NSE from -0.57 to 0.79, 0.58, 0.66 and 0.55 for the MFB, BSA, LB and CM driven models, respectively. The raw radar driven model provided an extremely poor prediction of the hydrographs at all SG locations, with values of NSE consistently less than zero. Clearly, the addition of rain gauge data to adjust radar data significantly increased model efficiency. In comparison with the RGO (OK) driven model, only the MFB driven model provided a statistically significant increase in model accuracy with a P-value of 0.043. All other gauge-radar merged rainfall driven models generated P-values greater than the 0.05 threshold, indicating that the observed increases in median accuracy were not statistically significant. These results indicate that the addition of radar data in hydrological modelling applications in the UTRb can increase modelling accuracy for particular gauge-radar merging methods (i.e., MFB).

Overall, as shown in Table 19, the MFB driven model provided the best median prediction of flows in the UTRb over the study period analysed, with an overall median NSE of 0.79. The spatially-dependent correction methods displayed the largest variation in the NSE with standard deviations of 0.42 and 0.43 for BSA and LB, respectively. The MFB displayed the smallest variation in accuracy with a standard deviation of 0.25. The variation observed in the spatially-dependent merging methods over the mean field bias method is attributed to spatio-temporal sampling errors outlined in Gjertsen et al. (2004) and discussed in Section 4.3.1. At higher temporal resolutions the MFB approach is able to smooth fluctuations in the gauge-radar comparison that can be identified in individual gauges. The spatially-dependent correction methods are prone to larger errors at smaller time-steps on account of these fluctuations. These large fluctuations in rainfall accuracy of the spatially-dependent correction methods translated into large fluctuations in the accuracy of predicted flows over the three rainfall events.

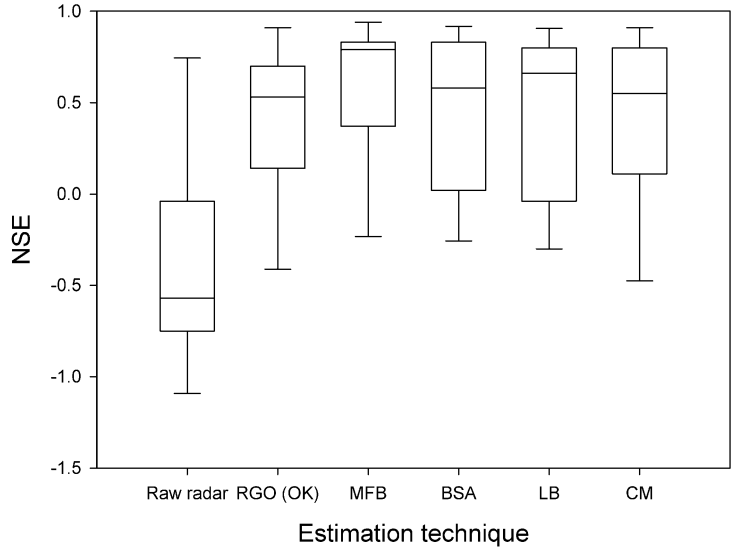

Figure 21: Box-plot based on median of the NSE for each model driven by each individual estimation technique for all events analysed combined

Table 18: Wilcoxon rank sum test P-values based on the comparison of each gauge-radar driven model with raw radar and RGO (OK) driven models

	Raw radar	RGO (OK)	MFB	BSA	LB	CM
Raw radar	X	0.001	0.000	0.000	0.000	0.000
RGO (OK)	0.001	X	0.043	0.247	0.247	0.525

Fig. 22 presents the box-plot for the PEPF for each model driven by the individual rainfall estimation techniques over all rainfall events analysed combined. Each estimation technique driven model typically under-estimated the peak flow. This is attributed to the spatial averaging of rainfall over the subbasins, which reduced the effect of small spatial scale high intensity rainfall cells on the stream flow. Raw radar is also known to under-estimate rainfall during heavy precipitation events (Smith et al. 2007). Each merging method provided a reduction in the median PEPF as compared to raw radar and RGO (OK) driven models. The MFB, BSA, LB and CM driven models reduced the median PEPF over the raw radar driven model by 69%, 61%, 55% and 57%, respectively, and

over the RGO (OK) driven model by 30%, 22%, 16% and 18%, respectively. Overall, as shown in Table 19, the MFB method driven model consistently provided the best estimate of the peak flow. The raw radar driven model displayed the largest variation in the PEPF with a standard deviation of 45%, while the other estimation techniques varied with similar magnitudes.

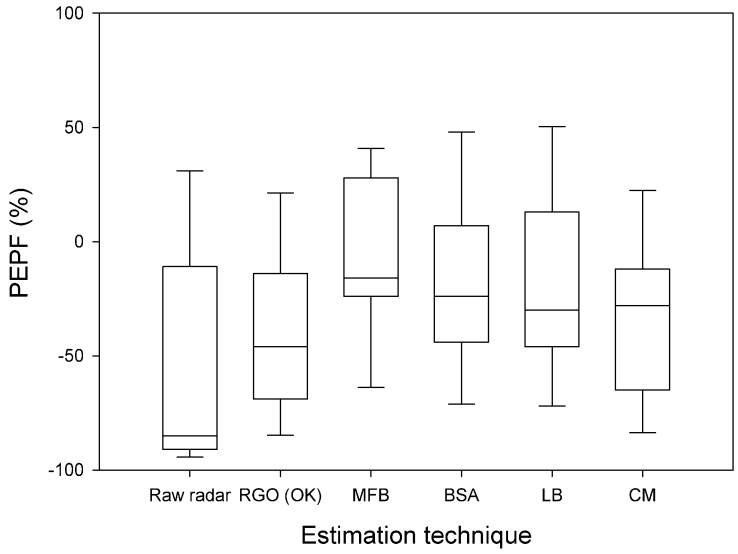

Figure 22: Box-plot based on median of the PEPF for all estimation techniques for all events analysed combined

Fig. 23 displays the box-plot for the PEV of each model driven by each individual estimation technique over all events analysed combined. The success of the MFB driven model outlined in Table 19 is attributed to the greater depth of rainfall estimated as compared to the other estimation techniques. This was evident in the PEV, with the MFB driven model providing a lower median PEV (-5%), as well as a smaller standard deviation in the PEV (29%), as compared to the other estimations techniques. The under-estimation of the total volume follows a similar trend in error to the under-estimation in the PEPF observed in Fig. 22.

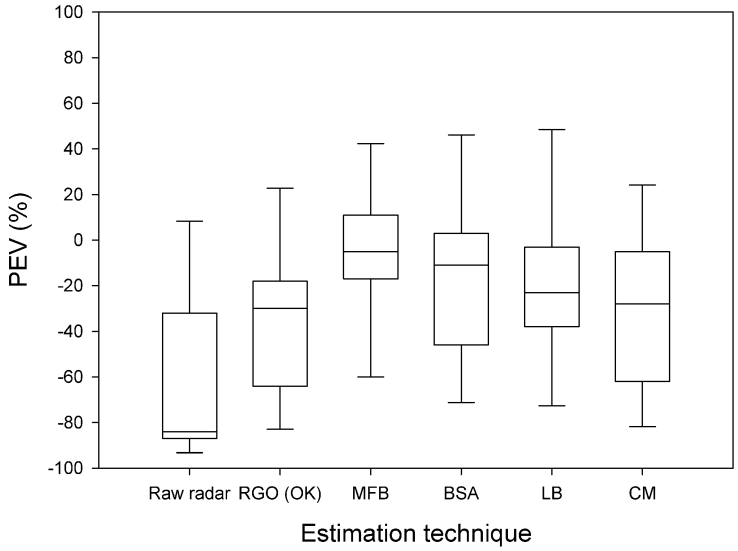

Figure 23: Box-plot based on the median of the PEV for all estimation techniques for all events analysed combined

Fig. 24 displays the box-plot for the PTE for each model driven by each individual rainfall estimation technique over the three events analysed combined. Overall, each model generally captured the shape of the observed hydrograph. Therefore, each model produced PTE values of similar magnitudes. This is attributed to each model using identical values in both the rainfall-runoff and flow routing model components.

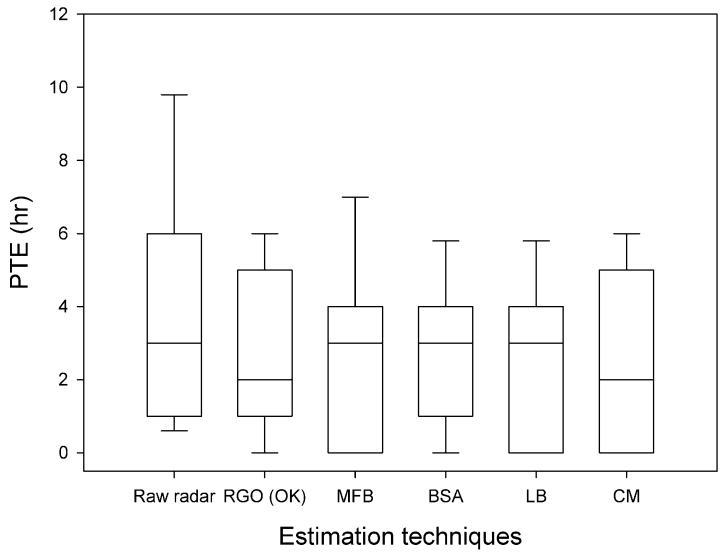

Figure 24: Box-plot based on the median of the PTE for all estimation techniques for all events analysed combined

Table 19: Median error for each estimation technique for all events analysed combined

Error Statistic	Raw Radar	RGO (OK)	MFB	BSA	LB	CM
NSE	-0.57	0.53	0.79	0.58	0.66	0.55
PEPF (%)	-85	-46	-16	-24	-30	-28
PEV (%)	-84	-30	-5	-11	-23	-28
PTE (hr)	3	2	3	3	3	2

5.6.5 Variation in storm type

In the above analysis it was evident that the success of individual gauge-radar merging methods varied depending on the storm event analysed. As displayed in Fig. 25 the storm events of 8 July 2014 and 5 September 2014 displayed similar magnitudes and trends in error for each of the merging methods. However, the trend in results varied from the analysis of the 10 September 2014 rainfall event. This storm-to-storm variation in accuracy is attributed to the possible difference in storm type (i.e., convective or frontal) and magnitude as discussed in Section 4.3.5. The success of the RGO (OK) during the 10 September 2014 rainfall event as compared to the gauge-radar merging methods is attributed to the even distribution of rainfall. Rain gauges alone can often accurately

characterize storm events of this nature. The RGO (OK) performed poorly during the 8 July 2014 and 5 September 2014 rainfall events which tended to be localized events. It was also evident that the local bias and geostatistical methods outperformed the MFB method during the 10 September 2014 event. The success of the geostatistical method (CM) is attributed to the ability of the rain gauges to properly measure the rainfall depths. The poor performance of the MFB method in comparison to the other merging methods during the 10 September 2014 rainfall event was due to substantial over-estimation of the peak flow at the St. Mary's SG and Innerkip SG. Due to the limited study duration further detailed analysis of different storm types and their effect on overall gauge-radar merging accuracy was not possible.

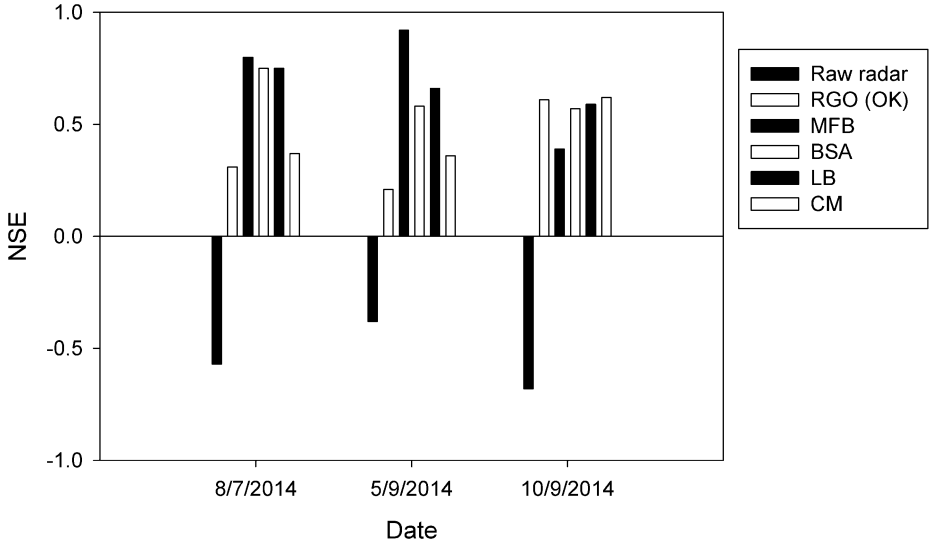

Figure 25: Median NSE for each model driven by each rainfall estimation technique at all stream gauges analysed based on storm event

5.6.6 Effect of basin characteristics

As displayed in Fig. 26 the performance of gauge-radar merging methods varied with the SG location analysed during each rainfall event. Although determining a quantifiable relationship between basin type and performance of merging method is difficult to establish, some notable trends based on the SG location analysed can be observed.

With the exception of the raw radar model, all estimation techniques performed well at the Mitchell SG over all events analysed, with the MFB, BSA and LB methods slightly outperforming the RGO (OK) and CM methods. The Mitchell SG typically produced larger increases in flows as a result of the rainfall events due to the higher percentage of cleared land and soil characteristics. The larger rainfall accumulation values measured by the MFB, BSA and CM methods over the Mitchell subbasin contributed to the success of these methods. The rain gauge network is sparse in the northern part of the watershed where the Mitchell SG is located, which contributed to the success of radar driven rainfall products over the RGO (OK) in this region. With the exception of MFB, BSA and LB methods during the 5 September 2014 rainfall event, the Byron SG consistently displayed a higher NSE for all merging methods over the three rainfall events analysed in comparison to the other SG locations. The variation in accuracy between the merging methods at the Byron SG is also less pronounced. This is attributed to two main factors: 1) the dampening of rainfall errors due to the size of the upstream catchment; and 2) the auto-correction of stream flow values at the Fanshawe Dam. As the contributing basin size increases, the errors within the flow due to errors in the rainfall field are averaged out and become less prominent (Zhu et al. 2013). The Fanshawe Dam is a major flood control structure on the North Branch of the Thames River and is situated upstream of the Byron SG. During heavy precipitation events the Fanshawe Dam can reduce flows by upwards of 50% on the North Branch. As discussed in Section 5.2.1, the reservoirs were removed in the model and replaced with a source-sink set. Consequently, the majority of the flow from the North Branch is corrected to match the observed flow at the Fanshawe Dam, which resulted in increased model efficiency at the Byron SG.

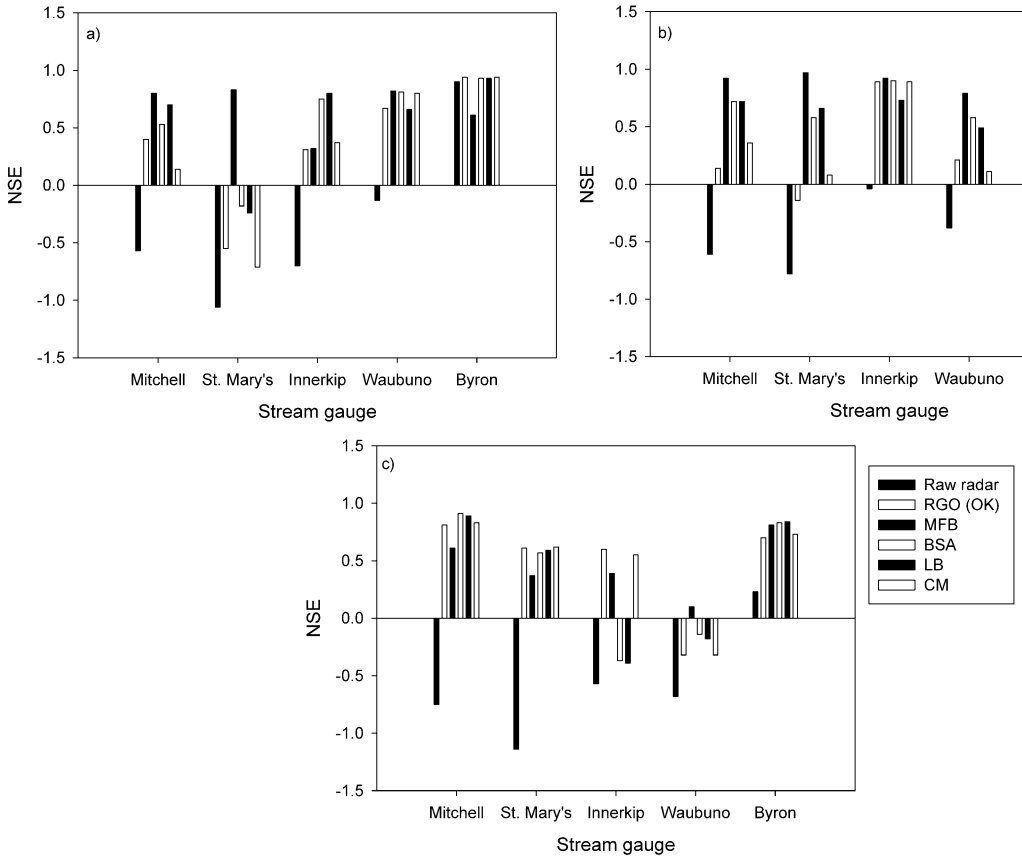

Figure 26: NSE for each model driven by each rainfall estimation technique at all stream gauges analysed for: a) 8 July 2014; b) 5 September 2014; and c) 10 September 2014

5.6.7 Rain gauge network density analysis

As discussed in Section 4.3.3, the accuracy of the estimated rainfall (and consequently, the accuracy of the predicted flows), depends on the density of the rain gauge network used in the adjustment procedures. In order to assess the effect of rain gauge network density on accuracy of predicted flows, rain gauges were systematically removed from the correction network as described in Section 4.3.3. The following three rain gauge network densities were analysed:

(1) 14 gauges (1 gauge per 244 km^2);
(2) 8 gauges (1 gauge per 427 km^2) ; and
(3) 5 gauges (1 gauge per 684 km^2).

The basin averaged rainfall for each rain gauge network density was generated and used as the rainfall input in the HEC-HMS model.

Fig. 27 presents the median NSE for each model driven by each individual rainfall estimation technique for the three rain gauge network densities considered. Results from all three rainfall events are combined in this analysis. As expected, the median model efficiency for each model decreased as the rain gauge network density decreased. In decreasing the gauge density from one gauge per 244 km^2 to one gauge per 644 km^2 the median NSE decreased from 0.53, 0.79, 0.58, 0.66 and 0.55 to 0.31, 0.46, 0.43, 0.48 and 0.25 for RGO (OK), MFB, BSA, LB and CM models, respectively. This indicates that gauge density has a considerable effect on the accuracy of the individual estimation techniques. All merging methods displayed a higher median NSE compared to raw radar alone at all gauge densities analysed in this study. This suggests that gauge-radar merging methods are still beneficial and provide a reduction in error even at lower gauge densities. The MFB correction method displayed the largest decrease in the median NSE as the gauge density decreased. Similar to the findings reported in Section 4.3.3, as the gauge density decreased the MFB, BSA and LB merging methods displayed a gradual decrease in accuracy, while the RGO (OK) and CM methods did not show a relatively large decrease in accuracy until a gauge density less than one gauge per 427 km^2 was reached. Beyond this gauge density the RGO (OK) and CM methods displayed a decrease in accuracy.

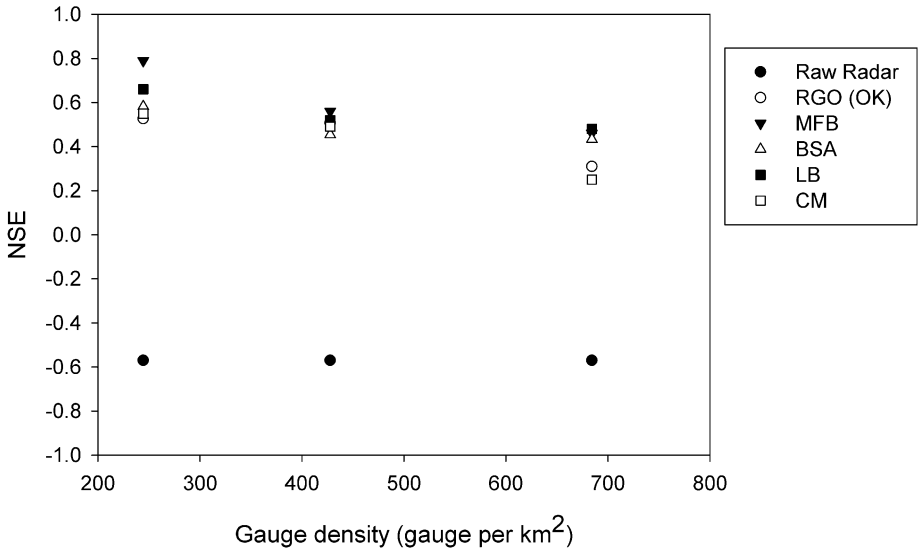

Figure 27: Rain gauge network density analysis for each model driven by each rainfall estimation technique for all events analysed combined

Chapter 6

6 Conclusions and discussion

This thesis provides a significant contribution to the water resources community. Results from this research provide a framework for analysing the addition of radar quantitative precipitation estimates (QPE) in hydrology. This research furthers the understanding of the effect of several operational, hydrological and environmental factors on the accuracy of gauge-radar merged rainfall estimates, and provides a basis for the application of radar based rainfall products in other geographic locations. This Chapter summarizes and discusses the main conclusions drawn from this thesis. The main findings from this thesis are divided into two categories:

(1) results from a comprehensive review assessing the performance of the use of rain gauges, radar and gauge-radar merging methods for quantitative precipitation estimations (Chapter 2); and
(2) results from the analysis of the effect of gauge-radar merging methods on the accuracy of rainfall estimation and hydrological modelling results (Chapters 4 and 5).

The last section of this Chapter provides recommendations for areas of future research.

6.1 Gauge-radar merging methods for quantitative precipitation estimation

Hydrological models are an important tool used in the water resources community. To develop a hydrological model that produces results with a high degree of confidence, it is imperative that the model be provided with accurate QPE as input (McMillan et al. 2011). For flood forecasting purposes in basins with rapid response times (e.g., hour(s) or less), QPE at high spatial and temporal resolutions are preferable (Gjertsen et al. 2004). Rain gauges and radar are the most widely used instruments for the near real-time collection of QPE (Sene 2013). Rain gauges directly measure rainfall intensity or accumulations at a single location and, therefore, provide relatively accurate depth measurements. Rainfall fields, however, can be highly variable in both space and time (Faures et al. 1995). Since

rain gauges only measure rainfall at a single point the spatial and temporal variability in the rainfall field is often mischaracterized. Consequently, this variability in rainfall fields can have an effect on stream flows and, therefore, the accuracy of hydrological models based on rain gauge data alone can suffer. Radar measures rainfall indirectly and remotely by measuring the reflectivity off particles within the atmosphere and converting the reflectivity to a rainfall rate based on the Marshall-Palmer relationship (Marshall and Palmer 1948). This measurement technique allows radar to accurately detect both the timing and location of rainfall, however, considerable error exists in the radar-generated depth values due to the indirect nature of the measurement (Creutin et al. 2000; Berne and Krajewski 2013). Due to the non-linearity of the transformation of rainfall to stream flow, errors in rainfall depth measurements are intensified within a hydrological model and can result in large errors in stream flow prediction (Zhu et al. 2013). Therefore, while rain gauges and radar demonstrate certain strengths, both instruments suffer from a wide variety of well-known errors which inhibit their ability to provide optimal QPE for hydrological models (Berne and Krajewski 2013).

Considering this, several methods have been developed to merge the estimates of these two instruments in order to minimize their individual weaknesses and take advantage of their respective strengths (Wilson and Brandes 1979). These methods are divided into two main categories: bias reduction techniques and error variance minimization techniques. Bias reduction techniques adjust radar rainfall estimates based on rain gauge accumulations, while error variance minimization techniques combine the two rainfall estimates. The bias reduction techniques investigated in this thesis included: mean field bias correction, Brandes spatial adjustment, local bias correction with ordinary kriging and range dependent bias reduction. The error variance minimization techniques investigated included: Bayesian data combination, conditional merging, kriging with external drift and statistical objective analysis. Following a comprehensive review of prominent gauge-radar merging methods it is evident that there is an opportunity for near real-time gauge-radar merging methods in hydrology. Several factors were identified which can considerably affect the accuracy of gauge-radar merging methods, including:

(1) gauge network design;
(2) storm type;
(3) basin characteristics;
(4) temporal resolution of adjustment; and
(5) proximity to the radar station.

These five factors have demonstrated a considerable effect on the overall accuracy of the application of a particular gauge-radar merging method (see, e.g., Kitchen and Blackall 1992; Michelson and Koistinen 2000; Kalinga and Gan 2006; Smith et al. 2007; Goudenhoofdt and Delobbe 2009; Berne and Krajewski 2013). While the application of near-real-time gauge-radar merging methods has been studied in other regions, few studies have been conducted in Canada. Clearly, the above factors suggest that the accuracy of gauge-radar merging methods depends on location-specific hydrological, environmental and operational conditions. Therefore, there exists a need to assess the performance of gauge-radar merging methods on a case-by-case basis, and to quantify the effect of these five factors on the performance of gauge-radar merging methods.

6.2 Application of gauge-radar merging methods in hydrology

In order to assess the performance of gauge-radar merging methods for hydrological applications, this thesis investigated the application of several well-known merging methods using radar data supplied by Environment Canada (EC) and the Upper Thames River basin (UTRb) in southwestern Ontario, Canada, as a case study. The following two objectives were accomplished:

(1) assessment of the effect of gauge-radar merging methods on the accuracy of estimated rainfall accumulations; and
(2) assessment of the effect of gauge-radar merging methods on the accuracy of predicted flows using a semi-distributed hydrological model.

Chapter 4 analysed the effect of gauge-radar merging methods on the accuracy of rainfall depth estimates, while Chapter 5 assessed the effect of gauge-radar merging methods on the accuracy of predicted flows using a semi-distributed hydrological model. Both

analyses were completed in the UTRb using tipping bucket (TB) rain gauges provided by the Upper Thames River Conservation Authority (UTRCA) and a corrected C-band radar product provided by the Canadian Meteorological Centre (CMC). Due to the availability of the radar rainfall product the study period was limited to the two periods between 1 June 2013 to 31 August 2013 and 1 April 2014 to 31 October 2014. Four gauge-radar merging methods were selected based on their prevalence in the literature, their operational use in other geographical locations and their ability to be implemented in near-real time in the UTRb (Gjertsen et al. 2004; Goudenhoofdt and Delobbe 2009; Berne and Krajewski 2013). The methods selected included a mean field bias correction (MFB), two spatially-dependent bias correction methods (BSA and LB) and a geostatistical merging method (CM). Both analyses were conducted on an hourly time-step. Several factors identified in Chapter 2, including rain gauge network density, time-step of adjustment, storm variation and radar range effects, were considered in the assessment of the effect of gauge-radar merging methods on rainfall accumulation accuracy. Rain gauge network density, storm variation and basin type were investigated in the assessment of the effect of gauge-radar merging methods on accuracy of predicted flows.

6.2.1 Effect of gauge-radar merging methods on rainfall accumulation accuracy

Chapter 4 investigated the effect of the gauge-radar merging methods on hourly rainfall accumulation accuracy. In the comparison of the gauge-radar merging methods to raw radar alone, each merging method provided (on average) an increase in the accuracy of the rainfall accumulation estimates. This indicates that that the accuracy of radar rainfall estimates is improved with the addition of rain gauge values for adjustment. In comparison against RGO (OK), only the MFB approach increased (on average) the accuracy of rainfall accumulation estimates. The BSA, LB and CM methods each provided (on average) rainfall accumulations with similar magnitudes of accuracy. The success of the RGO (OK) compared to the gauge-radar merging methods is attributed to the proximity of the verification gauges to the correction gauges, as well as the overall rain gauge network density used in this analysis.

Overall, the MFB method provided (on average) the best estimate of rainfall over the entire study period. The success of the MFB approach over the other gauge-radar merging methods is attributed to the one-hour time-step of adjustment. Due to the differences in the measurement techniques of rainfall by radar and rain gauges there exist spatio-temporal sampling errors that become increasingly prominent at shorter time-steps. These sampling errors can cause large fluctuations in the gauge-radar comparison. While the MFB method relies on a summation of all gauge-radar comparisons, averaging out the spatio-temporal sampling errors, these fluctuations affect the single gauge correction factors of the spatially-dependent correction methods resulting in large variations in correction accuracy. This was verified through alteration of the time-step of adjustment. These fluctuations decreased as the time-step of adjustment increased from 1 to 24 hours, and as a result, the overall error decreased. As expected, at the 24 hour time-step the spatially dependent adjustment methods outperformed the MFB method.

Correction gauges were systematically removed in order to assess the effect of rain gauge network density on the accuracy of rainfall accumulations determined by each gauge-radar merging method. As expected, the error of each gauge-radar merging method increased as the gauge-network density decreased. The MFB, BSA and LB methods displayed gradual increases in the average overall error as the gauge density decreased from one gauge per 244 km^2 to one gauge per 684 km^2. The RGO (OK) and CM methods, however, did not display an increase in the average error until a density of one gauge per 427 km^2 was reached. Once the density fell below one gauge per 427 km^2, an increase in the average error was observed for both the RGO (OK) and CM estimation techniques.

Results indicated a noticeable variation in error between events for the different gauge-radar merging methods. This trend was attributed to variations in storm type and magnitude. Range related errors were found to not be a concern in the UTRb due to the close proximity of the radar tower to all points in the watershed, verifying the assumptions of Kneble et al. (2004).

6.2.2 Effect of gauge-radar merging methods on hydrological model accuracy

Chapter 5 investigated the effect of gauge-radar merging methods on hydrological modelling accuracy. In order to accomplish this objective, each estimation technique was used as input into a semi-distributed hydrological model (HEC-HMS). The model was calibrated using RGO (OK) data for one of the largest rainfall events on record in the UTRb (a rainfall event that began on 9 July 2000).

In comparison with raw radar alone, the accuracy of the model driven by the rainfall inputs of each gauge-radar merging method significantly increased. Similar to the results from Chapter 4, this indicated that the addition of rain gauge values to adjust radar improves rainfall estimation and, therefore, model performance. In comparison with the use of RGO (OK) as input, all gauge-radar merging methods provided an increase in the median model accuracy, however, similar to Chapter 4 only the MFB driven model significantly increased model efficiency. Overall, the hydrological model driven by the MFB generated rainfall provided the best match in predicted flows to observed flows over the three rainfall events analysed combined.

As expected, as the density of the rain gauge network decreased from one gauge per 244 km^2 to one gauge per 644 km^2 the median model efficiency for each gauge-radar merging method subsequently decreased. The MFB, BSA and LB methods each displayed a gradual decrease in model accuracy. The RGO (OK) and CM methods, however, did not display a substantial decrease in accuracy until a gauge density below one gauge per 427 km^2 was reached.

In addition, variations in error between the three storm events analysed were observed. The 8 July 2014 and 5 September 2014 rainfall events displayed similar magnitudes and trends in error for each gauge-radar merging method. The same trends were not observed for the 10 September 2014 rainfall event. This variation in error is attributed to the difference in storm type and magnitude. The 8 July 2014 and 5 September 2014 rainfall events were characterized by localized rainfall, while the 10 September 2014 rainfall event was more widespread throughout the watershed. Variations in the accuracy of the

simulations were also observed to be dependent on SG location. The Mitchell SG and Byron SG generally displayed greater accuracy in modelled flows.

6.2.3 Comparison of rainfall accumulations and predicted flows

Based on examination of the trends between each analysis, it is apparent that there exist several expected similarities between the results of the two objectives. In both studies raw radar provided the worst estimation of rainfall, with the gauge-radar merging methods providing an increase in accuracy in both the estimated rainfall accumulations and predicted flows. The MFB method (on average) provided the best estimate of rainfall accumulations and predicted flows. In general, the performance of the BSA, LB and CM methods were found to be similar between the two analyses. In the analysis of rainfall accumulations the BSA, LB and CM methods provided (on average) estimates with similar or worse magnitudes of error as compared to RGO (OK), with no substantial difference between the estimates. Similarly, in the analysis of predicted flows these three methods were unable to provide statistically superior results over the model driven by RGO (OK).

Due to the non-linearity of the transformation of rainfall to runoff, errors within the rainfall estimates were more pronounced during the hydrological model simulations. This lead to larger discrepancies in the difference between the accuracy of each merging method during the assessment of predicted flows over the assessment of rainfall accumulations. Small errors in rainfall estimates can be increased in a hydrological model and can cause substantial variations in the accuracy of model predictions. These errors can cause considerable issues in the operational use of the model. Therefore, in assessing the accuracy of rainfall estimates it is recommended that they be used as input in a hydrological model rather than only assessing rainfall accumulations.

6.3 Recommendations for future research

The following are recommendations suggested for future research in this area.

(1) Extend the timeframe of the study period to increase the number of rainfall events analysed. This study period was limited due to the availability of corrected C-

band radar from the CMC. Therefore, variations in individual storm events have a larger influence on the average error of each merging method, which can skew the results. Extending the study period in order to analyse a larger base of rainfall events will reduce the effect that a single outlier event has on the overall error of each estimation technique.

(2) Investigate the effect of gauge-radar merging schemes at higher temporal resolutions. Decreasing the time-step of adjustment to 15 minutes will reduce the signal treatment of the raw radar (i.e., correction for AP). However, in small urban watersheds both the timing and location of rainfall is extremely important in modelling the resulting stream flow. As observed at the Byron SG, the HEC-HMS model missed the timing of the initial urban peak. Increasing the temporal resolution of the data is especially important in urban catchments where flash flooding is a major cause of damage.

(3) Categorize the storm events based on storm type to quantify this effect in the UTRb. Previous studies have indicated that storm type can have a considerable effect on radar rainfall accuracy. This analysis has indicated a variation in accuracy between storm events.

(4) Investigate the effect of gauge-radar merged rainfall estimates on the accuracy of predicted flows using a continuous hydrological model. Continuous models can offer additional information on watershed conditions over longer time-frames.

(5) Assess the effect of using gauge-radar merged rainfall estimates on predicted water surface elevations through use of a hydraulic model. By taking the results of the hydrological model and using them in a hydraulic model, the potential increase in the accuracy of water surface elevations can be examined.

References

Babish, G. 2000. *Geostatistics without tears: A pratical guide to geostatistics, Variograms and Kriging.* Regina, SK: Environment Canada: Ecological Research Division.

Barge, B.L., R.G. Humphries, S.J. Mah, and W.K. Kuhnke. 1979. Rainfall measurements by weather radar: applications to hydrology. *Water Resources Research* 15 (6): 1380-1386. doi: 10.1029/WR015i006p01380.

Barnes, S.L. 1964. A technique for maximizing details in numerical weather-map analysis. *Journal of Applied Meteorology* 3 (4): 396-409. doi: 10.1175/1520-0450(1964)003<0396:ATFMDI>2.0.CO;2.

Bell, V.A., and R.J. Moore. 1998. A grid-based distributed flood forecasting model with weather radar data: part 2 case studies. *Hydrology and Earth System Sciences* 2:265-281. doi: 10.5194/hess-2-283-1998.

Berne, A., and W.F. Krajewski. 2013. Radar for hydrology: unfulfilled promise or unrecognized potential? *Advances in Water Resources* 51:357-366. doi: 10.1016/j.advwatres.2012.05.005.

Beven, K. 2002. Towards an alternative blueprint for a physically based digitally simulated hydrologic response modelling system. *Hydrological Processes* 16 (2): 189-206. doi: 10.1002/hyp.343.

Beven, K.J., and G.M. Hornberger. 1982. Assessing the effect of spatial pattern of precipitation in modelling stream flow hydrographs. *Journal of the American Water Resource Association* 18 (5): 823-829. doi: 10.1111/j.1752-1688.1982.tb00078.x.

Biggs, E.M., and P.M. Atkinson. 2011. A comparison of gauge and radar precipitation data for simulating an extreme hydrological event in Severn Uplands, UK. *Hydrological Processes* 25 (5): 795-810. doi: 10.1002/hyp.7869.

Boodoo, S., D. Hudak, A. Ryzhkov, P. Zhang, N. Donaldson, and J. Reid. 2014. Quantitative precipitation estimation from C-band dual-polarized radar for the July 8th 2013 flood in Toronto, Canada. *ERAD - The Eighth European Conference on Radar in Meteorology and Hydrology*, Eds. K. Helmert and M. Hagen, 7pp. Garmisch-Partenkirchen, Germany: ERAD.

Borga, M. 2002. Accuracy of radar rainfall estimates for streamflow simulation. *Journal of Hydrology* 267:26-39. doi: 10.1016/S0022-1694(02)00137-3.

Borga, M., E.N. Anagnostou, and E. Frank. 2000. On the use of real-time radar estimates for flood predictions in mountainous basins. *Journal of Geophysical Research* 105 (D2): 2269-2280. doi: 10.1029/1999JD900270.

Borga, M., F. Tonelli, R.J. Moore, and H. Andrieu. 2002. Long-term assessment of bias adjustment in radar rainfall estimation. *Water Resources Research* 38 (11): 1226. doi: 10.1029/2001WR000555.

Brandes, E.A. 1975. Optimizing rainfall estimates with the aid of radar. *Journal of Applied Meteoology* 14 (7): 1339-1345. doi: 10.1175/1520-0450(1975)014<1339:OREWTA>2.0.CO;2.

Cole, S.J., and R.J. Moore. 2008. Hydrological modelling using raingauge and radar-based estimators of areal rainfall. *Journal of Hydrology* 358 (3-4): 159-181. doi: 10.1016/j.jhydrol.2008.05.025.

Collier, C.G. 1986. Accuracy of rainfall estimates by radar part II: Comparison with raingauge network. *Journal of Hydrology* 83 (3): 225-235. doi: 10.1016/0022-1694(86)90153-8.

Creutin, J.D., M. Borga, and J. Joss. 2000. Hydrometeorology: Storms and flash floods. In *mountainous natural hazards*, ed. F. Gillet and F. Zanolini, 349-366. Grenoble, France: Cemagref Edt.

Cunderlik, J., and S. Simonovic. 2004. *Selection of calibration and verification data for the HEC-HMS hydrologic model.* Project Report, London, Ontario: The University of Western Ontario.

Daley, R. 1991. *Atmospheric data analysis.* Cambridge: Cambridge University Press.

Dingman, S. Lawrence. 2008. *Physical Hydrology, 2nd Edition.* Long Grove, Illinois, USA: Waveand Press.

Environment Canada. 2014. *Canada's top ten weather stories for 2013: Alberta's Flood of Floods*. http://www.ec.gc.ca/meteo-weather/default.asp?lang=En&n=5BA5EAFC-1&offset=2&toc=hide. (accessed May 26, 2015).

Environment Canada. 2013a. *Cost of flooding*. http://www.ec.gc.ca/eau-water/default.asp?lang=En&n=02A71110-1. (accessed September 30, 2013).

—. 2013b. *Causes of flooding.* https://www.ec.gc.ca/eau-water/default.asp?lang=En&n=E7EF8E56-1. (accessed February 27, 2014).

—. 2013c. *Weather and meteorology*. http://www.ec.gc.ca/meteo-weather/default.asp?lang=En&n=108C6C74-1. (accessed May 25, 2014).

—. 2013d. *About radar.* http://www.ec.gc.ca/meteo-weather/default.asp?lang=En&n=2B931828-1. (accessed September 24, 2013).

Environment Canada. 2009. *Devices using ultra-wideband (UWB) technology*. Radio Standards Specification 220, Issue 1, Ottawa: Environment Canada. https://www.ic.gc.ca/eic/site/smt-gst.nsf/vwapj/smse-007-09-EC-comments.pdf/$FILE/smse-007-09-EC-comments.pdf (accessed May 7, 2014).

Erdin, R. 2009. Combining rain gauge and radar measurements of a heavy precipitation event over Switzerland: Comparison of geostatistical methods and investigation of important influencing factors. *Veroffentlichungen der MeteoSchweiz* 81, 108 pp. Zurich, Switzerland.

Faures, J.M., D.C. Goodrich, D.A. Woolhiser, and S. Sorooshian. 1995. Impact of small-scale spatial rainfall variability on runoff modeling. *Journal of Hydrology* 173 (1-4): 209-326. doi: 10.1016/0022-1694(95)02704-S.

Fortin, V., G. Roy, and N. Donaldson. 2014. Assimilation of radar QPE in the Canadian Precipitation Analysis (CaPA). *In ASCE International Symposium on Weather Radar and Hydrology,* eds. C. Pathak and R. Teegavarapu, 10 pp. Washington DC: American Society of Civil Engineers.

Gandin, L.S. 1965. Objective analysis of meteorological fields. *Gidrometeorologicheskoe Izdatel'stvo (GIMIZ),* Leningrad Trans. by Israel Program for Scientific Translations: Jerusalem, Ed. R. Hardin, 242 pp.

Garcia-Pintado, J., G.G. Barbera, M. Erena, and V.M. Castillo. 2009. Rainfall estimation by rain gauge-radar combination: a concurrent multiplicative-additive approach. *Water Resources Research* 45 (1): 1-15. doi: 10.1029/2008WR007011.

Gerstner, E.M., and G. Heinemann. 2008. Real-time areal precipitation determination from radar by means of statistical objective analysis. *Journal of Hydrology* 352 (3-4): 296-308. doi: 10.1016/j.jhydrol.2008.01.016.

Gjertsen, U., M. Salek, and D.B. Michelson. 2004. Gauge adjustment of radar-based precipitation estimates in Europe. Procceding of ERAD 2004. 7-11.

Golding, B.W. 2009. Uncertainty propagation in a London flood simulation. *Journal of Flood Risk Management* 2 (1): 2-15. doi: 10.1111/j.1753-318X.2008.01014.x.

Goudenhoofdt, E. and L. Delobbe. 2009. Evaluation of radar-gauge merging methods for quantatative precipitation estimates. *Hydrology and Earth Systems Science* 13:195-203. doi:10.5194/hess-13-195-2009.

Government of Canada. 2014. *Climate - Daily data report for July 2013.* http://climate.weather.gc.ca/climateData/dailydata_e.html?timeframe=2&Prov=ON&StationID=51459&dlyRange=2013-06-13|2014-08-26&Year=2013&Month=7&Day=01.(accessed August 27, 2014).

Habib, E., E. Meselhe, and A. Aduvala. 2008. Effect of local errors of tipping bucket rain gauges on rainfall-runoff simulations. *Journal of Hydrologic Enginering* 13 (6): 488-496. doi: 10.1061/(ASCE)1084-0699(2008)13:6(488).

Hamill, M. 1998. Hypothesis tests for evaluating numerical precipitation forecasts. *Weather and Forecasting* 2 (14): 155-167. doi: 10.1175/1520-0434(1999)014<0155:HTFENP>2.0.CO;2.

Hanchoowong, R., U. Weesakul, and S. Chumchean. 2012. Bias correction of radar rainfall estimates based on geostatistical technique *Science Asia* 38:373-385. doi: 10.2306/scienceasia1513-1874.2012.38.373.

Hayter, A. 2007. *Probability and statistics for engineers and scientists, third edition*. Belmont, California, USA: Thompson Brooks/Cole.

Hengl, T., G.B.M Heuvelink, and A. Stein. 2003. *Comparison of kriging with external drift and regression-kriging.* Technical Note, ITC, Available on-line at http://www.itc.nl/library/Papers_2003/misca/hengl_comparison.pdf.

Hitschfeld, W., and J. Bordan. 1954. Errors inherent in radar measurements of rainfall at attenuating wavelengths. *Journal of Meteorology* 11 (1): 58-67. doi: 10.1175/1520-0469(1954)011<0058:EIITRM>2.0.CO;2.

Hossain, F., E.N. Anagnostou, T. Dinku, and M. Borga. 2004. Hydrological model sensitivity to parameter and radar rainfall estimation uncertainty. *Hydrological Processes* 18 (17): 3277-3291. doi: 10.1002/hyp.5659.

Huff, F.A. 1970. Sampling errors in measurements of mean precipitation. *Journal of Applied Meteorology* 9 (1): 35-44. doi: 10.1175/1520-0450(1970)009<0035:SEIMOM>2.0.CO;2.

Insurance Bureau of Canada. 2015. *2015 facts of the property and casualty insurance industry in Canada*. Insurance Bureau of Canada, Toronto, Canada.

James, W.P., C.G. Robinson, and J.F. Bell. 1993. Radar-assisted real-time flood forecasting. *Journal of Water Resources Planning and Management* 119 (1): 32-44. doi: 10.1061/(ASCE)0733-9496(1993)119:1(32).

Jayakrishnan, R., R. Srinivasan, and J.G. Arnold. 2004. Comparison of raingage and WSR-88D Stage III precipitation data over the Texas-Gulf basin. *Journal of Hydrology* 292:135-152. doi: 10.1016/j.jhydrol.2003.12.027.

Jung, Y., H. Kim, J. Baik, and M. Choi. 2014. Rain-gauge evaluations using spatiotemporal correlation structure for semi-mountainous regions. *Terrestrial Atmospheric and Oceanic Sciences Journal* 25 (2): 267-278. doi: 10.3319/TAO.2013.10.31.01(Hy).

Kalinga, O.A., and T.Y. Gan. 2006. Semi-distributed modelling of basin hydrology with radar and gauged precipitation. *Hydrological Processes* 20 (17): 3725-3746. doi: 10.1002/hyp.6385.

Kampata, J.M., B.P. Parida, and D.B. Moalafhi. 2008. Trend analysis of rainfall in the headstreams of the Zambezi River basin in Zambia. *Physics and Chemistry of the Earth* 8-13 (33): 621-625. doi: 10.1016/j.pce.2008.06.012.

Kim, B.S., B.K. Kim, and H.S. Kim. 2008. Flood simulation using the gauge-adjusted radar rainfall and physics-based distributed hydrologic model. *Hydrological Processes* 22 (22): 4400-4414. doi: 10.1002/hyp.7043.

Kitchen, M., and R.M. Blackall. 1992. Representativeness errors in comparisons between radar and gauge measurements of rainfall. *Journal of Hydrology* 134: 13-33.

Kneble, M.R., Z.L. Yang, K. Hutchison, and D.R. Maidment. 2005. Regional scale flood modeling using NEXRAD rainfall, GIS and HEC-HMS/RAS: a case study for the San Antonio River basin summer 2002 storm event. *Journal of Environmental Management* 75: 325-336. doi: 10.1016/j.jenvman.2004.11.024.

Koistinen, J., and T. Puhakka. 1981. "An imporved spatial gauge-radar adjustment technique." In *Preprints. 20th Conference on Radar Meteorology*, 179-186. American Meteorological Society.

Kouwen , N. 1988. WATFLOOD: A micro-computer based flood forecasting system based on real-time weather radar. *Canadian Water Resources Journal* 13 (1): 62-77. doi: 10.4296/cwrj1301062.

Kouwen, N., and G. Garland. 1989. Resolution considerations in using radar rainfall data for flood forecasting. *Canadian Journal of Civil Engineering* 16:279-289.

Kovacs, P., S. Guilbault, and D. Sandink. 2014. *Cities adapt to extreme rainfall; celebrating local leadership.* Institute for Catastrophic Loss Reduction. http://www.iclr.org/images/CITIES_ADAPT_DIGITAL_VERSION.compressed.pdf. (accessed March 6, 2015).

Krajewski, W.F. 1987. Cokriging of radar-rainfall and rain gauge data. *Journal of Geophysical Research* 92 (D8): 9571-9580. doi: 10.1029/JD092iD08p09571.

Krajewski, W.F., G. Villarini, and J.A. Smith. 2010. Radar-rainfall uncertainties: Where are we after thirty years of effort. *Bulletin of the American Meteorological Society* 91 (1): 87-94. doi: 10.1175/2009BAMS2747.1.

Krause, P., D.P. Boyle, and F. Base. 2005. Comparison of different efficiency criteria for hydrological model assessment. *Advances in Geosciences* 5, 89-97.

Lane, R.J. 1999. *The Water Survey of Canada hydrometric technician career development program. Lesson package No. 10.1: principles of discharge measurement*. Fredericton, New Brunswick: Water Survey of Canada, Environment Canada.

Larson, L.W., and E.L. Peck. 1974. Accuracy of precipitation measurements for hydrological modeling. *Water Resources Research* 10 (4): 857-863. doi: 10.1029/WR010i004p00857.

Lobligeois, F., V. Andreassian, C. Perrin, P. Tobary, and C. Loumagne. 2014. When does higher spatial resolution rainfall information improve streamflow simulation? An evaluation of 3620 flood events. *Hydrology and Earth Systems Science* 18:575-594. doi: 10.5194/hess-18-575-2014.

Looper, J.P., and B.E. Vieux. 2012. An assessment of distributed flash flood forecasting accuracy using radar and rain gauge input for a physics-based distributed hydrologic model. *Journal of Hydrology* 412:114-132. doi: 10.1016/j.jhydrol.2011.05.046.

Mahfouf, J.F., B. Brasnett, and S. Gagnon. 2007. A Canadian precipitation analysis (CaPA) project: Description of preliminary results. *Atmosphere-Ocean* 45 (1): 1-17. doi: 10.3137/ao.v450101.

Mann, H.B., and D.R. Whitney. 1947. On a test of whether one of two random variables is stochastically larger than the other. *Institute of Mathematical Statistics* 18 (1): 50-60.

Marshall, J.S., and W.M. Palmer. 1948. The distribution of raindrops with size. *Journal of Meteorology* 5:165-166. doi: 10.1175/1520-0469(1948)005<0165:TDORWS>2.0.CO;2.

McClure, M, and T Howell. 2013. Forecast failure: How flood warnings came too late for southern Albertans. *Calgary Herald*, December 31.

McMillan, H., B. Jackson, M. Clark, D. Kavetski, and R. Woods. 2011. Rainfall uncertainty in hydrological modeling: An evaluation of multiplicative error models. *Journal of Hydrology* 400 (1-2): 83-94. doi: 10.1016/j.jhydrol.2011.01.026.

Michelson, D.B., and J. Koistinen. 2000. Gauge-Radar Network Adjustment for the Baltic Sea Experiment. *Physics and Chemistry of the Earth* 25 (10-12): 915-920. doi: 10.1016/S1464-1909(00)00125-8.

Michelson, D.B., T. Andersson, J. Koistinen, C.G. Collier, J. Riedl, J. Szturc, U. Gjertsen, A. Nielsen, and S. Overgaard. 2000. *BALTEX radar data center products and their methodologie,*. SMHI Reports Meteorology and Climatology RMK Nr. 90, SMHI, SE-601 76. Norrkoping, Sweeden: SMHI.

Moore, R. J., B. C. Watson, D. A. Jones, K. B. Black, M. A. Haggett, M. A. Crees, C. Richards. 1989. Towards an improved system for weather radar calibration and rainfall forecasting using raingauge data from a regional telemetry system. In New directions for surface water modelling. Proceedings of the 3rd Scientific Assemble IAHS, ed. M.L. Kavvas, 13-21. IAHS Publication no. 181. Baltimore, MD.

Morin, E., R.A. Goodrich, R.A. Maddox, X. Gao, H.V. Gupta, and S. Sorooshian. 2006. Spatial patterns in thunderstorm rainfall events and their coupling with watershed hydrological response. *Advances in Water Resources* 29 (6): 843-860. doi: 10.1016/j.advwatres.2005.07.014.

Nash, J.E., J.V. Sutcliffe. 1970. River flow forecasting through conceptual models: 1: Discussion of principles. *Journal of Hydrology* 10 (3): 282-290.

National Oceanic and Atmospheric Administration. 2015. *National Weather Service Glossary*. http://w1.weather.gov/glossary/. (accessed August 10, 2015).

Neary, V.S., E. Habib, and M. Fleming. 2004. Hydrologic modeling with NEXRAD precipitation in middle Tennesee. *Journal of Hydrologic Engineering* 9 (5): 339-349. doi: 10.1061/~ASCE!1084-0699~2004!9:5~339!

Pardo-Iguzquiza, E. 1998. Optimal selection of number and location of rainfall gauges for areal rainfall estimation using geostatistics and simulated annealing. *Journal of Hydrology* 210: 206-220.

Pereira, A.J., K.C. Crawford, and C.L. Hartzell. 1998. Improving WSR-88D hourly rainfall estimates. *Weather and Forecasting* 13:1016-1028.

Pettazzi, A., and S. Salson. 2012. Combining radar and rain gauges rainfall estimates using conditional merging: A case study. In *The Seventh European Conference on Radar in Meteorology and Hydrology.* Santiago de Compostela, Spain: MeteoGalicia, Galician Weather Service.

Rodriguez-Iturbe, I., and J.M. Mejia. 1974. The design of rainfall networks in time and space. *Water Resources Research* 10 (4): 713-728. doi: 10.1029/WR010i004p00713.

Sandink, D., P. Kovacs, G. Oulahen, and G. McGillvray. 2010. *Making floods insurable for Canadian homeowners.* A Discussion Paper, Toronto: Institute for Catastrophic Loss Reduction & Swiss Reinsurance Company Ltd.

Schilling, W., and L. Fuchs. 1986. Errors in stormwater modeling - a quantitative assessment. *Journal of Hydraulic Engineering* 112 (2): 111-123.

Schuurmans, J.M., M. F.P. Bierkens, E.J. Pebesma, and R. Uijlenhoet. 2007. Automatic prediction of high-resolution daily rainfall fields for multiple extents: the potential of operational radar. *Journal of Hydrometeorology* 8 (6): 1204-1224. doi: 10.1175/2007JHM792.1.

Sene, K. 2013. "Chapter 2: Precipitation measurement." In *Flash floods: forecasting and warning*, 33-67. http://download.springer.com/static/pdf/793/bok%253A978-94-007-5164
4.pdf?auth66=1418140762_5083b2dd411c7f5ccec85b79b605c4e2&ext=.pdf: Springer. (accessed December 9, 2014)

Seo, D.J., and J.P. Breidenbach. 2002. Real-time correction of spatially nonuniform bias in radar rainfall data using rain gauge measurements. *Journal of Hydrometeorology* 3 (2): 93-111. doi: 10.1175/1525-7541(2002)003<0093:RTCOSN>2.0.CO;2.

Shabbar, A., B. Bonsal, and M. Khandekar. 1997. Canadian precipitation patterns associated with the southern oscillation. *Journal of Climate* 10: 3016-3027. doi: 10.1175/1520-0442(1997)010<3016:CPPAWT>2.0.CO;2.

Sinclair, S., and G. Pegram. 2005. Combining radar and rain gauge rainfall estimates using conditional merging. *Atmospheric Science Letters* 6 (1): 19-22. doi: 10.1002/asl.85.

Smith, J.A., M.L. Baeck, K.L. Meierdiercks, A.J. Miller, and W.F. Krajewski. 2007. Radar rainfall estimation for flash flood forecasting in small urban watersheds. *Advances in Water Resources* 30 (10): 2087-2097. doi: 10.1016/j.advwatres.2006.09.007.

Steiner, M, and J.A. Smith. 2000. Reflectivity, rain rate, and kinetic energy flux relationship based on raindrop spectra. *Journal of Applied Meteorology* 39 (11): 1923-1940. doi: 10.1175/1520-0450(2000)039<1923:RRRAKE>2.0.CO;2.

Steiner, M., J.A. Smith, S J. Burges, C.V. Alonso, and R.W. Darden. 1999. Effect of bias adjustment and rain gauge data quality control on radar rainfall estimation. *Water Resources Research* 35 (8): 2487-2503. doi: 10.1029/1999WR900142.

Stellman, K.M., H.E. Fuelberg, R. Garza, and M. Mullusky. 2001. An examination of radar rain gauge derived mean areal precipitation over Georgia watersheds. *Weather and Forecasting* 16 (1): 133-144.

Takeuchi, K. 2001. Increasing vulnerability to extreme floods and societal needs of hydrological forecasting. *Hydrological Sciences Journal* 46 (6): 869-881. doi: 10.1080/02626660109492882.

Tao, T., B. Chocat, S. Liu, and X. Kunlan. 2009. Uncertainty analysis of interpolation methods in rainfall spatial distribution - a case study of small catchment in Lyon. *Journal of Environmental Protection* 1:50-58.

Thistlethwaite, J., and B. Feltmate. 2013. *Assessing the viability of overland flood insurance: the residential property market.* Waterloo, ON: University of Waterloo and The Co-operators Group Limited.

Todini, E. 2001. A Bayesian technique for conditioning radar precipitation estimates to rain-gauge measurements. *Hydrology and Earth System Sciences* 5 (2): 187-199. doi: 10.5194/hess-5-187-2001.

Upper Thames River Conservation Authority. 2015. *Fanshawe Dam and Reservoir*. http://thamesriver.on.ca/water-management/flood-control-structures/fanshawe-dam/. (accessed June 17, 2015).

Upper Thames River Conservation Authority. 2012. *Upper Thames River Watershed Report Cards*. London, Ontario: UTRCA.

USACE, 2013. *Hydrologic Modeling System HEC-HMS*. User's Manual. US Army Corps of Engineers, Hydrologic Engineering Center.

USACE, 1996. Hydrologic aspects of flood warning - Preparedness programs. Technical Letter 1110-2-540, Washington, DC.

Vehvilainen, B., M.K. Cauwenberghs, J-L. Cheze, A. Jurczyk, R.J. Moore, J. Olsson, M. Salek, and J. Szturc. 2004. Evaluation of operational flow forecasting systems that use weather radar. SMHI. http://www.smhi.se/cost717/doc/WDD_01_200408_1.pdf. (accessed January 6, 2014).

Vieux, B.E., and P.B. Bedient. 1998. Estimation of rainfall for flood prediction from WSR-88D reflectivity: A case study. *Weather and Forecasting* 13 (2): 407-415. doi: 10.1175/1520-0434(1998)013<0407:EORFFP>2.0.CO;2.

Volkmann, T., S. Lyon, H. Grupta, and P. Troch. 2010. Multi-criteria design of rain gauge networks for flash flood predicton in semi-arid catchments with complex terrain. *Water Resources Research* 46 (11): W1554. doi: 10.1029/2010WR009145.

Vuerich, E., C. Monesi, L.G. Lanza, L. Stagi, and E. Lanzinger. 2009. *WMO field intercomparison of rainfall intensity gauges.* Report No. 99, Vigna die Valle, Italy: World Meteorological Organization.

Wackernagel, H. 2003. *Multivariate geostatistics: An introduction with applications.* New York, New York: Springer.

Wang, L., S. Ochoa, N. Simoes, C. Onof, and C. Maskisimovic. 2013. Radar-raingauge data combination techniques: A revision and analysis of their suitability for urban hydrology. *Water Science and Technology* 68 (4): 737-747. doi: 10.2166/wst.2013.300.

Wilcox, I, C. Quinlan, C. Rogers, M. Troughton, I. McCallum, A. Quenneville, E. Heagy, and D. Dool. 1998. *The Thames River Watershed: Background study for nomination under the Canadian heritage rivers system.* London: Upper Thames River Conservation Authority.

Wilcoxon, F. 1945. Individual comparisons by ranking methods. *Biometric Bulletin* 1 (6): 80-83.

Wilson, J.W. 1970. Integration of radar and rain gauge data for improved rainfall measurement. *Journal of Applied Meteorology* 9 (3): 489-497. doi: 10.1175/1520-0450(1970)009<0489:IORARD>2.0.CO;2.

Wilson, J.W., and E.A. Brandes. 1979. Radar measurement of rainfall - a summary. *Bulletin of the American Meteorological Society* 60 (9): 1048-1058. doi: 10.1175/1520-0477(1979)060<1048:RMORS>2.0.CO;2.

World Meteorological Organization (WMO). 2008. Chapter 3: Precipitation measurement. In Guide to hydrological practices, Volume 1: Hydrology – From measurement to hydrological information, ed. C. Collier, 1.3-1–1.3-30. Geneva, Switzerland: World Meteorological Organization.

Xiaoli, J., C.Y. Xu, Q. Zhang, V.P. Singh. 2010. Parameter and modeling uncertainty simulated by GLUE and a formal Bayesian method for a conceptual hydrologic

model. *Journal of Hydrology* 383 (3-4): 147-155. doi: 10.1016/j.jhydrol.2009.12.028.

Xie, H., X. Zhou, J.M.H. Hendrick, E.R. Vivoni, H. Guan, Y.Q. Tian, and E.E. Small. 2006. Evaluation of NEXRAD stage III precipitation data over a semiarid region. *Journal of the American Water Resources Association* 42 (1): 237-256. doi: 10.1111/j.1752-1688.2006.tb03837.x.

Xu, H., C.Y. Xu, H. Chen, Z. Zhang, and L. Li. 2013. Assessing the influence of rain gauge density and distribution on hydrological model performance in a humid region of China. *Journal of Hydrology* 505:1-12. doi: 10.1016/j.jhydrol.2013.09.004.

Zhu, D., D.Z. Peng, and I.D. Cluckie. 2013. Statistical analysis of error propagation from radar rainfall to hydrological models. *Hydrology and Earth System Sciences* 17:1445-1453. doi: 10.5194/hess-17-1445-2013.

Appendices

The following appendices provides additional figures and text not included in the main body of the thesis.

Appendix A: Qualitative analysis of rainfall estimation techniques

a)

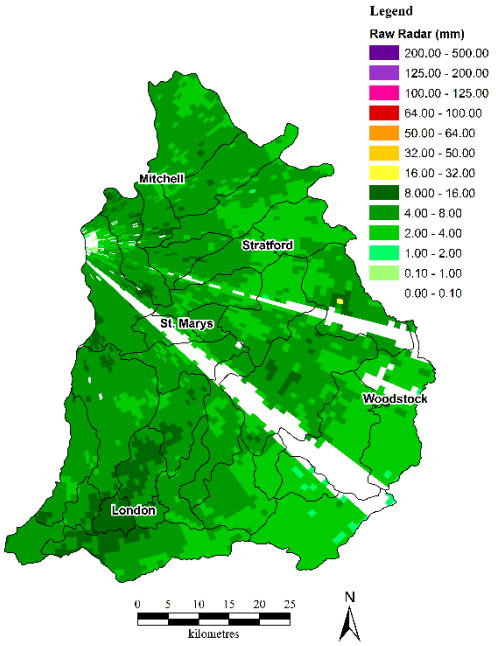

b)

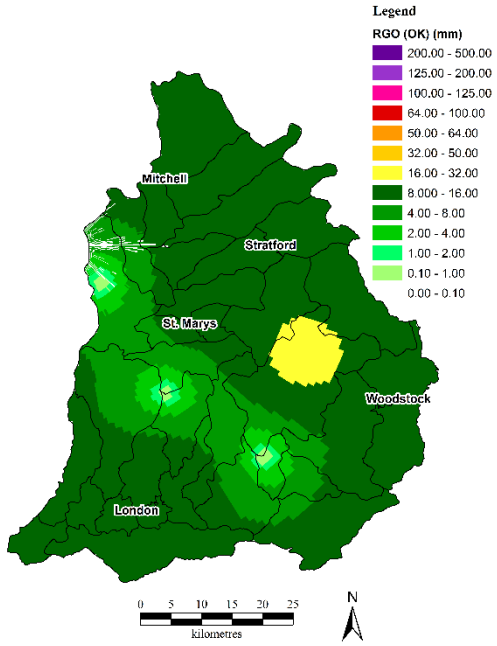

c)

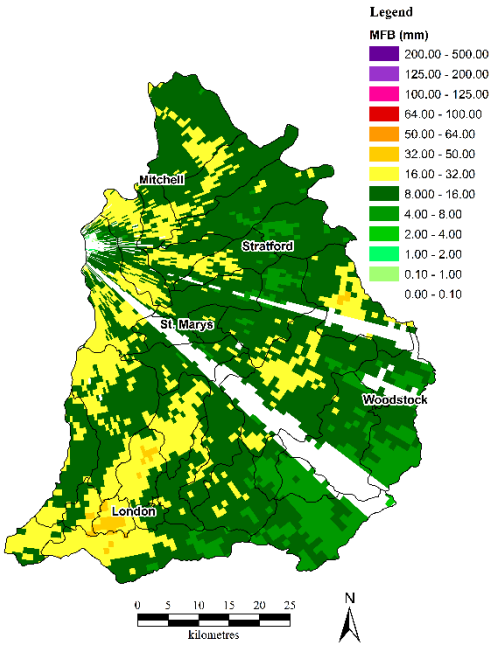

d)

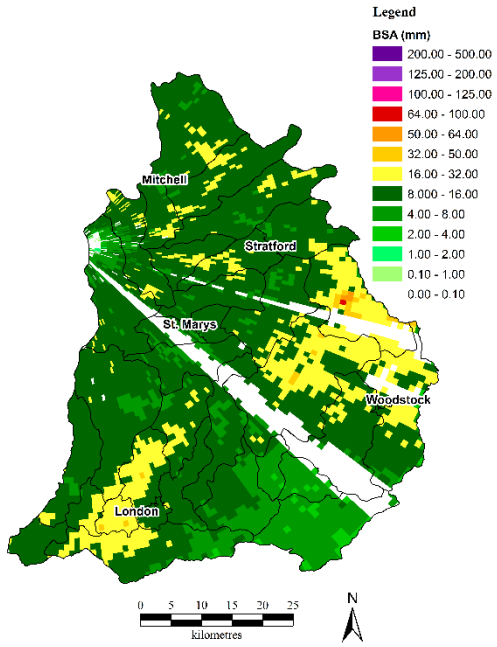

e) f)

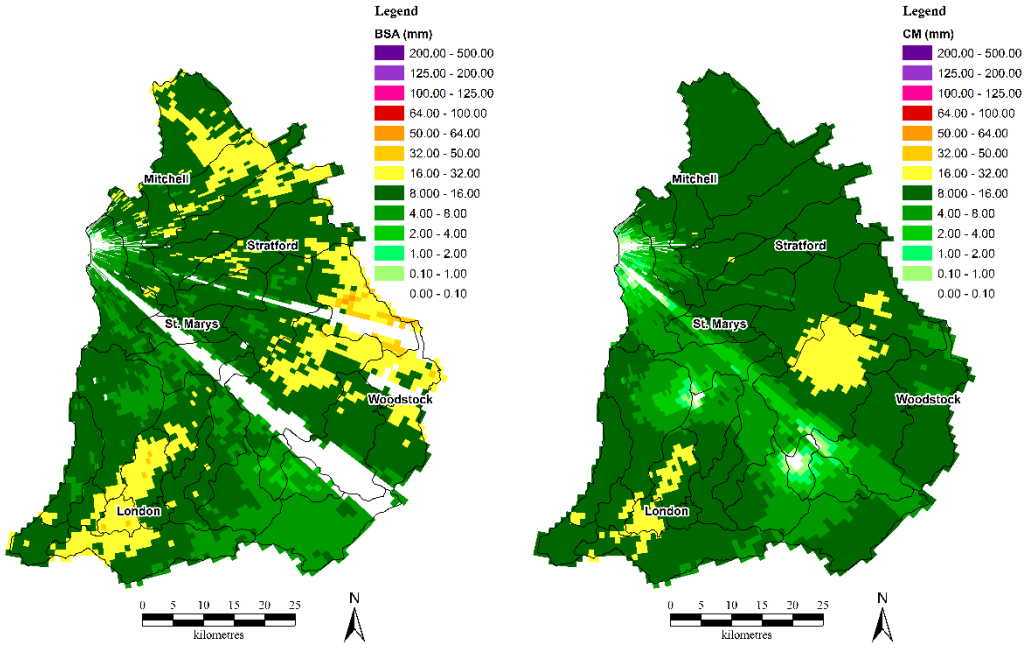

Figure 28: Hourly rainfall accumulations for the hour of 22:00 (UTC) on 10 September 2014 for: a) Raw radar; b) RGO (OK); c) MFB; d) BSA; e) LB; and f) CM

Appendix B: Rainfall accumulation error based on individual event analysis

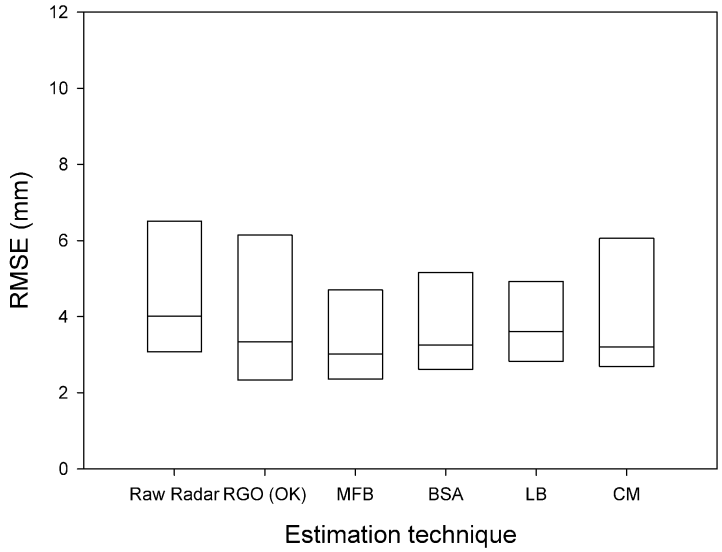

Figure 29: Box-plots based on the median of the RMSE for all individual events combined

Table 20: Error for each rainfall estimation technique for all events analysed

Event	RMSE (mm)					
	Raw radar	RGO (OK)	MFB	BSA	LB	CM
28 June 2013	3.110	3.672	2.195	2.890	3.060	3.535
31 July-August 2013	4.524	2.175	2.834	5.440	5.146	1.932
20-21 May 2014	4.740	6.169	2.968	2.767	2.819	6.516
7 July 2014	30.60	3.002	5.002	3.614	4.252	2.795
8 July 2014	3.490	2.806	3.065	2.567	2.836	3.055
27-28 July 2014	1.782	2.011	1.827	1.918	1.754	2.650
5-6 September 2014	10.608	7.082	6.787	7.179	7.610	8.208
10-11 September 2014	7.100	6.062	3.789	4.320	4.157	4.688

Appendix C: Summary of the calibrated RGO (OK) hydrological model parameters

Table 21: Initial loss model parameters for the RGO (OK) calibrated model

Basin #	Basin name	Area (km^2)	Loss model (Initial and Constant)		
			Initial abstraction (mm)	Constant rate (mm/hr)	% Impervious
1	N. Thames R. above Whirl Cr.	176	5	2	0
2	Whirl Cr. @ N. Thames R.	130	5	2	0
3	N. Thames R. above Black Cr.	48	15	2	0
4	Black Cr. @ N. Thames R.	151	15	2	0
5	N. Thames R. above Avon R.	77	20	2	0
7	Avon R. @ N. Thames R.	144	8	4	2
8	Flat Cr. @ N. Thames R.	88	20	2	0
9	N. Thames R. above St. Mary's	79	15	2	0
10	Trout Cr. above Wildwood Dam	141	5	2	0
11	Trout Cr. @ Thames R.	29	15	2	0
12	N. Thames R. above Fish Cr.	36	10	2	0
13	Fish Cr. @ N. Thames R.	154	15	2	0
14	N. Thames R. below Fish Cr. (incl. Gregory Cr.)	85	12	2	0
15	N. Thames R. @ Fanshawe Dam (incl. Wye Cr.)	94	5	2	0
16	N. Thames R. in London (incl. Stoney Cr.)	75	2	1	5
17	Medway Cr. @ N. Thames R.	203	10	2	12
18	S. Thames R. @ Innerkip	148	5	3	0

19	S. Thames R. @ Pittock Dam	97	5	2	0
20	Cedar Cr.	98	25	5	0
21	S. Thames R. @ Ingersoll	171	34	3	0
22	S. Thames R. @ Middle Thames R.	43	3	2	0
23	Middle Thames R. @ Thamesford	291	27	3	0
24	Middle Thames R. @ S. Thames R.	36	45	4	0
25	Reynolds Cr. @ S. Thames R.	166	45	2	0
26	S. Thames River @ Waubuno Cr.	121	50	2	0
27	Waubuno Cr. @ S. Thames R.	105	5	5	0
28	S. Thames R. @ Ealing (incl. Pottersburg Cr.)	61	50	2	0
29	S. Thames R. @ N. Thames R. (Forks)	23	1	2	40
30	Thames R. @ Byron	30	1	2	30
31	Thames R. @ Oxbow Cr.	32	1	4	0
32	Oxbow Cr. @ Thames R.	89	5	8	0
33	Thames R. @ Dingman Cr.	51	5	4	0
34	Dingman Cr. @ Thames R.	169	3	6	2

Table 22: Transform model parameters for the RGO (OK) calibrated model

Basin #	**Basin name**	**Area (km^2)**	**Transform (Clark unit hydrograph)**	
			Time of concentration (hr)	**Storage coefficient (hr)**
1	N. Thames R. above Whirl Cr.	176	12	22
2	Whirl Cr. @ N. Thames R.	130	8	13
3	N. Thames R. above Black Cr.	48	12	6
4	Black Cr. @ N. Thames R.	151	12	6

5	N. Thames R. above Avon R.	77	7	6
7	Avon R. @ N. Thames R.	144	3	18
8	Flat Cr. @ N. Thames R.	88	8	6
9	N. Thames R. above St. Mary's	79	5	6
10	Trout Cr. above Wildwood Dam	141	8	15
11	Trout Cr. @ Thames R.	29	9	10
12	N. Thames R. above Fish Cr.	36	10	8
13	Fish Cr. @ N. Thames R.	154	13	14
14	N. Thames R. below Fish Cr. (incl. Gregory Cr.)	85	14	10
15	N. Thames R. @ Fanshawe Dam (incl. Wye Cr.)	94	15	20
16	N. Thames R. in London (incl. Stoney Cr.)	75	8	8
17	Medway Cr. @ N. Thames R.	203	22	15
18	S. Thames R. @ Innerkip	148	15	18
19	S. Thames R. @ Pittock Dam	97	15	15
20	Cedar Cr.	98	15	22
21	S. Thames R. @ Ingersoll	171	4	20
22	S. Thames R. @ Middle Thames R.	43	24	9
23	Middle Thames R. @ Thamesford	291	8	21
24	Middle Thames R. @ S. Thames R.	36	8	15
25	Reynolds Cr. @ S. Thames R.	166	15	18
26	S. Thames River @ Waubuno Cr.	121	8	8
27	Waubuno Cr. @ S. Thames R.	105	15	15

28	S. Thames R. @ Ealing (incl. Pottersburg Cr.)	61	8	5
29	S. Thames R. @ N. Thames R. (Forks)	23	4	6
30	Thames R. @ Byron	30	7	10
31	Thames R. @ Oxbow Cr.	32	6	6
32	Oxbow Cr. @ Thames R.	89	40	14
33	Thames R. @ Dingman Cr.	51	8	7
34	Dingman Cr. @ Thames R.	169	12	8

Table 23: Baseflow model parameters for the RGO (OK) calibrated model

Basin #	Basin name		Baseflow (recession)		
		Area (km^2)	Initial discharge ($m^3/s/km^2$)	Recession constant	Ratio
1	N. Thames R. above Whirl Cr.	176	0.01	0.4	0.2
2	Whirl Cr. @ N. Thames R.	130	0.01	0.4	0.2
3	N. Thames R. above Black Cr.	48	0.01	0.4	0.2
4	Black Cr. @ N. Thames R.	151	0.01	0.4	0.2
5	N. Thames R. above Avon R.	77	0.01	0.4	0.2
7	Avon R. @ N. Thames R.	144	0.01	0.4	0.2
8	Flat Cr. @ N. Thames R.	88	0.01	0.4	0.2
9	N. Thames R. above St. Mary's	78	0.01	0.4	0.2
10	Trout Cr. above Wildwood Dam	141	0.01	0.4	0.2
11	Trout Cr. @ Thames R.	29	0.01	0.4	0.2
12	N. Thames R. above Fish Cr.	35	0.01	0.4	0.2
13	Fish Cr. @ N. Thames R.	154	0.01	0.4	0.2
14	N. Thames R. below Fish Cr. (incl. Gregory Cr.)	85	0.01	0.4	0.2
15	N. Thames R. @ Fanshawe Dam (incl. Wye Cr.)	94	0.01	0.4	0.2
16	N. Thames R. in London (incl. Stoney Cr.)	75	0.01	0.4	0.2
17	Medway Cr. @ N. Thames R.	202	0.01	0.4	0.2

18	S. Thames R. @ Innerkip	148	0.01	0.4	0.2
19	S. Thames R. @ Pittock Dam	97	0.01	0.4	0.2
20	Cedar Cr.	98	0.01	0.4	0.2
21	S. Thames R. @ Ingersoll	171	0.01	0.4	0.2
22	S. Thames R. @ Middle Thames R.	43	0.01	0.4	0.2
23	Middle Thames R. @ Thamesford	291	0.01	0.4	0.2
24	Middle Thames R. @ S. Thames R.	36	0.01	0.4	0.2
25	Reynolds Cr. @ S. Thames R.	166	0.01	0.4	0.2
26	S. Thames River @ Waubuno Cr.	121	0.01	0.4	0.2
27	Waubuno Cr. @ S. Thames R.	105	0.01	0.4	0.2
28	S. Thames R. @ Ealing (incl. Pottersburg Cr.)	61	0.01	0.4	0.2
29	S. Thames R. @ N. Thames R. (Forks)	22	0.01	0.4	0.2
30	Thames R. @ Byron	30	0.01	0.4	0.2
31	Thames R. @ Oxbow Cr.	32	0.01	0.4	0.2
32	Oxbow Cr. @ Thames R.	89	0.01	0.4	0.2
33	Thames R. @ Dingman Cr.	50	0.01	0.4	0.2
34	Dingman Cr. @ Thames R.	169	0.01	0.4	0.2

Appendix D: Summary of the calibrated BSA hydrological model parameters

Table 24: Initial loss model parameters for the BSA calibrated model

Basin #	Basin name	Area (km^2)	Loss model (Initial and Constant)		
			Initial abstraction (mm)	Constant rate (mm/hr)	% Impervious
1	N. Thames R. above Whirl Cr.	176	4	1	0
2	Whirl Cr. @ N. Thames R.	130	5	2	0
3	N. Thames R. above Black Cr.	48	15	2	0
4	Black Cr. @ N. Thames R.	151	15	2	0
5	N. Thames R. above Avon R.	77	20	2	0
7	Avon R. @ N. Thames R.	144	8	4	2
8	Flat Cr. @ N. Thames R.	88	20	2	0
9	N. Thames R. above St. Mary's	78	15	2	0
10	Trout Cr. above Wildwood Dam	141	5	2	0
11	Trout Cr. @ Thames R.	29	15	2	0
12	N. Thames R. above Fish Cr.	35	10	2	0
13	Fish Cr. @ N. Thames R.	154	14	2	0
14	N. Thames R. below Fish Cr. (incl. Gregory Cr.)	85	12	2	0
15	N. Thames R. @ Fanshawe Dam (incl. Wye Cr.)	94	5	2	0
16	N. Thames R. in London (incl. Stoney Cr.)	75	2	1	5
17	Medway Cr. @ N. Thames R.	202	15	2	12

18	S. Thames R. @ Innerkip	148	5	3	0
19	S. Thames R. @ Pittock Dam	97	5	2	0
20	Cedar Cr.	98	23	4	0
21	S. Thames R. @ Ingersoll	171	34	3	0
22	S. Thames R. @ Middle Thames R.	43	3	2	0
23	Middle Thames R. @ Thamesford	291	21	3	0
24	Middle Thames R. @ S. Thames R.	36	45	4	0
25	Reynolds Cr. @ S. Thames R.	166	45	2	0
26	S. Thames River @ Waubuno Cr.	121	50	2	0
27	Waubuno Cr. @ S. Thames R.	105	5	5	0
28	S. Thames R. @ Ealing (incl. Pottersburg Cr.)	61	50	2	0
29	S. Thames R. @ N. Thames R. (Forks)	23	1	2	40
30	Thames R. @ Byron	30	1	2	30
31	Thames R. @ Oxbow Cr.	32	1	4	0
32	Oxbow Cr. @ Thames R.	89	5	8	0
33	Thames R. @ Dingman Cr.	50	5	4	0
34	Dingman Cr. @ Thames R.	169	3	6	2

Table 25: Transform model parameters for the BSA calibrated model

Basin #	Basin name	Area (km^2)	Transform (Clark unit hydrograph)	
			Time of concentration (hr)	Storage coefficient (hr)
1	N. Thames R. above Whirl Cr.	176	12	22
2	Whirl Cr. @ N. Thames R.	130	12	13
3	N. Thames R. above Black Cr.	48	18	6
4	Black Cr. @ N. Thames R.	151	27	6
5	N. Thames R. above Avon R.	77	6	6
7	Avon R. @ N. Thames R.	144	4	18
8	Flat Cr. @ N. Thames R.	88	12	13
9	N. Thames R. above St. Mary's	79	3	6
10	Trout Cr. above Wildwood Dam	141	8	15
11	Trout Cr. @ Thames R.	29	20	15
12	N. Thames R. above Fish Cr.	36	22	8
13	Fish Cr. @ N. Thames R.	154	19	14
14	N. Thames R. below Fish Cr. (incl. Gregory Cr.)	85	21	16
15	N. Thames R. @ Fanshawe Dam (incl. Wye Cr.)	94	15	20
16	N. Thames R. in London (incl. Stoney Cr.)	75	8	8
17	Medway Cr. @ N. Thames R.	203	22	15
18	S. Thames R. @ Innerkip	148	22	18
19	S. Thames R. @ Pittock Dam	97	50	22
20	Cedar Cr.	98	22	22
21	S. Thames R. @ Ingersoll	171	6	34
22	S. Thames R. @ Middle	43	26	20

	Thames R.			
23	Middle Thames R. @ Thamesford	291	12	17
24	Middle Thames R. @ S. Thames R.	36	8	15
25	Reynolds Cr. @ S. Thames R.	166	15	18
26	S. Thames River @ Waubuno Cr.	121	8	8
27	Waubuno Cr. @ S. Thames R.	105	22	6
28	S. Thames R. @ Ealing (incl. Pottersburg Cr.)	61	1	5
29	S. Thames R. @ N. Thames R. (Forks)	23	4	6
30	Thames R. @ Byron	30	7	10
31	Thames R. @ Oxbow Cr.	32	6	6
32	Oxbow Cr. @ Thames R.	89	40	14
33	Thames R. @ Dingman Cr.	51	8	7
34	Dingman Cr. @ Thames R.	169	12	8

Curriculum Vitae

Name:	Jack McKee
Post-secondary Education and Degrees:	The University of Western Ontario London, Ontario, Canada 2009-2013 B.E.Sc.
	The University of Western Ontario London, Ontario, Canada 2013-Expected 2015 M.E.Sc.
Honours and Awards:	Natural Sciences and Engineering Research Council of Canada Industrial Postgraduate Scholarship 2013-2015
	First place, Latornell Conservation Symposium Student Poster Competition 2014
	Latornell Conservation Symposium Three-Day Grant 2014
	First place, London Capstone Design Competition 2013
Related Work Experience	Teaching Assistant The University of Western Ontario 2013-2015

Journal and Conference Publications:

McKee, J.L., M. Helsten, M. Shifflett, and A.D. Binns. 2015. Application of gauge-adjusted radar for hydrology. *22nd Canadian Hydrotechnical Conference.* Canadian Society for Civil Engineering. Montreal, Canada. 29 April – 2 May 2015.

McKee, J.L., and A.D. Binns. 2015. A review of gauge-radar merging methods for quantitative precipitation estimation in hydrology. Accepted to *Canadian Water Resources Journal* (Manuscript ID: TCWR-2014-0082).

McKee, J.L., A.D. Binns, M. Helsten, and M. Shifflett. 2014. Application of radar quantitative precipitation estimates. *Showcasing water innovation in the Upper Thames River basin.* Upper Thames River Conservation Authority. London, Canada. 3 December 2014.

McKee, J.L., M. Helsten, M. Shifflett, and A.D. Binns. 2014. Gauge-radar precipitation merging methods for reliable flood forecasting. *21st Annual A.D. Latornell Conservation Symposium*. 18-20 November, Alliston, Canada, 2014.

Gunsolus, E.H., J.L. McKee, J. Brand, and A.D. Binns. 2014. Water resources and hydraulic engineering: Mitigating impacts to surface water environments. *Western Environment and Sustainability Showcase*. 6 March, London, Canada, 2014.